
PRAJÑĀ ĪVG
JOURNAL OF PURE & APPLIED SCIENCES
Published by
SARDAR PATEL UNIVERSITY
VOL.15, December 2007

*** CONTENTS ***

BIOSCIENCES

- Biopharmaceutics classification system-biowaiver extension
for class III compounds** 01
Tejal G. Soni, N.P. Chotai and B.G. Patel

CHEMISTRY

- Synthesis of some schief bases and their biological activity** 14
*Shipra Baluja, Sumitra Chanda, Vaghasiya Yogeshkumar, Rathish Nair
and Asif Solanki*
- Extraction and characterization of oil from spent bleaching earth** 23
Sibban Singh

COMPUTER SCIENCE

- Knowledge-based decision support system for diagnosis of
abdomen pain** 28
Dipti Shah and Priti Srinivas Sajja
- A web based fuzzy expert system for insect pest management in
groundnut crop** 36
P.V. Virparia

ELECTRONICS

- Fabrication of enzyme based glucose biosensor** 42
U.B. Trivedi, D. Laxminarayana, I.L. Kothari, K.K. Makhija and H.N. Kapse
- Fabrication of p-AgGaTe₂ / n-ZnSe photodiode** 49
Shahera S. Patel and B.H. Patel

PRAJÑĀ
ĪVG



JOURNAL OF PURE & APPLIED SCIENCES
VOLUME 15
DECEMBER 2007

VALLABH
VIDYANAGAR



PUBLISHED BY
SARDAR PATEL UNIVERSITY
Vallabh Vidyanagar

JOURNAL OF PURE & APPLIED SCIENCES - PRAJÑA

Published by
Sardar Patel University

Original research papers in the fields of basic and applied sciences are invited from scientists, engineers, industrialists, faculty and research students of post-graduate departments and affiliated colleges of universities in Gujarat for the next volume of the research journal, JOURNAL OF PURE & APPLIED SCIENCES - "PRAJÑA", published by Sardar Patel University, Vallabh Vidyanagar. The papers for publication may be submitted in duplicate to Prof. Ramesh Tikekar, Managing Editor, Department of Mathematics, Sardar Patel University, Vallabh Vidyanagar 388 120, Gujarat. Also, the paper on floppy diskette using PageMaker 6.5/Word 7 would be most appreciated. Short communications and announcements of unpublished results will be also considered for publication.

Instructions for preparation of manuscripts :

- (i) The Paper should be written in English and be neatly typed with double spacing on one side of bond paper.
- (ii) The "Abstract" of the paper, in not more than 150 words, should be provided on a separate sheet.
- (iii) Displayed formulae, mathematical equations and expressions be numbered serially.
- (iv) Tables, if any, should have a titles in addition to a serial number for each.
- (v) Photographs / figures be original with good contrast so as to be in a form suitable for direct reproduction / scanning.
- (vi) Original tracings of line diagrams should be provided.
- (vii) Footnotes be avoided.
- (viii) The title of the paper and the name(s) of the author(s) be in capital letters. The name of the institution be given in small letters below the name(s) of the authors(s).
- (ix) All figures must be numbered serially as they appear in the text, and their legends/ captions should necessarily be provided.
- (x) References in the text be made by the name (surname) of the author. At the end of the paper, the references should be cited in numerical order with the last name first.

HOME SCIENCE

- Thiamin and riboflavin status of rats fed on *phulka* supplemented with dietary fat** 55
Harshada J. Shah and S.S. Sail

MATERIALS SCIENCE

- Effect of chemical activation on deodorizing properties of activated carbon from banana stem** 61
J.H. Bhagat and S. Manocha
- Property modification of conventional castor oil based polyurethane using novel frame retardant polyurethanes** 66
R.H. Patel and H.B. Patel

MATHEMATICS

- Algebraic computations in general relativity using Mathematica** 77
A.H. Hasmani and G.A. Rathava
- Binachi type I bulk viscous string dust cosmological model in general relativity** 82
Raj Bali and Anjali

PHYSICS

- Microstructural analysis of zirconium triselenide single crystals** 91
K.R. Patel, R.D. Vaidya, M.S. Dave, A.J. Patel and S.G. Patel
- Growth and characterization of TaSe₂ single crystals grown by chemical vapour transport technique** 98
A.J. Patel, K.R. Patel, Rajiv Vaidya, A.R. Jani and S.G. Patel
- Synthesis, thermal and structural properties of zinc substituted barium hexaferrite powders prepared by a gel route** 105
R.B. Jotania and C.C. Chauhan
- Electron-molecule interactions in complex potential formulation: eH₂O example** 111
Sumona Gangopadhyay and K.N. Joshipura
- Temperature sensitivity of characteristic parameters of MoSe₂ solar cells** 122
Deepa Makhija, T.S. Maniar, R.J. Pathak, K.D. Patel. V. M. Pathak and R.Srivastava
- Growth and X-ray diffraction studies of ZnSe crystals** 127
J.R. Gandhi, G.K. Solanki, K.D. Patel and S.G. Patel
-

PRAJÑĀ
fvG

JOURNAL OF PURE & APPLIED SCIENCES

Published by **SARDAR PATEL UNIVERSITY**

Volume 15, December 2007

Biosciences

Chemistry

Computer Science

Electronics

Home Science

Materials Science

Mathematics

Medical Science & Pharmacy

Physics

Statistics

SARDAR PATEL UNIVERSITY
Vallabh Vidyanagar - 388 120, Gujarat, India

EDITORIAL BOARD

Dr B.G. Patel (Patron)	Vice-Chancellor, Sardar Patel University
Dr Ramesh Tikekar (Managing Editor)	Department of Mathematics
Dr K.N. Joshipura	Department of Physics
Dr S.J. Bhatt	Department of Mathematics
Dr Datta Madamwar	Department of Biosciences
Dr A.K. Ray	Department of Chemistry
Dr Rema Subhash	Department of Home Science
Dr (Mrs) S.L. Manocha	Department of Materials Science
Dr Darshan Choksi	Department of Computer Science

The University is grateful to Prof. Vithalbhai A. Patel of Humboldt State University, Arcata, California, U.S.A., whose generous donation to organise academic activities in the name of Shri Ishwarbhai Ambalal Patel (Shertha) helped to meet a part of the publication cost of this Journal.

Published by the Registrar, Sardar Patel University, Vallabh Vidyanagar - 388 120

Printed at Sardar Patel University Press, Vallabh Vidyanagar

Microstructural analysis of zirconium triselenide single crystals <i>K.R. Patel, R.D. Vaidya, M.S. Dave, A.J. Patel and S.G. Patel</i>	23
Growth and characterization of TaSe₂ single crystals grown by chemical vapour transport technique <i>A.J. Patel, K.R. Patel, Rajiv Vaidya, A.R. Jani and S.G. Patel</i>	30
Knowledge-based decision support system for diagnosis of abdomen pain <i>Dipti Shah and Priti Srinivas Sajja</i>	37
Synthesis, thermal and structural properties of zinc substituted barium hexaferrite powders prepared by a gel route <i>R.B. Jotania and C.C. Chauhan</i>	45
Fabrication of enzyme based glucose biosensor <i>K.K. Makhija and H.N. Kapse</i>	51
Thiamin and riboflavin status of rats fed on phulka supplemented with dietary fat <i>Harshada J. Shah and S.S. Sail</i>	58
A web based fuzzy expert system for insect pest management in groundnut crop <i>Dr. P.V. Virparia</i>	64
Electron-molecule interactions in complex potential formulation: eH₂O example <i>Sumona Gangopadhyay and K.N. Joshipura</i>	70
Temperature sensitivity of characteristic parameters of MoSe₂ solar cells <i>Deepa Makhija, T.S. Maniar, R.J. Pathak, K.D. Patel. V. M. Pathak and R.Srivastava</i>	81
Growth and X-ray diffraction studies of ZnSe crystals <i>J.R. Gandhi, G.K. Solanki, K.D. Patel and S.G. Patel</i>	86
Fabrication of p-AgGaTe₂ / n-ZnSe photodiode <i>Shahera S. Patel and B.H. Patel</i>	91
Effect of chemical activation on deodorizing properties of activated carbon from banana stem <i>J.H. Bhagat and S. Manocha</i>	97
Binachi type I bulk viscous string dust cosmological model in general relativity <i>Raj Bali and Anjali</i>	102
Algebraic computations in general relativity using Mathematica <i>A.H. Hasmani and G.A. Rathava</i>	111
Property modification of conventional castor oil based polyurethane using novel frame retardant polyurethanes <i>R.H. Patel and H.B. Patel</i>	116
Extraction and characterization of oil from spent bleaching earth <i>Sibban Singh</i>	127

BIOPHARMACEUTICS CLASSIFICATION SYSTEM- BIOWAIVER EXTENSION FOR CLASS III COMPOUNDS

Tejal G. Soni, N.P. Chotai* and B.G. Patel*

Anand Pharmacy College, Anand

*A.R. College of Pharmacy and G.H. Patel Institute of Pharmacy, Vallabh Vidyanagar

Abstract

The review article encompasses the recent inputs on Biopharmaceutics Classification System (BCS), biowaiver extension potential of BCS for class III drugs, its application as a framework for optimization of new chemical entity. The aim of this review is to present the status of the BCS and discuss its future application in pharmaceutical product development. The importance of the dissolution media selection considering BCS classification and similarity of dissolution profile using Moore and Flanner equation has been highlighted.

Introduction

The oral route of drug administration is the route of choice for the formulators and continues to dominate the area of drug delivery technologies. However, though popular, this route is not free from limitations of absorption and bioavailability in the milieu of gastrointestinal tract. The drug in the dosage form is released and dissolves in the surrounding gastrointestinal fluid to form a solution. This process is solubility limited. Once the drug is in the solution form, it passes across the membranes of the cells lining the gastro-intestinal tract. This process is permeability limited. Then onwards the drug is absorbed into systemic circulation. In short, the oral absorption and hence bioavailability of drug is determined by the extent of drug solubility and permeability.⁽¹⁾

The Food and Drug Administration (FDA) published its position on biowaivers in an August 2000 Guidance for Industry, Waiver of In Vivo Bioavailability and Bioequivalence Studies for Immediate-Release (IR) Solid Oral Dosage Form containing certain active moieties/ active ingredients based on a Biopharmaceutics Classification System (BCS) proposes to further expand the regulatory applications of BCS and also recommends methods for classifying drugs and IR drug products. The conditions under which a drug may be eligible for a waiver of in vivo bioavailability and bioequivalence studies termed as a biowaiver. The biowaiver provision applies to immediate-release, solid oral dosage forms in order to demonstrate equivalent bioavailability, for which the active ingredient does not have a narrow therapeutic index.⁽²⁾

Biopharmaceutics Classification System-Biowaiver...

In many cases the FDA is now asking for data documenting the BCS classification of new drugs early in the approval process, regardless of whether or not the sponsor has requested a biowaiver. In terms of development time and cost, it makes sense to classify new drug candidate within the BCS as early as possible.

Currently, only Class I (highly soluble and highly permeable) drugs that dissolve rapidly are eligible for a biowaiver. This policy is based on systemic exposure to a drug, which is proportional to its rate and extent of absorption, is in turn related to its solubility and permeability, especially when the rate of dissolution is rapid in relation to gastric emptying. There is currently an ongoing dialogue regarding the idea that Class III (high-solubility, low-permeability) compounds should also be eligible for a biowaiver. The rationale is that, once a compound is in solution, its systemic bioavailability is then dependent only on its permeability. If it can demonstrate comparable solubility and rate of dissolution in two different formulations, the bioavailability will be comparable. Permeability is based on the chemical structure of a compound and is less dependent than, e.g., the rate of dissolution or stability, on the excipients in a given formulation. Thus, a compound that has low permeability (Class III) will not have a much higher permeability in one formulation than another. On the other hand, a compound with low permeability is not going to have even lower permeability in a different formulation.⁽³⁾

In addition, IR solid oral dosage forms are categorized as having rapid or slow dissolution. Within this framework, when certain criteria are met, the BCS can be used as a drug development tool to justify requests for biowaivers.

The Biopharmaceutics Classification System

In 1995, Amidon et al. devised Biopharmaceutical Classification System (BCS) to classify drugs based on the aqueous solubility and intestinal permeability.⁽⁴⁾ Since then the BCS, has become a benchmark in the regulation of bioequivalence of oral drug products. The aim of the BCS is to provide a regulatory tool for replacing certain BE studies by accurate in-vitro dissolution tests. The future revision of the BCS guidelines by the regulatory agencies in communication with academic and industrial scientists is exciting and will hopefully result in an increased applicability in drug development. Finally, use of the BCS as a simple tool in early drug development to determine the rate-limiting step in the oral absorption process. This increased awareness of a proper biopharmaceutical characterization of new drugs may in the future result in drug molecules with a sufficiently high permeability, solubility and dissolution rate, and that will automatically increase the importance of the BCS as a regulatory tool over time.

The BCS guidance takes into account three major factors, dissolution, solubility and intestinal permeability, which govern the rate and extent of drug absorption from immediate release

Tejal G. Soni, N.P. Chotai and B.G. Patel

solid dosage forms.^(5,6,7) Proper in vitro surrogates for these two properties should allow prediction of a drug's absorption in vivo from in vitro assays.

According to the BCS, drug substances are classified as follows:

Class IV: LS/LP Low Solubility – Low Permeability Furosemide, Hydrochlorothiazide	Class III: HS/LP High Solubility – Low Permeability Ranitidine, Cimetidine, Atenolol
Class II: LS/HP Low Solubility – High Permeability Carbamazepine, Ketoprofen, Naproxen	Class I: HS/HP High Solubility – High Permeability Verapamil, Propranolol, Metoprolol

Drug Substance Solubility Class:

A drug substance is considered highly soluble when the highest dose strength is soluble in 250 ml or less of aqueous media over the pH range of 1-8. The volume estimate of 250 ml is derived from typical bioequivalence study protocols that prescribe administration of a drug product to fasting human volunteers with a glass (about 8 ounces) of water. This boundary value is a reflection of the minimum fluid volume anticipated in the stomach at the time of drug administration during a typical fasting bioequivalence study.⁽⁵⁾

Solubility Determination:

A sufficient number of pH conditions should be evaluated to define the pH-solubility profile. The number of pH conditions for a solubility determination can be based on the ionization characteristics of the test drug substance.

Depending on study variability, additional replication may be necessary to provide a reliable estimate of solubility methods other than the traditional shake-flask method, such as acid or base titration methods can be used to predict equilibrium solubility of the test drug substance.

Concentration of the drug substance in selected buffers (or pH conditions) should be determined using a validated stability-indicating assay. Stability in the gastrointestinal tract may be documented using gastric and intestinal fluids obtained from human subjects. Drug solutions in these fluids should be incubated at 37°C for a period that is representative of in

Biopharmaceutics Classification System-Biowaiver...

vivo drug contact with these fluids; for example, 1 hour in gastric fluid and 3 hours in intestinal fluid. Drug concentrations should then be determined using a validated stability-indicating assay method. Significant degradation (>5%) of a drug could suggest potential instability.

Drug Substance Permeability Class:

The permeability class boundary is intended that highly permeable drugs when administered as a solution exhibit complete absorption. The high permeability class membership may be considered when the extent of absorption in humans is greater than 90%.

Permeability Determination

The permeability class boundary is based on the rate of extent of absorption of a drug substance in humans by measurements of the rate of mass transfer and absolute BA. Mass balance studies can be used by using unlabeled, stable isotopes or a radiolabeled drug substance. Determination of total radioactivity in urine will help to establish permeability.

The following intestinal perfusion methods can also be used to determine the permeability of a drug substance from the gastrointestinal tract:

- In vivo intestinal perfusion studies in humans;
- In vivo or in situ intestinal perfusion studies using suitable animal models; (e.g., rats),
- In vitro permeation studies using excised human or animal intestinal tissues; (e.g., Caco-2 cell cultures).

An interesting alternative to intestinal tissue models is the use of well-established in vitro systems based on the human adenocarcinoma cell line Caco-2.⁽⁸⁾ These cells serve as a model of small intestinal tissue. The differentiated cells exhibit the microvilli typical of the small intestinal mucosa and the integral membrane proteins of the brush-border enzymes. In addition, they also form the fluid-filled domes typical of a permeable epithelium. Recent investigations of Caco-2 cell lines have indicated their ability to transport ions, sugars and peptides. The directed transport of bile acids and vitamin B12 across Caco-2 cell lines has also been observed. These properties have established the Caco-2 cell line as a reliable in vitro model of the small intestine.

- In Vitro Permeation Studies across a Monolayer of Cultured Epithelial Cells.

In vivo or in situ animal models and in vitro methods using cultured monolayer of animal or human epithelial cells are considered appropriate for passively transported drugs. The

Tejal G. Soni, N.P. Chotai and B.G. Patel

observed low permeability of some drug substances in humans could be caused by efflux of drugs via membrane transporters such as P-glycoprotein (P-gp). Pharmacokinetic studies on dose linearity may provide useful information for evaluating the relevance of observed in vitro efflux of a drug.

Chemical structure and/or certain physicochemical attributes of a drug substance (e.g., partition coefficient in suitable systems) can provide useful information about its permeability characteristics.

Biowaivers Based on BCS

BCS based biowaivers apply for situations during both pre- new drug application (NDA) and abbreviated new drug application (ANDA) and post approval phases. Considering the uncertainties associated with in vitro dissolution tests, BCS recommends biowaivers for rapidly dissolving products of highly soluble and highly permeable drugs Class I drug (The drug should not be a narrow therapeutic index), rate of dissolution should be greater than 85% in 30 minutes in the three recommended dissolution media (acidic media, such as 0.1 N HCl or Simulated Gastric Fluid USP without enzymes, a pH 4.5 buffer; and a pH 6.8 buffer or Simulated Intestinal Fluid USP without enzymes).⁽⁹⁾

In vivo differences in the rate and extent of absorption of a drug observed from two pharmaceutically equivalent solid oral products may be due to differences in drug dissolution in vivo. However, when in vivo dissolution of an IR solid oral dosage form is rapid in relation to gastric emptying and the drug has high permeability, the rate and extent of drug absorption is unlikely to be dependent on drug dissolution and/or gastrointestinal transit time. Under such circumstances, demonstration of in vivo BA or BE may not be necessary for drug products containing Class I drug substances, as long as the inactive ingredients used in the dosage form do not significantly affect absorption of the active ingredients.

A waiver of BA/BE studies is being proposed also for Class III compounds (high solubility and low permeability) in fast dissolving products with excipients which may not modify gastrointestinal transit or membrane permeation. This type of drug substance may be an even better candidate for a waiver as; in this case, bioavailability will not so much depend on the formulation characteristics, as on drug substance properties (e.g. permeability).^(10,11)

There is sufficient evidence that excipients used to formulate BCS Class III APIs in IR solid oral dosage forms have not effect on permeability and not alter the GI transit time. Dissolution similarity provide bioequivalency. In fact, it appears that the f_2 criterion for similarity of dissolution profiles represents a rather conservative approach, for Class III

Biopharmaceutics Classification System-Biowaiver...

APIs, since the rate-limiting step in the absorption process is the permeability, rather than the dissolution for these APIs. Thus, it appears that the f_2 criterion is more than sufficient to assure BE of BCS Class III APIs products in the absence of any excipient effects. Because permeability is the critical step in the absorption of the BCS Class III APIs, excipients that alter the GI motility and/or membrane permeation have the highest potential to affect the absorption.

When these two criteria are met, together with the "rapidly dissolving" criterion as per BCS, and the f_2 criterion. Biowaivers for other BCS Class III APIs have also been evaluated to be reasonably safe.

The results of the absorption of cimetidine from IR tablets is limited by permeability rather than dissolution. In vivo-in vitro correlation (IVIVC) analysis demonstrated that only when the release was deliberately retarded (tablets containing 26% methacrylate copolymer), did the dissolution represent the rate-limiting step to drug absorption. On the in vitro side, it seems that 85% dissolution within 30 minutes, as currently required by the US FDA Guidance, is more than sufficient to guarantee bioequivalence of IR cimetidine products.⁽⁹⁾ However, the data evaluated show that it would be safe to grant biowaivers for IR solid oral dosage forms of cimetidine, provided that the test product is formulated with excipients, in amounts typically used in IR solid oral dosage forms.⁽¹²⁾

Atenolol is indicated as a BCS Class III substance. In a provisional classification of the WHO Essential Drugs, this API was also classified to be BCS Class III. Atenolol might be a candidate for a biowaiver, as excipient interaction appeared not to be critical with regard to the absorption of atenolol, provided that tablets are formulated with well-known excipients show rapid in vitro dissolution, and meet the dissolution profile comparison criteria. As per USP specification for dissolution of atenolol tablets is NLT 80% dissolved in 30 min in 900 mL acetate buffer pH 4.6, using the paddle method operated at 50 rpm.⁽⁸⁾ Cimetidine and atenolol are both hydrophilic and are transported paracellularly through the intestinal membrane.^(13,14)

Dissolution

Dissolution test for oral solid dosage forms was first introduced in *United States Pharmacopoeia (USP)* 18 in 1969. The rationale behind this test is that a drug should be appropriately dissolved within the gastrointestinal tract (GIT) in order to be absorbed. Dissolution hence has become the most important test to determine product quality and drug release behavior in addition to other applications.⁽¹⁵⁾ *In vitro* dissolution characterization is encouraged the establishment of an *in vitro-in vivo* correlation. When an *in vitro-in vivo* correlation or association is available the *in vitro* test can serve not only as a quality

Tejal G. Soni, N.P. Chotai and B.G. Patel

control specification for the manufacturing process, but also as an indicator of how the product will perform *in vivo*.^(16, 17)

Compounds belonging to class I with high solubility and permeability should go into solution quickly when they are housed in immediately release dosage forms and also be rapidly transported across the gut wall. Therefore it is expected that they will be well absorbed unless they are unstable, form insoluble complexes, and secreted directly from the gut wall or undergo first pass metabolism. Dissolution for IR products is needed only to verify that the drug is indeed rapidly released from the dosage form under mild aqueous conditions. An IR drug product is considered *rapidly dissolving* when no less than 85% of the labeled amount of the drug substance dissolves within 30 minutes.

For Class II drugs, rate of dissolution is the rate limiting step for drug absorption. The limitation can be equilibrium or kinetic in nature. Equilibrium can be checked by calculating the dose: solubility ratio. In the case of a kinetic problem, the drug dissolves too slowly for the entire dose to become dissolved before the drug has passed by its site of uptake. Because the poor driving force for dissolution supplied by the solubility, combined with the low surface area of drug at larger particle size, is insufficient to ensure timely dissolution. For class II drugs, it should be possible to establish a strong correlation between the results of IVIVC. Adequate comparison of the dosage form for class II drugs, require dissolution test with multiple sampling times in order to characterize dissolution profile.⁽¹⁸⁾

Class III drugs are rapidly dissolving and the test criteria should be that the formulation can release the drug under the mild conditions within a predetermined time. Rapid dissolution is particularly desirable for class III drugs, in order to maximize the contact time between the dissolved drug and the absorbing mucosa, and consequently the bioavailability of the compound. Therefore the duration of the dissolution test should be at least as stringent for class III drugs as for class I drugs.

Class IV drugs are expected to have poor absorption in general as in case of Class II drugs, poor formulation could have an additional negative influence on both the rate and extent of the drug absorption. Thus for all four categories it is anticipated that well designed dissolution test can be a key prediagnostic tool in the assessment of both the drug's potential for oral absorption and of the bioequivalence of its formulations.

Media Selection:

The choice of medium is depend upon purpose of the dissolution test. For batch - batch consistency selection of medium is based on solubility data and the dose range of the drug product to ensure that sink conditions are met. The term sink condition is defined as the

Biopharmaceutics Classification System-Biowaiver...

volume of medium at least greater than three times that required to form a saturated solution of a drug substance. A medium that fail to provide the sink condition can be justified because absence of sink conditions may result in unpredictable release kinetics and suppression of release profiles. When dissolution test is used to indicate the biopharmaceutic property of dosage form, it is more important that the proposed biorelevant test closely simulate the environment in the gastrointestinal tract that necessarily produce sink conditions. According to some other references the drug concentration in the dissolution medium should not exceed 15% to 20% of saturation solubility of the drug in order to provide sink conditions.

Different techniques have been employed by scientists to improve solubility and ensure sink conditions.⁽¹⁹⁾

- Addition of organic solvents to aqueous medium,
- Use of 2-phase solvent system,
- Use of large dissolution volume,
- Removal of dissolved drug,
- pH changes, and
- Addition of surfactants or their combinations.

For some low solubility compounds, adequate dissolution can not be obtained with aqueous solutions within the physiologic pH ranges. For these compounds, aqueous solution containing a surfactant may be used to enhance drug solubility. A surfactant can be used as either a wetting agent or when the critical micelle concentration is reached, to stabilize the drug substance.⁽²⁰⁾ The need for surfactant as well as their type and concentration should be justified. Commonly acceptable ionic or nonionic surfactants include

- Sodium lauryl sulfate,
- Polyoxyethylenesorbitan monolaurate (Tween),
- Cetyltrimethylammoniumbromide (CTAB),
- Polyoxyyl castor oil (Cremophor),
- Hexadecyltrimethylammonium bromide (HTAB),
- Polyethylene glycol tert-octphenyl ether (Triton),
- Nonphenol ethoxylate (Tergitol),
- Cyclodextrins, and
- Lecithin.

Tejal G. Soni, N.P. Chotai and B.G. Patel

In general nonionic detergent (Tween) is considered more biologically relevant, and thus are often the first choice when considering the addition of a surfactant. Depending on the dose size and solubility characteristics of low solubility drugs, a meaningful and discriminatory power of dissolution rate testing can be demonstrated.

Saturation solubility of fenofibrate and glipizide in different media were determined. Solubility of fenofibrate increased directly with SLS concentration. For a 54-mg fenofibrate tablet, SLS at 0.025 M level is required for a discriminative dissolution test, while for 160-mg tablet, dissolution condition and levels of SLS should be optimized; higher concentrations may be effective (i.e., 0.052 M, ~1.5%). A pH 6.8 phosphate buffer medium is appropriate for glipizide 10-mg tablet dissolution study, when formulation ingredients include excipients with surface activity (e.g., HPMC).⁽²²⁾

The pH dependency relates to changes occurring in the gums and other necessary excipients and whether these result in a pH dependency in those properties reflecting release of drug from its matrix. At low pH (simulated gastric fluid, pH 1.5), the dissolution of metaxalone from Skelaxin tablets was less than 10% over 75 minutes; whereas, dissolution at pH 4.5 showed greater than 90% release in the same time period.⁽²³⁾

Dissolution Profile Similarity

An intensive screen of dissolution profiles between brands demonstrates clear products difference. A series of careful bioavailability studies were commissioned using the products selected from a dissolution rate screen.

Using the rationale of the BCS, it can be argued that biowaivers can, however, also be granted on the basis of standard pharmacokinetic data. If a drug exhibits dose-linear pharmacokinetics and a sufficiently fast dissolution profile, it can be concluded that this drug appears to pose no problem with respect to absorption. It should be noted that a change of an immediate-release tablet formulation can only lead to a deviating rate and/or extent of absorption when release of the drug from the formulation is altered. Logically, the dissolution profiles of the different formulations should be equal to guarantee bioequivalency. Thus, both BCS and the alternative linear pharmacokinetics approach require an evaluation of dissolution profiles. Hence a change in formulation without any effect on the dissolution profile is not expected to cause a change in availability.^(24,25)

Dissolution profiles (multiple data points, 0, 10, 15, 20, and 30 minutes) generated in a minimum of 12 dosage units should be evaluated at different agitation speeds for *U.S. Pharmacopoeia* (USP) Apparatus I at 100 rpm or Apparatus II at 50 rpm at least three dissolution media (1)0.1 N HCl or Simulated Gastric Fluid USP without enzymes;

Biopharmaceutics Classification System-Biowaiver...

(2) a pH 4.5 buffer; and (3) a pH 6.8 buffer or Simulated Intestinal Fluid USP without enzymes.⁽¹⁵⁾ Water can be used as an additional medium. If the drug being considered is poorly soluble, appropriate concentrations of surfactants are recommended.⁽²⁶⁾

Dissolution testing apparatus used in this evaluation should conform to the requirements in USP. Selection of the dissolution testing apparatus (USP Apparatus I or II) during drug development should be based on a comparison of in vitro dissolution and in vivo pharmacokinetic data available for the product. The USP Apparatus I (*basket method*) is generally preferred for capsules and products that tend to float, and USP Apparatus II (*paddle method*) is generally preferred for tablets. For some tablet dosage forms, in vitro (but not in vivo) dissolution may be slow due to the manner in which the disintegrated product settles at the bottom of a dissolution vessel. In such situations, USP Apparatus I may be preferred over Apparatus II. If the testing conditions need to be modified to better reflect rapid in vivo dissolution such modifications can be justified by comparing in vitro dissolution with in vivo absorption data.

The dissolution profile comparison may be carried out using model independent or model dependent methods. E.g. by linear regression of the percentage dissolved at specified time points, by statistical comparison of the parameter of the Weibull function or by calculating a similarity factor. A simple dissolution model independent approach uses a difference factor (f_1) and similarity factor (f_2). The similarity factor has been adopted by the Center for Drug Evaluation and Research (US FDA) and by Human Medicines Evaluation Unit of The European Agency for the Evaluation of Medicinal Products (EMA) as a criterion for the assessment of the similarity between two dissolution profiles.^(27,28) The US Food and Drug Administration's (FDA's) guidance for industry on dissolution testing of immediate-release, solid, oral dosage forms describes the model-independent mathematical approach proposed by Moore and Flanner for calculating a dissimilarity factor (f_1) and a similarity factor (f_2) of dissolution across a suitable time interval. It is included in various guidance documents. The similarity factor f_2 is defined as logarithmic reciprocal square root transformation of one plus the mean squared (the average sum of squares) differences of drug percent dissolved between the test and reference products:

The similarity factor f_2 is a measurement of the similarity in the percent (%) of dissolution between the two curves.

$$f_2 = 50 \cdot \log \left\{ \left[1 + \frac{1}{n} \sum_{t=1}^n (R_t - T_t)^2 \right]^{-0.5} \cdot 100 \right\}$$

$$f_1 = \left\{ \frac{\sum_{t=1}^n (R_t - T_t)}{\sum_{t=1}^n R_t} \right\}$$

Two dissolution profiles are considered similar when the f_2 value is (50-100) and f_1 values up to 15 (0-15). f_1 values should be close to 0 and f_2 values should be close to 100 ensure equivalence of the two curves. To allow the use of mean data, the coefficient of variation should not be more than 20% at the earlier time points (e.g., 10 minutes), and should not be more than 10% at other time points. Note that when both test and reference products dissolve 85% or more of the label amount of the drug in 15 minutes using all three dissolution media recommended above, the profile comparison with an f_2 test is unnecessary. ^(29, 30, 31)

References

1. Gibaldi, M., *Biopharmaceutical and Clinical Pharmacokinetics*, Fourth edition, Lea & Febiger, Philadelphia. 1991, 24-79.
2. Guidance for Industry: Immediate Release Solid oral Dosage Forms, Scale-Up and Post-Approval Changes: Chemistry, Manufacturing and Controls, In Vitro Dissolution Testing, and In Vivo Bioequivalence Documentation. US Food and Drug Administration, Rockville, MD, USA, 1995.
3. Blume HH, Schug BS. The biopharmaceutics classification system (BCS): Class III drugs—Better candidates for BA/BE waiver, *Eur J PharmSci*, 1999, 9, 117–121.
4. Amidon, G. L., H. Lennernäs, V. P. Shah, and J. R. Crison, A Theoretical Basis For a Biopharmaceutics Drug Classification: The Correlation of In Vitro Drug Product Dissolution and In Vivo Bioavailability, *Pharmaceutical Research*, 1995, 12, 413-420.
5. Tammara, V. K., Hossain, M., Malinowski, H., and Hussain, A. S. Evaluation of the Proposed Biopharmaceutics Classification System (BCS) Class Boundaries: A Survey of Recent Neuropharmacological Drugs. AAPS Annual Meeting, Boston, MA, November 1997.
6. Kaus, L. C., Gillespie, W. R., Hussain, A. S., and Amidon, G. A. The effect of in vivo dissolution, gastric emptying rate, and intestinal transit time on the peak concentration and area-under-the-curve of drugs with different gastrointestinal permeabilities. *Pharm. Res.*, 1999, 16, 272-280.
7. Abrahamsson B. et al., The use of biopharmaceutic classification of drugs in drug discovery and development: current status and future extension. *J Pharmacology*. 2005, 57, 273-285.
8. Collett A, Sims E, Walker D, He YL, Ayrton J, Rowland M, Warhurst G. Comparison of HT29-18-C1 and Caco-2 cell lines as models for studying intestinal paracellular drug absorption. *Pharm. Res.*, 1996, 13, 216–221.

Biopharmaceutics Classification System-Biowaiver...

9. Guidance for Industry: BA and BE studies for orally administered drug products, General considerations, US Department of Health and Human Services, Food and Drug Administration, Center for Drug Evaluation and Research, August 1999 .
10. Jantratid, Ekarat; Prakongpan, Sompol; Amidon, Gordon L.; Dressman, Jennifer B. Feasibility of Biowaiver Extension to Biopharmaceutics Classification System Class III Drug Products: Cimetidine Clinical Pharmacokinetics, 2006, 45,385-399.
11. Cheng CL, Yu LX, Lee HL, Yang CY, Lue CS, ChouCH. Biowaiver extension potential to BCSC Class III high solubility-low permeability drugs: Bridging evidence for metformin immediate release tablet. *Eur J Pharm Sci.*, 2004, 22,297–304.
12. Adkin DA, Davis SS, Sparrow RA, Huckle PD, Wilding IR. The effect of mannitol on the oral bioavailability of cimetidine. *J Pharm Sci.*, 1995, 84, 1405–1409.
13. Vogelpoel H, Welink J, Amidon GL, Junginger HE, Midha KK, Miller H, Olling M, Shah VP, Barends DM. Biowaiver monographs for immediate release solid oral dosage forms based on biopharmaceutics classification system literature data: Verapamil hydrochloride, propranolol hydrochloride, and atenolol. *J Pharm Sci.*, 2004, 93, 1945–1956.
14. Lindenberg M, Kopp S, Dressman JB. Classification of orally administered drugs on the World Health Organization Model list of Essential Medicines according to the biopharmaceutics classification system. *Eur J Pharm Biopharm*, 2004, 58,265–278.
15. Guidance for Industry: Dissolution Testing of Immediate Release Solid Oral Dosage Forms. US Food and Drug Administration, Rockville, MD, USA, 1997.
16. Dressman JB Amidone GL, Reppas C, Shah VP. Dissolution testing as a prognostic tool for oral drug absorption: immediate release dosage forms. *Pharm Res.* 1998, 15, 11-22.
17. Pillay V, Fassihi R. Evaluation and comparison of dissolution data derived from different modified release dosage forms: an alternative method *Control Release.* 1998, 55, 45-55.
18. B.R. Rohrs, “Invitro Dissolution Testing of Poorly Soluble Compounds: Impact of formulation Design”. Presented at the phRMA Acceptable Analytical Practice Workshop, Washington, DC, 2003, 9, 23-25.
19. Shah V P, Konecny J J, Everett R L, McCullough B, Noorizadeh A C, Skelly J P. Invitro dissolution profile of water-insoluble drug dosage forms in the presence of surfactants. *Pharm Res.* 1989, 6, 612-618.

Tejal G. Soni, N.P. Chotai and B.G. Patel

20. Jinno J, Oh DM, Crison JR, Amidon GL. Dissolution of water-insoluble drugs: the combined effect of pH and surfactant *Pharm Sci*, 2000, 89,268-274.
21. Jamzad S, Fassihi R. Role of Surfactant and pH on Dissolution Properties of Fenofibrate and Glipizide—A Technical Note. *AAPS PharmSciTech* 2006, 7, Article 33
22. Cacace J, Reilly EE, Amann A. Comparison of the Dissolution of Metaxalone Tablets (Skelaxin) Using *USP* Apparatus 2 and 3. *AAPS PharmSciTech*. 2004;5, Article 6.
23. Faassen, Fried I; Vromans, Herman I 2Biowaivers for Oral Immediate-Release Products: Implications of Linear Pharmacokinetics. *Clinical pharmacokinetics*. 2004, 43, 1117-1126.
24. Liebenberg R, Amidon GL. Modern bioavailability, bioequivalence and biopharmaceutics classification system. New scientific approaches to international regulatory standards. *Pharm Res*, 2000, 10, 1027–1030 .
25. Moore, J.W.; Flanner, H. H. Mathematical comparison of curves with an emphasis on in-vitro dissolution profiles. *Pharm.Tech*. 1996, 20, 64-74.
26. Adams, E.Maesschalck, R. D. Spiegeleer, B. D. Heyden, Y. V. Verbeke, J. S. Massart, D. L. Evaluation of dissolution profiles using principal component analysis. *Int. J.Pharm*. 2001, 212, 42-53.
27. Mukesh C. Gohel, K.G. Sarvaiya, N.R. Mehta, C.D. Soni, Vinita Vyas, R.K. Dave, Assessment of similarity Factor using Different Weighing Approaches. *Dissolution technologies*, 2005, 12, 22-27.
28. Note for Guidance on the investigation of Bioavailability and Bioequivalence. EMEA. London, 2001.
29. Bartoszynski, R.; Powers, J. D.; Herderick, E. E.; Pultz, J. A. Statistical comparison of dissolution curves. *Pharmacol. Res*. 2001, 43, 371-387.
30. Sarandasa, H.; Krishnamoorthy, K. A multivariate tests for similarity of two dissolution profiles. *J. Biopharm. Stat*. 2005, 15, 265-278.
31. Shah P.; Tsong, Y.; Sathe, P.; Liu, J. P. In vitro Dissolution Profile Comparison- Statistics and Analysis of the Similarity Factor, f2. *Pharm. Res*. 1998, 15, 889-895.

SYNTHESIS OF SOME SCHIFF BASES AND THEIR BIOLOGICAL ACTIVITY

Shipra Baluja*, **Sumitra Chanda****, **Vaghasiya Yogeshkumar****, **Rathish Nair****
and Asif Solanki*

*Department of Chemistry, **Department of Biosciences
Saurashtra University, Rajkot – 360 005

Abstract

Some new Schiff bases were prepared by the condensation of 3-chloro-4-fluoroaniline with different aromatic aldehydes. The structure characterization of these compounds was done on the basis of spectral data. The antimicrobial activity of the compounds was obtained in two polar solvents; DMF and DMSO and the compounds are found to be effective against both Gram +ve and Gram -ve bacteria.

Introduction

Fighting disease with drugs is a time less struggle. Man's survival on this planet has depended upon its success. Due to multi-drug resistant pathogens and cancers, we are faced with ever-increasing health threats from exotic and opportunistic infections. In order to combat these important health problems, discovery of new medicinal agents with novel modes of activity is imperative. Interest in research for compounds with antimicrobial properties has been revived due to current problems faced by people with the use of antibiotics. Drug design is an integrated developing discipline, which deals with development of new drugs on rational basis; the ultimate goal is to offer appropriate and efficient antimicrobial drugs to people.

Day by day Schiff bases are integrally applied for human welfare. Extensive investigation in the field of Schiff bases have been reported, their preparation, chemical and physical properties have been described. They are known to be important due to their wide applications such as preparation of dyes, liquid crystals, as powerful corrosion inhibitors⁽¹⁻²⁾, chelating agent, analytical reagent and as a catalyst for epoxidation of olefins⁽³⁻⁵⁾. Schiff's bases are known to be associated with broad spectrum of biological activities such as bactericidal, anti-pyretic, anticancer, antitumour, antituberculer and steerage inhibitory.⁽⁶⁻¹¹⁾ Furthermore, many Schiff bases possess bacteriosites fungicidal, medicinal and agrochemical activity⁽¹²⁾.

Considering the above, the aim of present work was to synthesize some Schiff bases from 3-chloro-4-fluoro aniline and to evaluate their potency as antibacterial agents.

Experimental

The following Schiff bases have been synthesized

N-[(1*Z*)-1-anthrylmethylene]-*N*-(3-chloro-4-fluorophenyl) amine (HAS-I)

4-{(*E*)-[(3-chloro-4-fluorophenyl) imino] methyl} phenol (HAS-II)

N-(3-chloro-4-fluorophenyl)-*N*-[(1*E*)-(3-nitrophenyl)methylene]amine (HAS-III)

N-(3-chloro-4-fluorophenyl)-*N*-[(1*E*)-(4-fluorophenyl) methylene] amine (HAS-IV)

N-(3-chloro-4-fluorophenyl)-*N*-[(1*E*)-(4-methoxyphenyl)methylene]amine (HAS-V)

N-(3-chloro-4-fluorophenyl)-*N*-{(1*E*)-[4-(dimethylamino)phenyl] methylene} amine (HAS-VI)

2-{(*E*)-[(3-chloro-4-fluorophenyl) imino] methyl} phenol (HAS-VII)

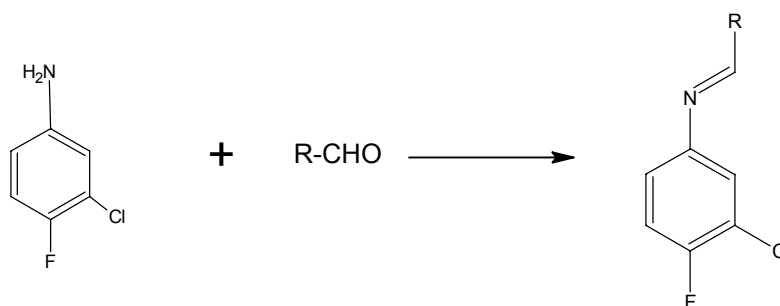
N-(3-chloro-4-fluorophenyl)-*N*-[(1*E*)-(4-chlorophenyl) methylene] amine (HAS-VIII)

5-{(*E*)-[(3-chloro-4-fluorophenyl)imino]methyl}-2-methoxyphenol (HAS-IX)

Synthesis of Schiff bases

An ethanolic solution of 0.01 mole 3-chloro-4-fluoroaniline was added to 0.01 mole of aldehyde and few drops of glacial acetic acid. The mixture was refluxed on water bath at 80-90 °C for 12 to 13 hours. The resulting reaction mixture was then poured on crushed ice. The solid was separated out, washed with distilled water and dry product was recrystallized from ethanol.

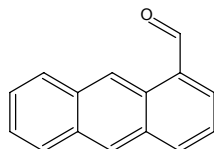
Reaction Scheme



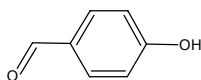
Synthesis of Some Schiff Bases and Their.....

Where Aldehydes are

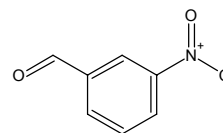
HAS-I



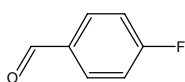
HAS-II



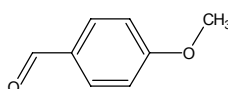
HAS-III



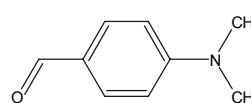
HAS-IV



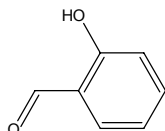
HAS-V



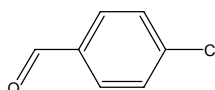
HAS-VI



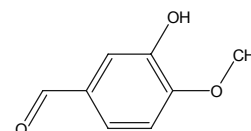
HAS-VII



HAS-VIII



HAS-IX



Melting points were determined by Capillary method and are uncorrected. Purity of compounds was checked by TLC on silica gel-G coated plates. Table-1 shows the physical properties and IR spectral data of all the synthesized Schiff bases.

Antimicrobial Activity

Test Microorganisms

The bacterial strains studied are identified strains and were obtained from National Chemical Laboratory (NCL), Pune, India. The investigated microorganisms are *E. Coli* ATCC 25922, *S. aureus* ATCC 25923, *P. vulgaris* NCTC 8313, *K. Pneumoniae* NCIM 2719. and *P. aeruginosa* ATCC 27853.

Preparation of test compound solution

Three different concentrations i.e., 2 mg/0.1mL, 0.2 mg / 0.1 mL and 0.02 mg / 0.1 mL were prepared for all the Schiff bases in both DMF and DMSO.

Preparation of the plates and microbiological assays

A loopful of the given test strain was inoculated in 20 mL of N-broth (Nutrient Broth). To activate the given bacterial strain, it was incubated for 24 hours in an incubator at 37 °C.

Shipra Baluja, Sumitra Chanda, Vaghasiya Yogeshkumar, Rathish Nair and Asif Solanki

The Agar well diffusion method⁽¹³⁾ is used for antibacterial assay. 28-30 mL of molten agar (Mueller Hinton Agar No. 2) was added into the 100 mm diameter petri plate. Care should be taken to avoid air bubbles during inoculation and pouring. To maintain sterile condition, all these procedures were done in the laminar air flow. The media was allowed to solidify. After solidification of the media, well was made in the plates with the help of cup-borer (0.85 cm) and then it was filled with the synthesized Schiff bases solution (dissolved in DMF/DMSO).

The antibacterial activities of these synthesized bases were determined by the inhibition zone formed by these compounds against the particular test bacterial strain.

Results and Conclusion

All the Schiff bases produced different inhibition zone against tested bacteria in the two solvents. The results are shown in Figures 1 to 3. Out of the three concentrations studied, the lowest concentration 0.02 mg/0.1 mL was not effective at all. The concentration 0.2 mg/0.1 mL was slightly effective whereas solution of the concentration 2 mg/0.1 mL gave significant results. In the present paper, the data of third concentration is only reported.

Composition of inhibition zones produced in DMF and DMSO in Fig.1 shows that in DMF for *E. Coli.*. Maximum inhibition is exhibited by VI and minimum by II, IV and VII. VIII shows no effect at all on *E. Coli.* The same compounds when tested in DMSO showed different trend. For the same bacteria *E. Coli.* in DMSO, II showed maximum inhibition. VII and VIII had very little effect whereas I and III had no effect at all.

The different inhibition zone of different compounds for the same bacteria is because of their molecular structures. All these Schiff bases has common 3-chloro-4-fluoroaniline moiety with different side chains. Further, it is observed that solvent plays important role in inhibition.

In DMF, III showed maximum inhibition against *S. aureus* whereas I exhibited minimum. The compounds IV, V, VII and VIII showed no effect at all. In DMSO also, III exhibited maximum inhibition followed by II and IX. All other compounds had no effect on *S. aureus*.

Fig.2 shows for *P. vulgaris*, in both DMF and DMSO, IX showed maximum activity and I showed no activity at all. In DMF, all Schiff bases exhibited inhibition against *K. Pneumoniae* but each compound had a different level of inhibition. VII showed maximum and VIII showed minimum inhibition. In DMSO, except I, all other bases showed inhibition and IX exhibited maximum activity. This again confirms our earlier conclusion that there is a direct and strong relation between structures of the compound, used solvent and the bacterial strain against which it is being studied.

Synthesis of Some Schiff Bases and Their.....

Fig.3 shows that inhibition of Schiff bases against *P.aero*. It is observed that IV shows maximum inhibition zone in DMF followed by V and IX. Rest of the schiff bases had no effect on *P.aero*. However, in DMSO VI had maximum effect followed by II and IX, other compounds did not affect the *P.aero*.

The differential response of the synthesized Schiff bases is because of the difference in their side chains. All the compounds have 3-chloro-4-fluoroaniline moiety.

Over all, IX is observed to be the most effective in inhibiting *S.aureus*, *P.vulgaris* and *P.aero* in DMF whereas in DMSO, it is highly effective for *P.vulgaris* and *K.Pneu*. VI followed next in inhibition against *E.Coli*. in DMF medium and *P.aero* in DMSO. The vanilline group is present in IX and VI contain N, N-di methyl benzaldehyde.

From the above, it can be concluded that out of all synthesized Schiff bases, those having vanillin (IX) and N, N-dimethyl (VI) are best. Out of two solvents DMF and DMSO, DMF is proved to be better solvent.

Some other bases with o, p-hydroxy benzaldehyde, m-nitro benzaldehyde, fluoro benzaldehyde side chains are also effective.

Thus, the 3-chloro-4-fluoro aniline with vanillin and N, N-dimethyl side chain can be used as lead molecule due its good inhibitory activity.

References

1. H. Ashassi-Sorkhabi, B.Shhabani and D.Seifzadch, Applied Surface Science, **239**, 154 (2005)
2. A. Aytac, U. Ozmen and M. Kabasakaloglu, Materials Chemistry and Physics, **89**, 176 (2005)
3. K. Lal; Ind.J.Chem. **20**, 853 (1981)
4. K. Srinivasan, P.Michand and J.K. Kochi; J. Am. Chem. Soc., **108**, 2309 (1986)
5. P.K.Bhattachariya, Proc. Ind. Acad. Sci., **102**, 247 (1990)
6. P.R.Panditrao, S.P.Deval, S.M.Gupta, S.D.Samant and L.D.Deodhar, Ind. J. Chem, **20**, 929 (1981)
7. J.H.Jedrut, Chem. Abstr., **70**, 3927 (1969)
8. M.S.Shingare and D.B.Ingle, Ind. J. Chem.Soc, **53**, 1036 (1976)
9. C. Deliwaliw, J. Med. Chem. **49**, 450 (1971)
10. J. R. Merchant and D.S.Chothia, J.Med.Chem, **40**, 194 (1970)
11. K. Sengupta and Hijeria, Chem.Abstr, **99**, 158177 (1983)
12. D. Sebla, Ind. J. Chem, **33**, 1335 (1996)
13. R. Nair, A. Shah, S. Baluja and S. V. Chanda, Med. Chem. Res, **11**, 463 (2002)

Fig. 1: Comparative study of Schiff bases in DMF (A) and DMSO (B)

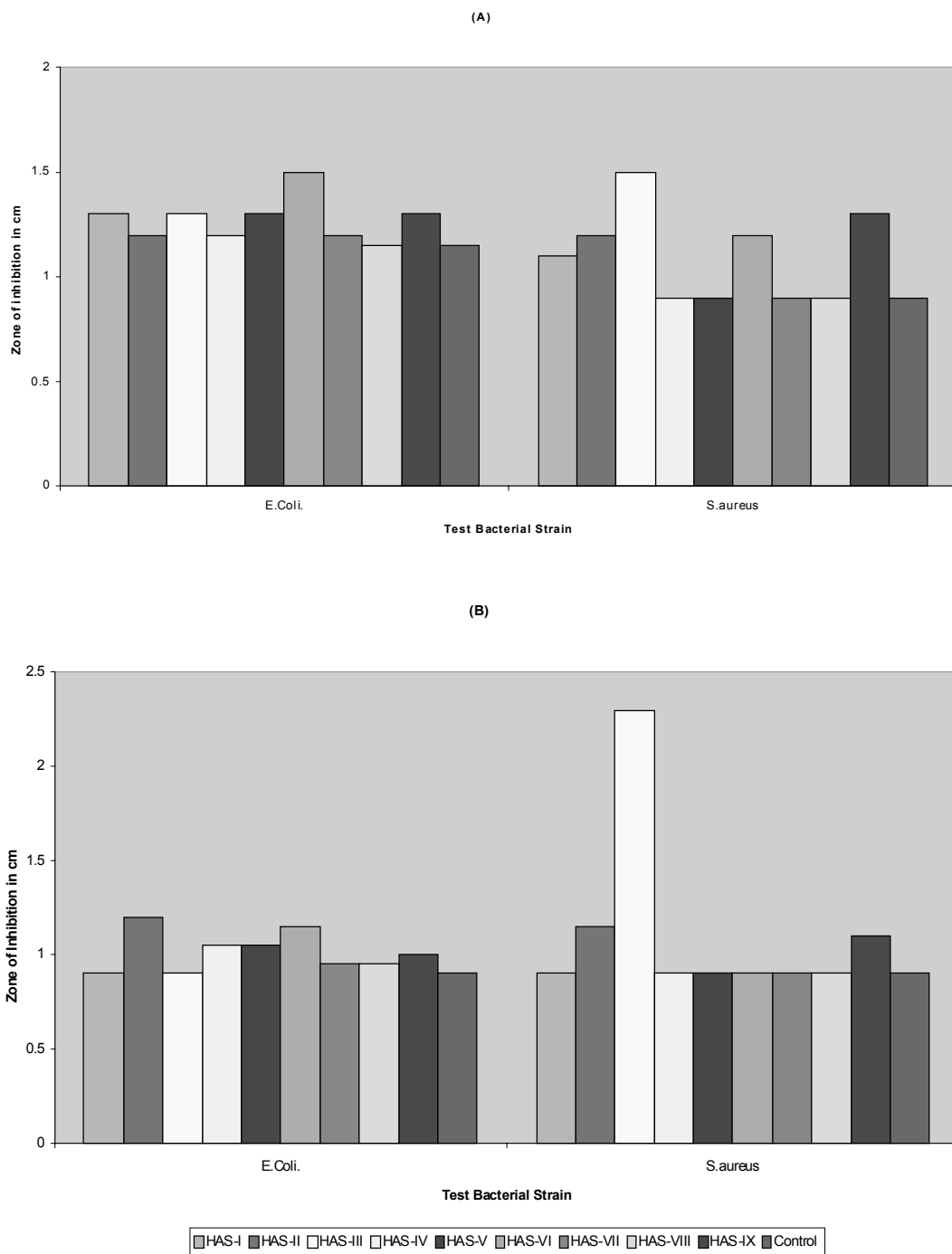


Fig. 2 : Comparative study of Schiff bases in DMF (A) and DMSO (B)

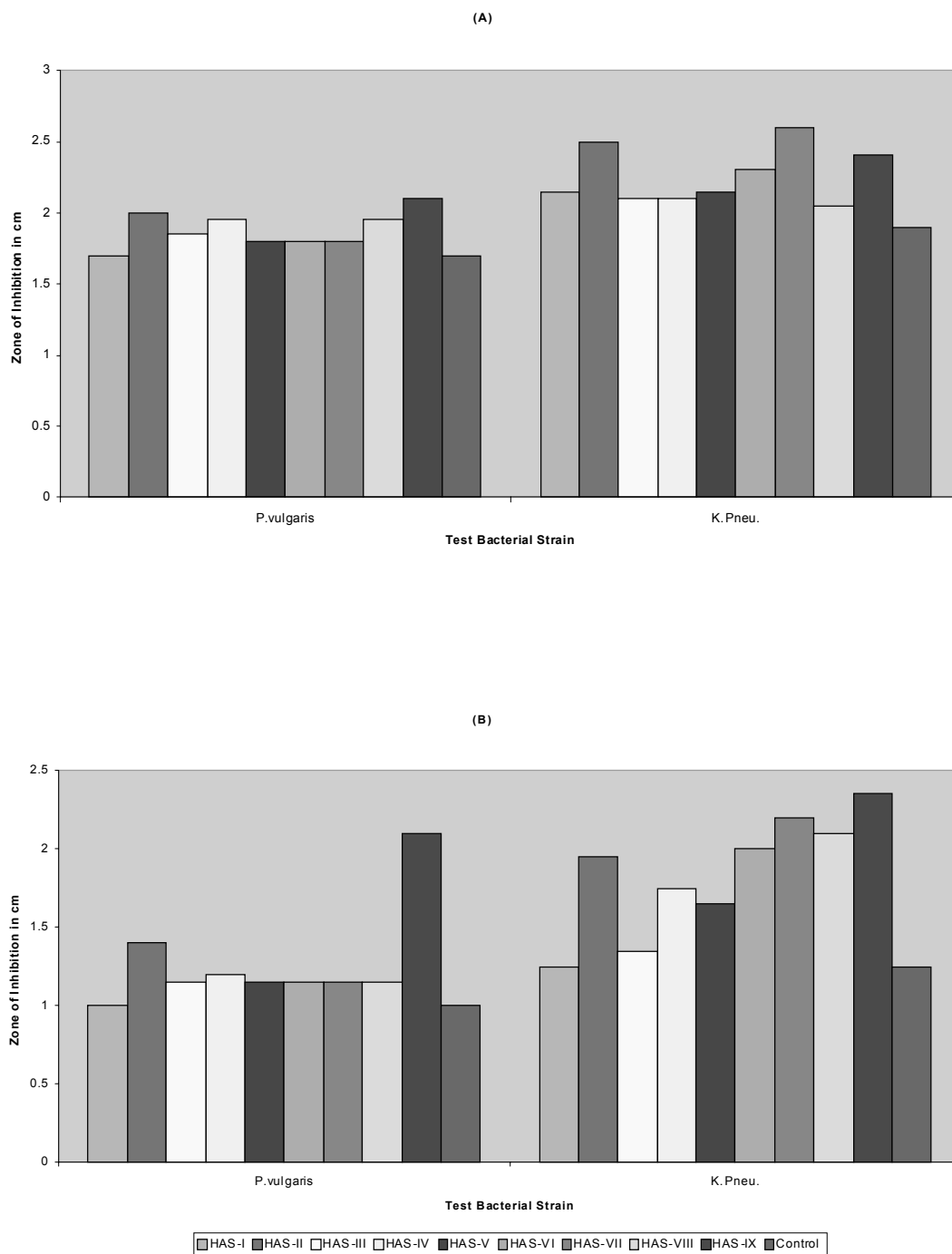


Fig. 3 : Comparative study of Schiff bases in DMF (A) and DMSO (B)

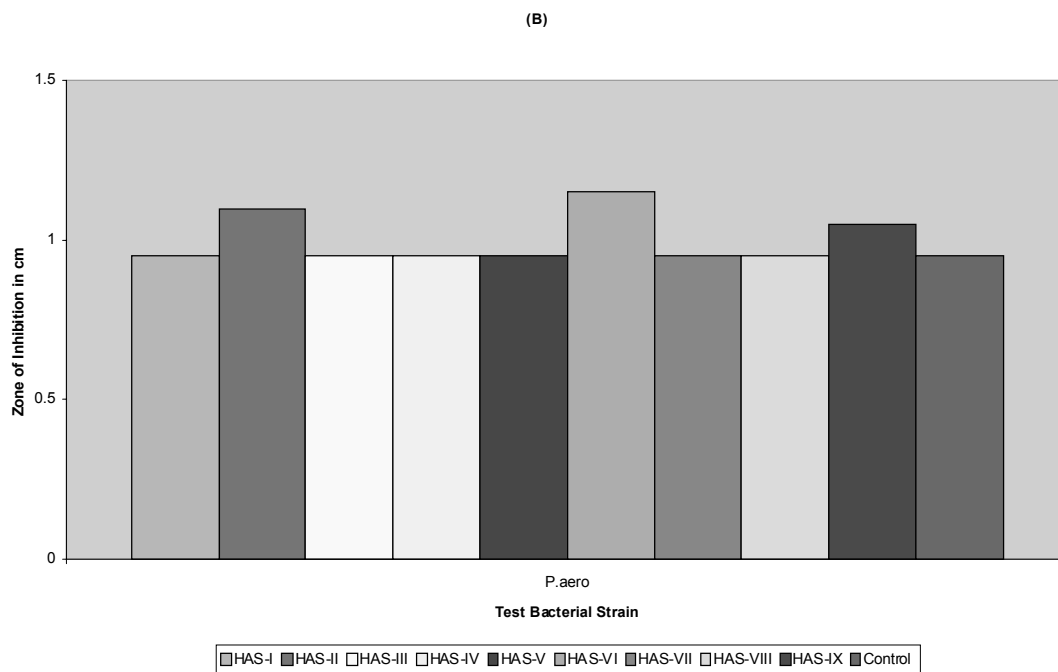
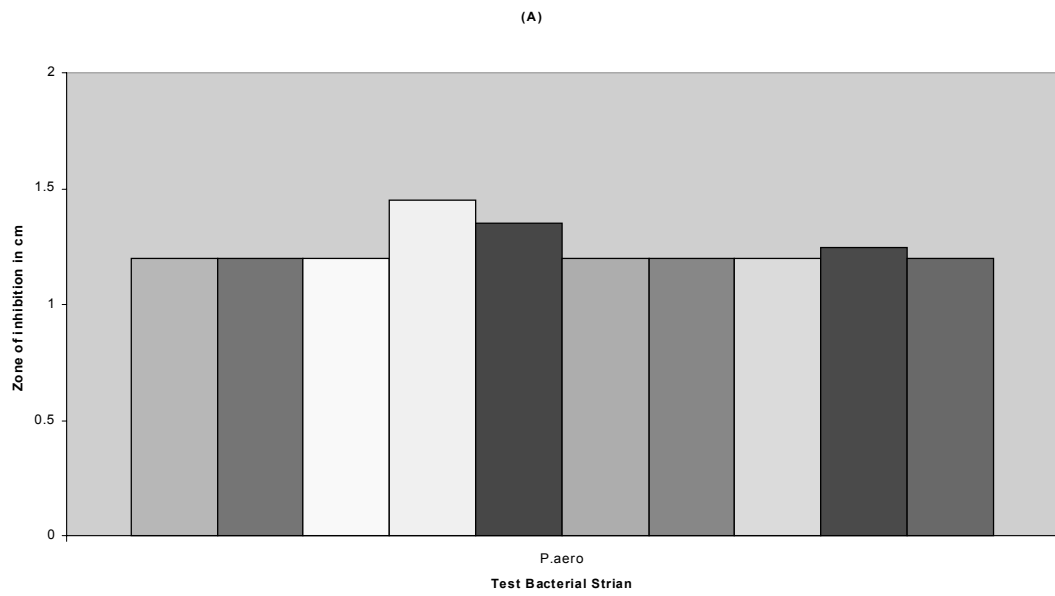


Table-1: Physical Constants and IR Spectral Data

Sr. No.	Aromatic Aldehydes	Code	M.Wt. (g)	M.F.	R _f * Value	M.P. °C	Yield %	IR (cm)
1.	9-anthraldehyde	HAS-I	337.786	C ₂₁ H ₁₃ ClFN	0.66	162	55	(C=C) 1545, (C=N) 1622, (Ar-H) 3033
2.	p-hydroxy	HAS-II	249.668	C ₁₃ H ₉ ClFNO	0.51	138	81	(C=C) 1511, (O-H) 3410 (C=N) 1609, (Ar-H) 3011
3.	m-nitro	HAS-III	278.666	C ₁₂ H ₈ ClFN ₂ O ₂	0.59	114	79	(C=C) 1521, (C=N) 1617, (Ar-H) 3026
4.	p-Fluoro	HAS-IV	251.659	C ₁₃ H ₈ ClF ₂ N	0.39	51	66	(C=C) 1498, (C=N) 1598, (Ar-H) 3023
5.	p-Methoxy	HAS-V	263.694	C ₁₄ H ₁₁ ClFNO	0.43	89	78	(C=C) 1567, (C=N) 1604, ((Ar-H) 3019, (OCH ₃) 2839
6.	N,N-Dimethyl	HAS-VI	276.736	C ₁₅ H ₁₄ ClFN ₂	0.61	110	73	(C=C) 1533, (C=N) 1609, (Ar-H) 3039
7.	Salicylaldehyde	HAS-VII	249.668	C ₁₃ H ₉ ClFNO	0.68	123	85	(C=C) 1516, (C=N) 1633, (Ar-H) 3010, (-OH) 3454
8.	p-Chloro	HAS-VIII	268.113	C ₁₂ H ₈ Cl ₂ FN	0.73	102	71	(C=C) 1571, (C=N) 1613, (Ar-H) 3016, (OCH ₃) 2882
9.	Vanilline	HAS-IX	279.694	C ₁₄ H ₁₁ ClFNO ₂	0.56	65	66	(C=C) 1511, (C=N) 1624, (Ar-H) 3026

* Benzene:Acetone 8:2 for 1 to 5 and E.A. : Hexene- 6:4 for 6 to 9

EXTRACTION AND CHARACTERIZATION OF OIL FROM SPENT BLEACHING EARTH

Sibban Singh

Department of Ind. Chem. (Oils, Fats & Waxes)
Institute of Science and Technology for Advanced Studies and Research
Vallabh Vidyanagar-388 120

Abstract

The environment friendly disposal of spent earth has many problems like hazards due to chemical and self ignition property. Apart from this it also contains significant amount of valuable fatty oils which get lost while disposing the spent earth for land filling. In the present experimental study the extraction of this entrained oil from the earth before its disposal has been worked out. Furthermore, the recovered oil was characterized and found to be a suitable feed stock for soap making and other oleochemical preparation.

Key words : Spent earth, fatty oil, hexane, oxidative deterioration.

Introduction

The bleaching of fatty oil is conducted by commonly employed adsorbents i.e. activated earth and carbon. These used adsorbents often called as 'Spent Earth' is obtained as a by-product from oil refinery. It represents a substantial amount of solid waste material [1]. Both activated earth and carbon have a high adsorption capacity. During the bleaching operation, they adsorb not only the undesirable matter but also a certain amount of oil. This property is known as 'Oil Retention', which is 20-40% of the spent earth used and depends on the filtration technique employed. Besides oil, spent earth is normally loaded with water, biological degradation products, and leachable heavy metals.

The normal mode of disposal of spent earth these days is to dump it in a land fill. In the discharge area, which remains absolutely dirty and hazardous due to self ignition quality, one has to pour water to extinguish and that makes it dirtier. Also the waste should be disposed off about 5-10 km away from the factory. It is hoped that the recovery method presented here will help to keep the discharge area clean. Also, a substantial amount of oil can be recovered from the spent earth. Various experimental methods are reported about the quantity and quality of associated oil (Biller et al. [2] and Paul Mailer [3]) and also safety aspect and hazardous property of the spent earth (Guenther and Meschede [4] and Pala et al. [5]). However, the techno-economical feasibility of extraction

Extraction and Characterization of...

process for safe disposal of spent earth still remains a problem. Therefore, in the present work the principal aim was to recover the oil from the earth by optimizing the process conditions and also see the possible application area of the extracted oil.

Materials and Methods

Analysis : The spent bleaching earth was obtained from local industry. All other chemicals used for analysis and extraction were of LR grade. The spent bleaching earth was analyzed for its oil content by extracting a five gram sample with petroleum ether (b.p. 60^o C to 80^o C) for three hr. in a Soxhlet apparatus by AOCS method (AOCS [6]). The extracted oil was further used to determine its physico-chemical characteristics such as Free fatty acid[7], Saponification value[8], Iodine value[9] and Peroxide value[10].

Extraction of Oil from Spent Earth by Klein's Method: The spent earth sample and solvent hexane in the required proportion were charged into three-neck flask, fitted with water condenser. The mixture was continuously agitated at set temperature and time interval. After completion of extraction process, the mixture was filtered at reduced pressure. Finally the oil was recovered from the filtrate by distillation of hexane.

The extraction of oil from the earth was carried out for one to three hour period at 40^o C and 60^o C temperature by varying the proportion of earth and solvent from 1:1 to 1:3 (w/v).

Results and Discussion

Analysis of Experimental Spent Bleaching Earth : The earth was analyzed for the oil content and the physico-chemical characteristics of the extracted oil are depicted in Table 1. It is clear from the table that the spent earth contains 34.2% oil. The free fatty acid and peroxide value of oil as represented in the table were 3.1 % and 51.2 respectively. It shows the higher degree of hydrolytic and oxidative deterioration of the oil.

Extraction of Oil from Spent Bleaching Earth : The percentage extraction of oil from spent earth at 40^o C and 60^o C for 1 hr. to 3 hr. by varying the earth and solvent ratio have been shown in the Table 2 to Table 4. It is apparent from these tables that the higher temperature and longer period of extraction provides higher yield. Apart from this the effect of tripling the quantity of solvent increases the oil recovery from 73.1 to 98.0 % at 60^o C. But the cost of separation of hexane by distillation restricts the use of higher amount

Sibban Singh

of solvent. However, the effect of extraction on further deterioration of oil quality is negligible as little changes are observed in free fatty acid and peroxide value.

Thus, the extracted oil though was inferior quality from the human consumption point of view, would be very well useful in soap making and other oleochemical preparation so, it can reduce the gap of demand and supply of oil in this competing world since, a drop of oil saved is a drop of oil produced.

Table 1 : Analysis of Experimental Spent Bleaching Earth

Characteristics	Value
Oil content	34.2%
Free fatty acid ^a	3.1%
Saponification value	185.4
Iodine value	82.4
Peroxide value	51.2

a – calculated as half of acid value of the oil

**Table 2: Extraction of Oil from Spent Earth
Earth : Solvent = 50 : 50 (w/v)**

Temperature (°C)	Time (hrs)	Recovery of Oil (%)	Free fatty acid^a	Peroxide value
40	1.0	64.1	3.1	51.7
	2.0	66.9	3.1	51.8
	3.0	68.1	3.2	52.3
60	1.0	65.7	3.1	52.8
	2.0	72.2	3.2	53.3
	3.0	73.3	3.2	53.8

a – calculated as half of acid value of the oil

Extraction and Characterization of...

Table 3: Extraction of Oil from Spent Earth
Earth : Solvent = 50 : 100 (w/v)

Temperature (°C)	Time (hrs)	Recovery of Oil (%)	Free fatty acid ^a	Peroxide value
40	1.0	64.9	3.1	54.4
	2.0	68.4	3.2	55.2
	3.0	71.0	3.2	55.7
60	1.0	73.4	3.1	56.2
	2.0	76.2	3.2	56.7
	3.0	82.7	3.2	57.2

a – calculated as half of acid value of the oil

Table 4: Extraction of Oil from Spent Earth
Earth : Solvent = 50 : 150 (w/v)

Temperature (°C)	Time (hrs)	Recovery of Oil (%)	Free fatty acid ^a	Peroxide value
40	1.0	67.5	3.2	57.7
	2.0	72.8	3.2	58.2
	3.0	79.5	3.3	59.7
60	1.0	87.6	3.3	60.2
	2.0	94.5	3.2	60.7
	3.0	98.0	3.3	61.2

a – calculated as half of acid value of the oil

Sibban Singh

References

1. Treaty on fats, fatty acids and oleochemicals, Narula O.P. (Ed) Part 2, P.T.4
2. Biller G. and Guhr G., 'Journal of American Oil Chemists' Society' 55:728(1978)
3. Paul Mailer, 'Chemical Abstract' R192170r(1997)
4. Guenther K. and Mesch T., ' Chemical Abstract' R19760k(1992)
5. Pala O.K. and Nwoke N.N., 'Chemical Abstract' 196833x(1989)
6. Official and tentative method of AOCS, Champaign, IL, USA(1976)
7. Indian standard methods of sampling and test for oils and fats, part-I (Third revision), IS: 548, p-29(1964)
8. Indian standard methods of sampling and test for oils and fats, part-I (Third revision), IS: 548, p-50(1964)
9. Indian standard methods of sampling and test for oils and fats, part-I (Third revision), IS: 548, p-47 (1964)
10. Indian standard methods of sampling and test for oils and fats, part-I (Third revision), IS: 548, p-63(1964)
11. Ohta H., Ida S., Milkani B. and Morti Y., *Agrie, Boil, Chem.* 50 : 31165 (1936)

KNOWLEDGE-BASED DECISION SUPPORT SYSTEM FOR DIAGNOSIS OF ABDOMEN PAIN

Dipti Shah and Priti Srinivas Sajja

G H Patel Post Graduate Department of Computer Science and Technology,
Sardar Patel University, Vallabh Vidyanagar

Abstract

Decision support through Information Technology is an integral part of our lives. It is being increasingly used for decision-making in the medical science also. This article introduces the information explosion in medical field justifying need of a knowledge-oriented decision support for diagnosis of abdomen pain. Main objective of the system is to assist doctors, assistants and social workers in their decision making process for the various kinds of the abdomen diseases and create awareness in the area. To impart the fuzziness of the domain, modified Prolog rule format is used, which is illustrated in a case of appendicitis. Such knowledge-based system can be used for the rural locality/remote place; especially where expertise is not available on demand. The system can be utilised to identify the information on the cause, diagnosis, symptoms, complications, prevention and treatment. The system also offers advantages of self-learning and explanation to improve overall quality of decision-making.

Introduction

There is an increasing appreciation of the role that computers and informatics can play in improving the overall health delivery systems. Medicine requires far more critical decision-making on a wide range of options. It also requires a large amount of humanism [2]. Medical informatics has high visibility through applications in areas such as diagnostic techniques in ultrasonography, x-ray, computerised tomography scanning, nuclear magnetic resonance imaging etc. The other areas can be clinical laboratories, pathological investigations and computer-assisted decision-making. In medical practice, data acquisition as well as subsequent storage, retrieval and manipulation of the data are enhanced by efficient computerisation through database in static fashion. Such decision-making through computers can improve accuracy and increases cost efficiency [5]. However, the decision support should be knowledge-oriented to improve effectiveness of the decisions made. Knowledge-oriented decision-making by its nature helps in identifying most plausible diagnosis and provides ease of choosing an appropriate treatment. Large amount of existing medical knowledge and rapid growth of the knowledge have resulted in a situation where even specialists find it increasingly difficult to assimilate and use the information that would be useful in making effective decisions. This leads the decision making a tedious and time-consuming process. Moreover, in India most of the population is living in rural areas.

Doctors and specialists are scarce resources in rural locality. Due to scarcity of experts and information explosion in the field of medicine, it is felt that knowledge-oriented decision-making systems are appreciated. The main objective of the system is to assist doctors, assistants and social workers in decision-making process for the various kinds of the abdomen diseases. Information on the cause, diagnosis, symptoms, complications, prevention and treatment needs to be identified, documented and inferred by the system for benefits of the rural locality; especially where expertise is not available on demand. This type of system will be an efficient means to store and to pass experts knowledge in documental form for long time and it can provide primary advice to the health workers and patients in initial stage. Hence, an advisory system that applies the knowledge in diagnosis and determines patient's condition is the prime necessity in the medical field. This article proposes a general framework of knowledge-oriented decision support system for advisory, diagnosis and awareness for the field. As an illustration, few sample fuzzy rules are formed with the help of domain experts for appendicitis case.

Knowledge-oriented Decision-making

A Knowledge-Based System (KBS) has interdisciplinary approach of various disciplines like computer science, cognitive science, hardware field etc. The society and industry are becoming knowledge-oriented and rely on different experts' decision-making abilities depending on the information available. When expertise is unavailable, a KBS can act as an expert on demand to save time. KBS can save money by leveraging expert, allowing users to function at higher level and promoting consistency[4]. One may consider the KBS as a productive tool, having knowledge of more than one expert for long period of time. Large percentage of the population in India lives in rural and remote areas, where medical facilities are unavailable. Hence, there is a need of a system that supports decisions and increases awareness in the area. Such system can potentially alleviate the immense diagnostic workload of rural health workers and medical practitioners. Also, it can assist in prevention of various diseases. In addition, by using such systems, user will get the advantage of the knowledge of more than one specialist. Such KBS uses Artificial Intelligence techniques for efficient and effective decision making in unstructured domain and apply reasoning and explanation facility for the domain problem to achieve high level of performance.

The large amount of existing medical knowledge and the rapid growth of that knowledge during the last quarter of the 20th century, resulted in a situation where most clinicians find it increasingly difficult to assimilate the field information, which could be useful in making optimal clinical judgment. The system can provide a solution to much of the problem created

A Knowledge-Based Decision Support...

by such information explosion. Decision making by the clinician in the management of patient's data is a highly intellectual activity, which involves: (i) skill in gathering and evaluating the information about the patient; and (ii) ability to effectively utilise the large body of medical knowledge. The system can facilitate to improve the clinician's performance of each of this task.

Structure of the System

The model of the discussed system is given in Figure 1 representing the overall process structure of KBS for medical diagnosis. The basic components of the system are the knowledge base, inference engine, and a workspace. The knowledge base of the system plays a key role in the procedure of decision-making[6] by efficiently storing the domain knowledge and patients history. Temporary results can be stored in workspace. The inference engine is a program, which infers the knowledge available in the knowledge base[7].

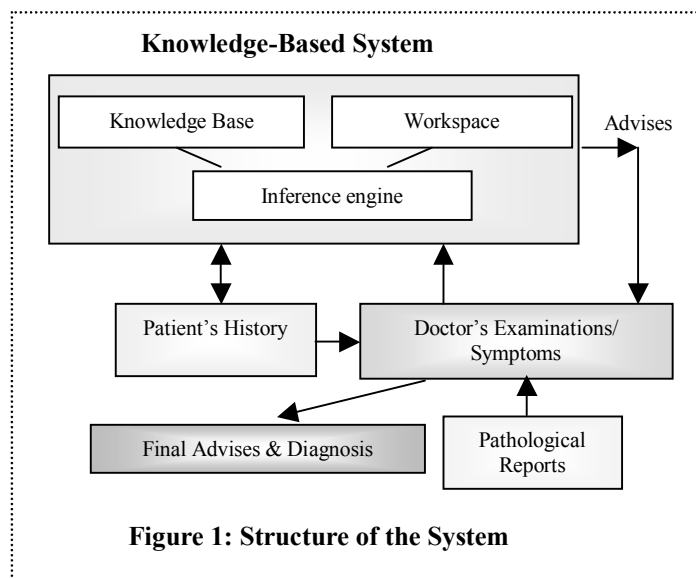


Figure 1: Structure of the System

The knowledge base of the proposed system first receives the preliminary information from the patient through self-administrated questionnaires and retrieves the patient's history, if any, stored in the knowledge base. After evaluating the inputs, the program presents a new questionnaire to the patient. Using the information, the system suggests actions/advisory for further tests and/or conclusion about the patient's disease. An expert may have a manual

control/justification of the given suggestions and alternatives depending on degree of uncertainty associated with the patient's response and overall decision-making process.

The knowledge of the expert in the decision-making can be represented in various forms. The knowledge of expert can be easily represented into rule-based format as a set of conditional rules[1]. Rules may be chained according to the knowledge it represents. Considering the uncertainty of the diagnosing process, the fuzzy rules are used here. To accommodate such fuzziness, the typical Prolog rule format is modified. Each rule has a basic form

IF antecedents THEN consequent

If certain antecedents are evaluated as True, then it logically follows the consequent. As denoted above, the modified Prolog rule format is

Hypothesis (Name, Disease, Probability):-
Symptom (Name, Indication, Probability),
Symptom (Name, Indication, Probability),
...
...
Symptom (Name, Indication, Probability).Eq. (1)

Here Hypothesis and Symptoms are the user defined predicates in Prolog [8]. These predicates use symbols (variables) like Name (user name), Disease (disease name) and Probability (chances in percentage). Probability factors given along with the rules for the concerned advises are considered as the degree of the uncertainty related with the decision taken. These values are determined by taking samples from experts. The hypothesis proved true if patient's data has all the indications given in symptom lists. Systems knowledge base consists of such multiple fuzzy rules representing the domain knowledge in form of Prolog code.

An Illustrative Case of an Appendicitis Problem

An intelligent advisory system for abdomen pain can also take care for the appendicitis problem including various other abdomen diseases. Interactive sample rules are proposed here, that can directly assist doctors or other health workers in finding the probability of having particular disease like appendicitis. Appendicitis usually commences as in inflammation of the mucous membrane or lymph follicles, which may terminate in one of the following ways [3]:

A Knowledge-Based Decision Support...

- ☞ Resolution
- ☞ Gangrene
- ☞ Ulceration
- ☞ Fibrosis
- ☞ Suppuration

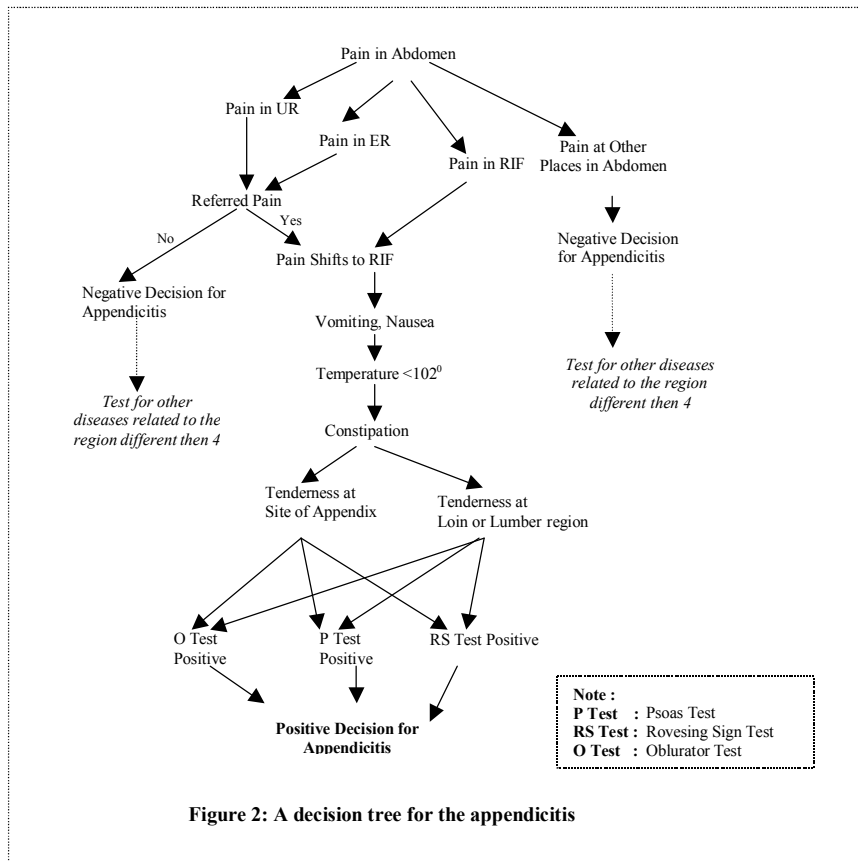
The system prepares the history of patient by asking several questions in the language understood by layman and predicts the probability of having a disease and presents advice for further treatment.

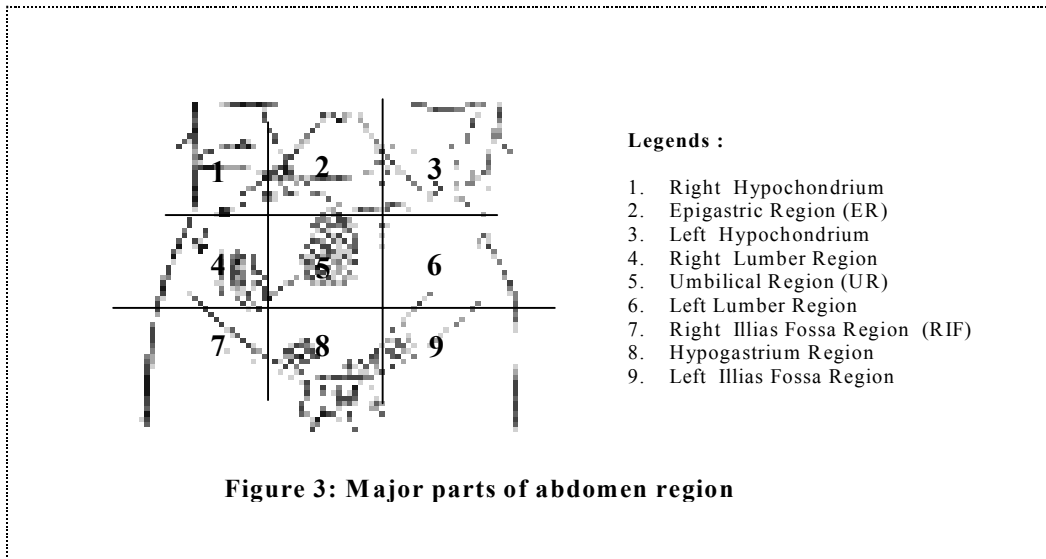
Sample Rules for the Above Case

	Rules		Rules
R1	hypothesis(Patient, appendicitis, 0.1) :- symptom(Patient,pain_ur, 0.4), symptom(Patient, pain_shift_rif, 0.1), symptom(Patient, o_test_result, 0.2).	R7	hypothesis(Patient, appendicitis, 1.0) :- symptom(Patient,pain_rif, 1.0), symptom(Patient, o_test_result, 1.0).
R2	hypothesis(Patient,rs_test, 1.0) :- symptom(Patient,pain_rif, 1.0), symptom(Patient, vomit, 0.8), symptom(Patient, less_temp, 1.0), symptom(Patient, tenderness_site, 0.8).	R8	hypothesis(Patient,p_test, 1.0) :- symptom(Patient,pain_ur, 0.7), symptom(Patient, pain_shift_rif, 0.6), symptom(Patient, vomit, 0.8), symptom(Patient, less_temp, 0.8), symptom(Patient, tenderness_site, 0.6).
R3	hypothesis(Patient, appendicitis, 0.6) :- symptom(Patient,pain_ur, 0.7), symptom(Patient, o_test_result, 1.0).	R9	hypothesis(Patient, appendicitis, 1.0) :- symptom(Patient,pain_rif, 1.0), symptom(Patient, rs_test_result, 1.0).
R4	hypothesis(Patient,o_test, 1.0) :- symptom(Patient,pain_rif, 1.0), symptom(Patient, vomit, 0.8), symptom(Patient, less_temp, 1.0), symptom(Patient, tenderness_site, 0.8).	R10	hypothesis(Patient,p_test, 1.0) :- symptom(Patient,pain_rif, 1.0), symptom(Patient, vomit, 0.8), symptom(Patient, less_temp, 1.0), symptom(Patient, tenderness_site, 0.8).
R5	hypothesis(Patient, appendicitis, 0.4) :- symptom(Patient,pain_ur, 0.7), symptom(Patient, o_test_result, 0.3).	R11	hypothesis(Patient, appendicitis, 1.0) :- symptom(Patient,pain_rif, 1.0), symptom(Patient, p_test_result, 1.0).
R6	hypothesis(Patient,p_test, 0.8) :- symptom(Patient,pain_ur, 0.7), symptom(Patient, pain_shift_rif, 0.6), symptom(Patient, vomit, 0.6), symptom(Patient, less_temp, 0.8), symptom(Patient, tenderness_site, 0.5).	R12	hypothesis(Patient, appendicitis, 0.1) :- symptom(Patient,pain_ur, 0.2), symptom(Patient,pain_er, 0.2), symptom(Patient, pain_rif, 0.1), symptom(Patient, vomit, 0.8), symptom(Patient, less_temp, 0.8), symptom(Patient, o_test_result, 0.2).

As stated above, the knowledge collected from the field expert is codified in the Prolog language to form a rule base for the application. These rules are sequentially executed to come to a conclusion/diagnosis. Above table presents some of the sample rules in the modified Prolog format. If the mentioned symptoms match, the hypothesis of having the appendicitis is true to some extent. For example, according to rule 6 (R6) 'If patient has pain in Umbilical Region and the pain shifts to Right Illias Fossa Region along with vomiting and tenderness symptoms at the site of appendicitis' (Region 4, in Figure 3), then Psoas Test is recommended with 80% probability. When rule 6 (R6) is true, the system will check all rules sequentially and fires rule 11 (R11) concerning the Psoas Test result in the symptom and conclude the probability of appendicitis.

Such multiple rules can be developed from a decision tree by maintaining the decision sequence. This is illustrated in Figure 2 in the form of decision tree that has critical information with proper directions for the discussed case. For structured decision-making, the whole abdomen region is divided into nine major parts as shown in Figure 3. For each of these 9 parts a separate tree can be prepared.





Acknowledgement

The authors are thankful to Dr. Balmukund Shah, Surgeon, "Krishna Hospital", Borsad for providing the domain knowledge regarding the abdomen diseases along with their concern tests and all the necessary support for automation of the decision making process for the system.

Conclusion

In this paper, a scenario of using knowledge-oriented decision-support system in medical science is presented. A model for a overall process structure with KBS for medical diagnosis is given for smooth medical decision making followed by a decision tree covering major decision points in the discussed case of appendicitis. Sample rules are implemented in Prolog. In the similar manner, such system can be enhanced further for all possible cases in abdomen pain. This type of system can be proved an efficient means to store and pass experts knowledge in documental form for long time.

References

1. Lee Brownston, Robert Farrell, Elaine Kant, Nancy Martin "Programming Expert Systems in OPS5, An Introduction to Rule Based programming", Addison Wesley Pub. USA (1986)
2. Lele RD "Computer in Medicine", Tata McGraw Hill Publishing Company Ltd., New Delhi (1988)

Dipti Shah and Priti Srinivas Sajja

3. Patel TN "A System of Surgical Diagnosis", BI Publications Ltd, Bombay (1985)
4. Paul Harmon, Rex Maus, William "Expert Systems Tools & Applications", John, Wiley & Sons, Newyork (1988)
5. Shah D.M. and Patel S.M. "IT in Healthcare", Proceeding of The National Seminar on Computer Applications, Department of Computer Science, Sardar Patel University, India, (2001)
6. Turban Efrain "Decision Support and Expert Systems", Mac. Publication Company (1993)
7. Waterman Donald A "A Guide to Expert Systems", IEEE Press, Newyork (1988)
8. W F Clockin, C S Melish, "Programming in Prolog", B P B Publications, (2002)

A WEB BASED FUZZY EXPERT SYSTEM FOR INSECT PEST MANAGEMENT IN GROUNDNUT CROP

P.V. Virparia

Department of Computer Science and Technology
Sardar Patel University
Vallabh Vidyanagar

Abstract

Information Technology has been found the most dynamic technology, having the greatest impact on national development. Due to the effect of uncertainties and dynamic interaction between decisions and events in agricultural systems, it is very difficult to handle some of the problems. Fuzzy theory can help to solve this type of situations. Consultation of Internet for data, information and knowledge has become a popular activity. Expert systems, which provide consultation and suggest diagnosis, can prove to be more useful if they are made available on the World Wide Web (WWW). Web based fuzzy expert system is an expert system that uses fuzzy logic instead of Boolean logic on WWW. In this paper, I have try to develop a prototype web based fuzzy expert system for controlling the Groundnut insect pests, which can perform the identification of various externally observable symptoms, identify the actual insect pest and recommends the appropriate control measures.

Keywords : World Wide Web, Expert System, Fuzzy Logic, Knowledge Base.

Introduction

Information Technology (IT), being a well-proven development tool, can be very useful for proper development of rural areas and can provide real-time solutions to the problems that consume a lot of time and human labour. In India, 74% of the population is engaged in agricultural activities and contributes just 32% of the national income[2]. As a result, there is an increasing challenge of what, when and how new technologies are to be utilized. The accepted aim of development planning is to maximize the rate of growth of per capita income. And a predominantly agricultural country like India cannot hope for a healthy economic growth unless sustained and substantial growth is ensured in the agricultural sector. The domain of agriculture is large and complex. It encompasses on many fields like land management, water management, soil conservation, seed production, plant protection etc. Also, these fields are very interconnected which becomes a constraint in identifying the critical problems and selecting a strategy to improve the crop growth and finally yield. It is also difficult to get human experts/decision makers who have thorough understanding of all these fields, to give effective solutions.

P.V. Virparia

Expert System

'Expert System' is one of the important application-oriented branch of Artificial Intelligence. The Expert Systems approach attempts to model the domain knowledge of experts in their respective areas of specialization, for example, diagnosis, planning, forecasting etc. Expert System is based on the knowledge including not only models and data, but more emphasizing on experiences of domain experts. An expert system is a computer application that solves complicated problems that would otherwise require extensive human expertise. It can be operated by a less educated person or a layman in a particular field of knowledge. It simulates the human reasoning process by applying specific knowledge and interfaces. Expert systems also use human knowledge to solve problems that normally would require human intelligence. These expert systems represent the expertise knowledge as data or rules within the computer, which can be called upon when needed to solve problems.

Fuzzy Expert System

Fuzzy sets are used to describe uncertainty, imprecision, and vagueness in a non-probabilistic framework. This goal is largely accomplished through extending traditional, binary set theory to a transitional set theory where the degree to which an element belongs to a set is defined by the level of membership. Fuzzy logic attempts to capture imprecise relations, and then use these relations to make inferences about system behavior with if/then rules. Use of fuzzy logic, which helps in knowledge based computing in the situations where knowledge is imperfect, has been extended to calculate more useful results in expert system. Fuzzy logic lets expert systems perform optimally with uncertain or ambiguous data and knowledge. With a fuzzy logic framework, one can efficiently implement linguistically expressed rules derived from experts.

A fuzzy logic system (as shown in figure-1) consists of following three steps:

1. Fuzzification : Real variables are transformed to linguistic variables with several terms, each with a membership function with a range of $[0,1]$. For example, the real variable milk yield is transformed to a linguistic variable milk yield with the terms "low," "moderate," and "high." For a particular cow, the real yield value of 25 litre may be transformed to membership 0.0 of "low", membership 0.5 of "moderate", and membership 0.9 of "high", indicating that the yield is certainly not low, rather high and also somewhat moderate.
2. Fuzzy Inference : The terms of the linguistic variables are applied in IF/THEN rules, where combinations of conditions lead to conclusions. For example: "IF yield is low AND milk temperature is high THEN health status

A Web Based Fuzzy Expert...

is bad." Given these conditions, the health status is considered bad. Rules are grouped in rule boxes.

3. Defuzzification : The conclusions of the rules relate to terms of linguistic variables that have to be transformed back to real variables, e.g., a cow is healthy or not.

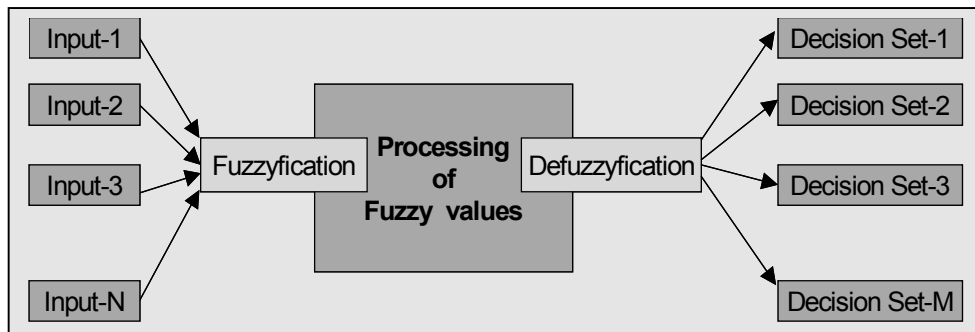


Figure-1 : Steps of Fuzzy Logic System

First phase in this system use fuzzy rules of inference and a good level of accuracy is achieved in results of identification. In an Integrated Pest Management system, IF (S) THEN P with CF rules have been used for inferences, where S is crop damage symptoms, P is active pest and CF is confidence factor associates with the rule.

Fuzzy logic has the ability to perform approximate reasoning knowledge which is inexact and incomplete can be used to draw inferences. Fuzzy logic has been incorporated in the system rules of inference to calculate the fuzzy confidence values representing activity of insect-pests and to control uncertainty. A fuzzy confidence value is a number or interval or a set of values in the range of 0 to 1. Fuzzy logic due to its power of expression, leads to system which help in computing with linguistic variables i.e. variables which can take words or sentences of natural languages as their values.

Fuzzy logic is ideal for approximate reasoning through the use of linguistic variables. The damage rates are classified into three categories in the form of linguistic options like 'low damage', 'medium damage' and 'high damage'. Similarly, related pest identification confidence values are 'may be active', 'active', and 'highly active'.

Fuzzyness is related to the use of predicates like 'pest is active' proposition. The idea is that it belongs to a set 'ACTIVE' admits a degree that is not necessarily just 0 or 1, as it is in the case with the classical set theory. For elements in the universe of discourse considered by us, we cannot definitely say that it belongs or does not belong to the set. At the most, we can assess some degree of membership $\mu(x)$ of the element x to the fuzzy set like

P.V. Virparia

A=ACTIVE. This function generalizes the classical indicator to a membership function $\mu(x)$ of a set :

$$\mu(x) = 1 \text{ if } x \text{ belongs to } A$$

$$\mu(x) = 0 \text{ if } x \text{ does not belongs to } A$$

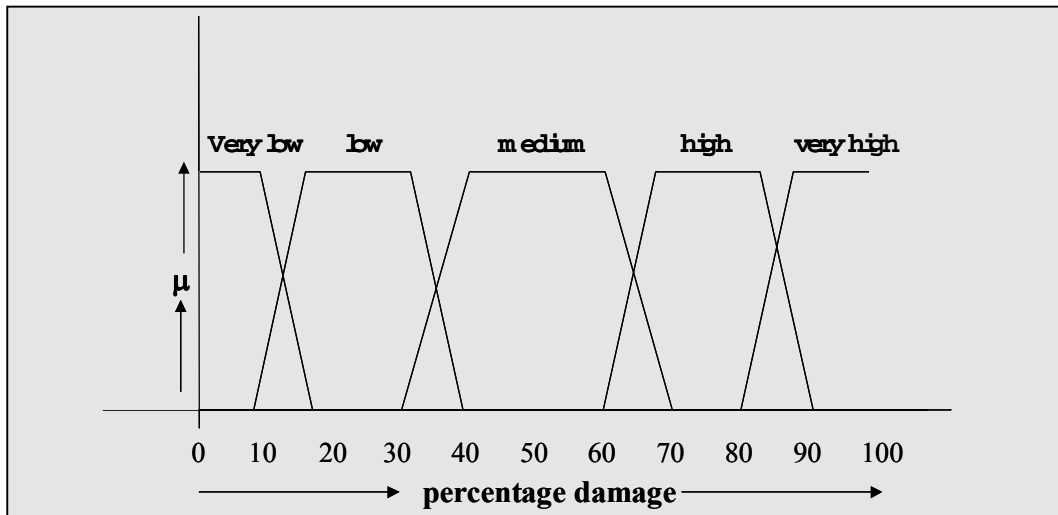


Figure-2 : The application to map the damage levels

The user selects one out of the granules 'very low', 'low', 'medium', 'high' and 'very high'. The figure-2 covers damage level range from 0% to 100%, which also matches to the commonsense and perception of the user. These values of the level of percentage damage perception are internally converted into the rule membership values (0.0 to 1.0).

A fuzzy expert system is an expert system that uses fuzzy logic instead of Boolean logic. In other words, a fuzzy expert system is a collection of membership functions and rules that are used to reason about data. Unlike conventional expert systems, which are mainly symbolic reasoning engines, fuzzy expert systems are oriented toward numerical processing.

Web Based Fuzzy Expert System

Internet is being used by researchers in data collection, analysis and as a tool for publishing. Electronic survey have proved to be cost effective and a convenient method of collecting data for extension and agricultural specialists. WWW provides a cost-effective medium to exchange research-based information. WWW technologies have rapidly transformed the

A Web Based Fuzzy Expert...

entire design, development and implementation process for all types of systems including expert systems. The legacy expert systems developed for standalone PC's can also be of better use if they are made accessible through the web.

Web based information systems are freely accessible by the users, professional consultants or extension workers. Web based expert systems are most appropriate in the situations where large number of users are spread over geographically far off places or different agro-climatic regions in case of agriculture applications.

Web based system has been developed to fulfill the objectives like :

- Making availability of decision support and expert system consultation independent of distance; global and free availability of expert knowledge,
- Quicker response to queries, increased interaction and better availability & utility of national expert talent for the problems,
- Generating feedback for improvement extendibility and enrichment through global suggestions,
- Benefit the common man (farmer in this case) through use of Internet based expert system consultation.

The Problem

Agriculture has been the most prominent industry in India and lot of research is currently being carried out in this field to increase its overall efficiency. On the various factors responsible for limiting the crop yield, insect pests are one of them. An annual loss due to insect pests problem is estimated to be around Rs. 1,5000 million. In India, about 115 insect pest species cause damage, of which only 9 species like leafminer, white grub, jassid, thrips, aphid, tobacco caterpillar, gram caterpillar, red hairy caterpillar and termites, are found to be more harmful, in the Groundnut crop[2]. The first principle underlying the control of an insect is its correct identification. When it is correctly identified, we can refer to the available information on the biology and habits of that insect and determine its most vulnerable stage, the appropriate time and the most suitable method(s) to control it. Control measures for a particular problem depend on a variety of factors such as crop, environmental conditions, chemicals & equipment available and economic condition of the farmer.

If by effective application of modern scientific methods of insect control, we prevent or at least reduce the damage to the minimum, the yield per acre could be significantly increased. Here, I have tried to develop a Prototype web based fuzzy expert system, which can perform:

P.V. Virparia

- (a) the identification of various externally observable symptoms in the Groundnut crop, and
- (b) conclude the actual problem(s) and recommend appropriate control measures.

The system is divided into mainly two parts viz. part-[i] is used to identify the externally observable symptoms on crop as well as on insect and part-[ii] is used to identify the actual problem(s) and recommend appropriate control measure. Any user can take the help of this system to identify the insect pest by giving some preliminary information about the plant condition, crop condition, and appearance of insect and results of the microscopic observations.

A graphical user interface has been developed to display a sequence of questions, to handle the inputs which are used in fuzzy rules of inference as well as outputs leading to the display of images and the results from inferences. The process of questioning and answering could be continued until at least any one of the rules in the knowledge base gets succeeded.

Conclusion

Insect pest management is a challenging problem for scientists engaged in increasing the productivity of groundnut crops. The web technology, expert system technology, fuzzy logic etc. are very useful and valuable to the developed as well as developing countries for solving such problems. The above mentioned package serves as an assistant to a field officer, an expert to a farmer, and an excellent teaching aid to a student.

References

1. Efraim Turban : Decision Support and Expert Systems, Macmillan Publishing Company, 1990.
2. Handbook of Agriculture, Indian Council of Agricultural Research, New Delhi.
3. Singh Harvinder : Web based Fuzzy Expert Information system for Pest Management, Ph. D. Thesis, 2002.
4. Toshiro Terano, Kiyoji Asai & Michio Sugeno: Applied Fuzzy Systems, AP Professional, 1994.
5. Virparia P V & Patel S M : INPEX - An Expert system in Agriculture, Proceedings of the 32nd Annual Convention of Computer Society of India, Ahmedabad, 1997.
6. Waterman A. Donald : A guide to Expert Systems, Addition-Wesley Publishing Company, 1985.
7. www.austinlinks.com/fuzzy/expert-systems.html

FABRICATION OF ENZYME BASED GLUCOSE BIOSENSOR

**U.B. Trivedi, D. Lakshminarayana, I.L .Kothari*,
K.K. Makhija and H.N. Kapse****

Department of Electronics, *Department of Biosciences,

**Institute of Science and Technology for Advanced Studies and Research,
Sardar Patel University, Vallabh Vidyanagar

Abstract

An amperometric glucose biosensor based on the immobilization of the glucose oxidase enzyme has been fabricated. A polymer matrix of Polyethylenimine (PEI) and Polycarbomylsulphonate (PCS) hydrogel is utilized for the immobilization. The paper describes the fabrication details and the performance of the sensor. The effects of buffer solution pH and temperature on the performance of the fabricated biosensor have been studied and reported. The biosensor has been tested with the real samples of soft drinks and human blood. The results obtained during the analysis are compared with those of commercial methods and the implications are presented.

Introduction

Glucose is a major component of animal and plant carbohydrates. A quantitative determination of glucose has, therefore, become an important aspect in biochemistry, clinical chemistry and food analysis. Numerous methods like spectrophotometry, amperometry, high performance liquid chromatography (HPLC), polarimetry, capillary electrophoreses etc. have been widely reported. However, most of these methods are lengthy and/or expensive in nature. Also, these methods are not found to be very appropriate for rapid field tests. In view of the increasing concern over the quantitative determination of glucose, a need has been arising, of late, for developing rapid, portable and low cost alternate methods for the glucose analysis. Biosensors have been emerging as potential and alternate methods of food and clinical analysis. The biosensor, a device incorporating a biological molecular recognition component connected to a transducer, can output an electronic signal proportional to the concentration of the analyte (glucose in the present case) being sensed [1].

The high selectivity in biosensors due to the biological recognition systems including antibodies, enzymes, nucleic acids, receptors, and cells has been used to detect important biological molecules such as antigens, nucleic acids, amino acids, creatinine, urea and glucose [2]. Enzymes are the biological recognition molecules commonly employed in research and

U.B. Trivedi, D. Lakshminarayana, I.L. Kothari, K.K. Makhija and H.N. Kapse

development because most chemical reactions in living systems are catalyzed by enzymes. Enzymes are often immobilized on solid substrates so that they can be reused. As a consequence, immobilization strategies for enzymes are of paramount importance to preserve their biological activity. The general methods of immobilization of enzymes include adsorption, cross linking, covalent bonding, entrapment and encapsulation of enzyme in a porous membrane. Depending upon the mechanism of transduction, the biosensors can be of different types like amperometric, potentiometric, conductometric, piezoelectric etc. Recently, Baoli Wu et.al [3] reported the fabrication of a glucose biosensor with glucose oxidase (GOD) enzyme immobilized on an eggshell membrane. Dawei Pan et.al [4] reported a glucose biosensor by the electrochemical co-polymerization of GOD and o-aminophenol monomer. However, these biosensors are highly complex in nature so far as the fabrication and response are concerned.

The authors in the present communication report the fabrication of a simple, low cost and disposable type of a glucose biosensor. An amperometric glucose biosensor, based on glucose oxidase (GOD) enzyme immobilized in a polymer matrix, has been developed for the glucose determination in food products and also for clinical analysis.

Experimental

Chemicals and Reagents

The various solutions utilized in the present investigation were all prepared with analytical reagent grade chemicals and double distilled water. The glucose oxidase (EC: 1, 1:34, 50,000 Units, G-6641) enzyme was procured from Sigma, Germany. The polymers of Polyethylenimine (50% w/v aqueous solution)(PEI) and Poly (carbomylsulphonate) (PCS) hydrogel were procured from Sigma and Sens Lab, Germany respectively. A buffer solution was prepared by mixing the sodium dihydrogen orthophosphate with potassium chloride (0.1M KCl) and disodium hydrogen orthophosphate with potassium chloride (0.1M KCl) to obtain a pH of 6.8. The pastes of platinum, graphite and Ag/AgCl (used in the screen printed fabrication of the electrodes) were all from ERCON (Germany). A polyester sheet of DuPont (Germany) was used as the base material for the electrode preparation in the thick film screen printing.

Fabrication of Transducer

The fabrication of glucose biosensor involves Screen printing, Lamination and Immobilization. The graphite electrodes were fabricated using the screen printing technique on the polyester sheet. Screens (DuPont) having mesh sizes of 300 μ m were used for the electrode fabrication. The graphite paste was squeezed through the UV-exposed screen on the polyester sheet

Fabrication of Enzyme...

for obtaining the desired pattern of basal track of electrodes. After drying at an optimum temperature (353K), the screen-printed tracks on the polyester sheet were used for further process. The transducing tip was formed of platinum paste over the graphite track so as to conduct a current through it. The lamination of electrode was carried out leaving a 2-mm tip diameter opened for the purpose of immobilization of the glucose oxidase (GOD) enzyme. The Platinum working electrode was accompanied with the graphite counter and Ag/AgC

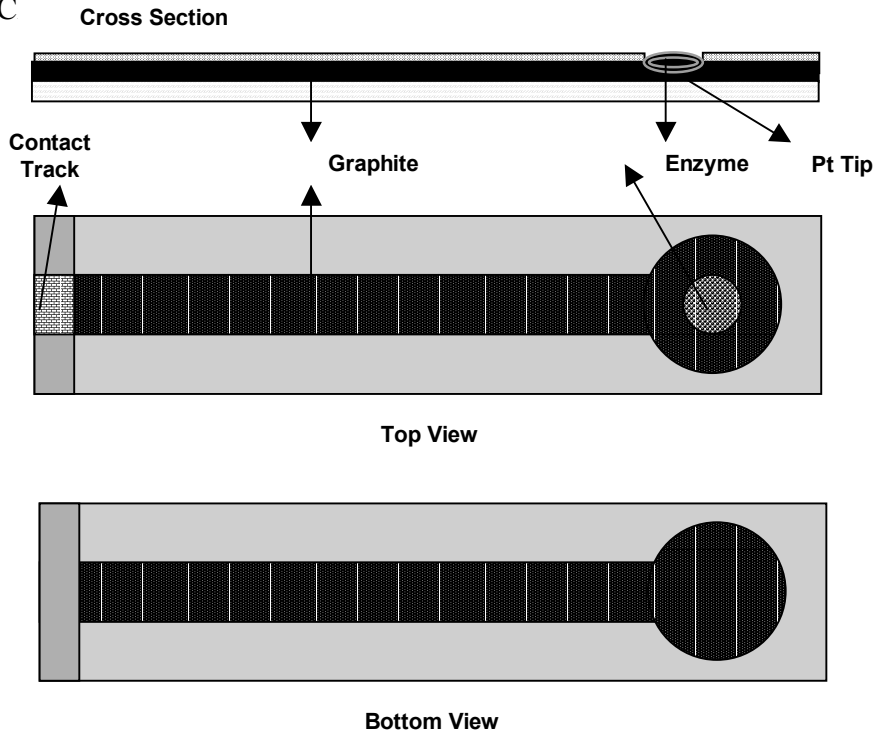


Figure 1: Schematic diagram of transducer with platinum working electrode

For enzyme immobilization, the GOD solution was prepared by dissolving 4.18mg GOD in 100 μ l buffer to make 418 μ l solutions. PCS solution was prepared by dissolving 150mg PCS hydrogel in 400 μ l water. This solution was mixed with PEI (2.5% in aqueous solution) until its pH value reached 5.4. Then, the GOD solution was added to the mixture of PEI and PCS in a proportion of 1:1. A volume of 2 μ l of the well mixed solution was applied on top of each laminated electrode. It is to be noted that a reasonably good number of about 60 transducers were prepared in a fabrication cycle. The biosensors, thus prepared, were all kept at 277K in humid atmosphere overnight and were kept ready for investigation later. The results reported in the present investigation represent the work carried out repeatedly on a number of transducers. The schematic diagram of a typical transducer used is shown in Figure1.

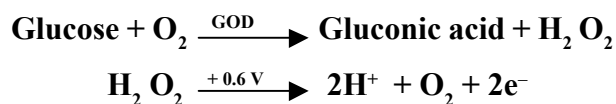
Measurements

A four channel potentiostat (ICB, Munster, Germany) was used in electrode configuration for amperometric measurements. The fabricated enzyme based biosensor was used as the working electrode with Ag/AgCl as a reference electrode. At the working electrode, a potential of +600mV with reference to the Ag/AgCl reference electrode was applied for the glucose analyte determination. Before starting the first measurement with the fabricated biosensor, a pre conditioning step was carried out by applying a potential of +1.2V at the working electrode (against Ag/AgCl).

Test Sample and Sensor Operation

The sensor was investigated in a phosphate buffer (pH 6.8) of 20ml solution in a measuring cell. 1M glucose stock solution of 10ml was added to the buffer. The solution was then continuously stirred for about 10 to 12 minutes to get the stable base line. Then, solutions of known glucose concentrations were carefully added to the above buffer to study the glucose testing ability of the sensor.

The glucose, in the presence of GOD, produces gluconic acid and hydrogen peroxide (H_2O_2). By applying a potential of +600mV to platinum electrode (against Ag/AgCl electrode) electrochemical oxidation of H_2O_2 takes place. The electrochemical reactions are as follows:



The electron current thus generated is an indicative of the glucose concentration. A calibration curve can then be obtained and used for detecting the unknown glucose concentrations.

Results and Discussion

The effect of the working potential on the amperometric response of the enzyme electrode was examined in the potential range of 0.5 – 0.9 V against Ag/AgCl reference. The highest amperometric response was obtained at a potential of 0.6 V. The amperometric responses of the enzyme electrode to the additions of stock glucose solutions were found to be 10 to 15 seconds. The recovery time was about 30 seconds.

Fabrication of Enzyme...

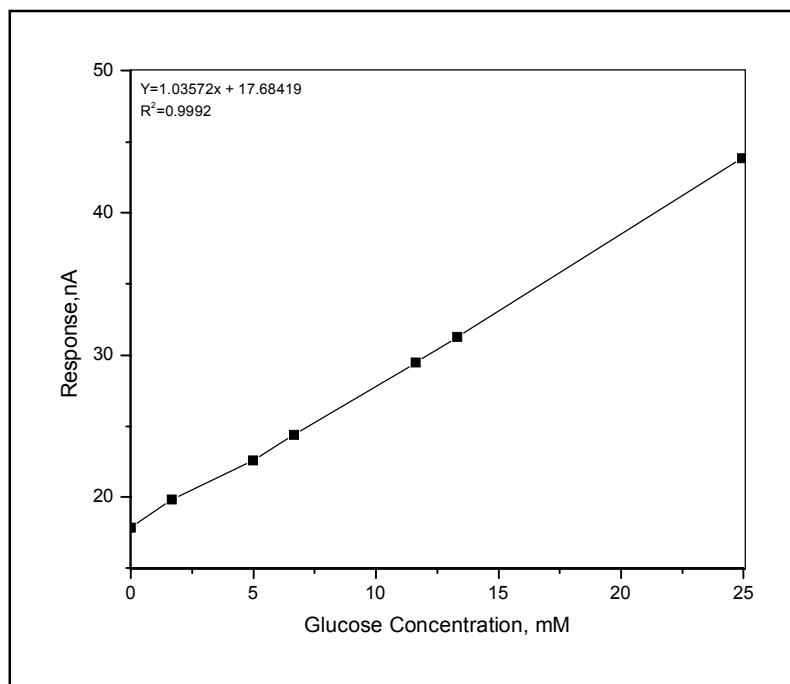


Figure 2: Calibration curve of the enzyme electrode for glucose analyte.

Using the biosensor response, a typical calibration curve for the glucose analyte of the optimized enzyme electrode was obtained as shown in Figure 2. It is clearly seen that the enzyme electrode produces a linear steady state amperometric response up to 20mM glucose. The calibration curve exhibits a good linearity with a correlation coefficient of 0.9992 ($n=8$). The existence of this linear relationship between the current and concentration of glucose is important for the accurate determination of glucose levels in human blood which lies within the narrow range of 3.5 to 5.0 mM [5].

The pH dependence of the buffer medium on the amperometric response to the glucose of the enzyme electrode was studied over the clinically and commercially relevant range. The pH optimum of immobilized enzyme may not be the same as that of the soluble enzyme. Bound to a negatively charged matrix, the pH optimum shifts to higher value, while on a positively charged support, the converse may be true. [6] Figure 3 shows the biosensor response against the pH of the buffer solution used. The highest response was observed at pH 6.8 which was subsequently utilized in further studies (Figure 4). However, it is important to note that the glucose assay is based on the electrochemical oxidation of the hydrogen peroxide which it self is a pH dependent redox process.

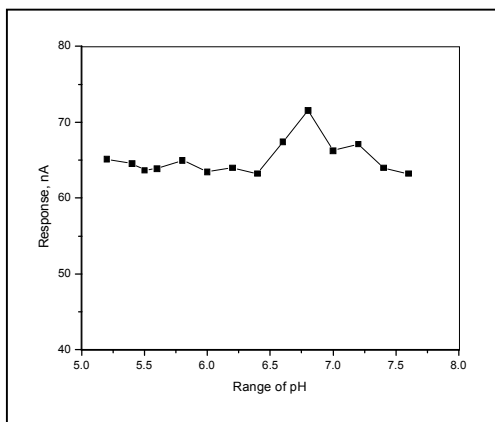


Figure 3: The influence of pH on the response of the glucose biosensor

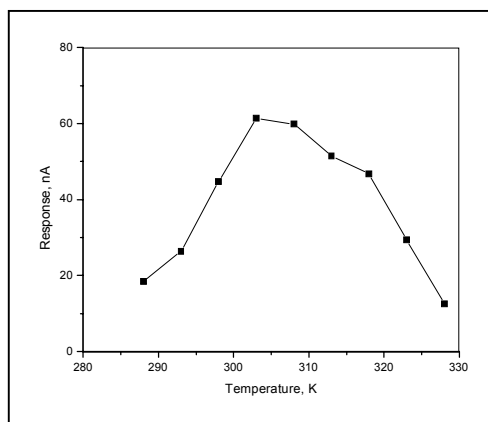


Figure 4: Effect of temperature on the response of the glucose biosensor

The effect of temperature of the buffer solution on the response of the enzyme electrode was studied in the range of 278 – 333 K (Figure 4). It is seen that the amperometric response initially increases with the temperature and decreases later. The response reached a maximum at about 303 K. The decrease of the response after 313 K may be attributed to the thermal inactivation of the enzyme or the enhanced disproportionation kinetics of hydrogen peroxide at higher temperatures which is favored over the electrochemical oxidation at the platinum electrode [7].

In order to confirm the specificity of the enzyme electrode, the amperometric responses to glucose injections without the enzyme were checked. Since, no measurable amperometric response could be observed, it has been concluded that the enzyme layer in polymer matrix was not only essential but also responsible for the observed results. The influence of the possible electrochemical interferents in the form of ascorbic acid and lactose on the performance of the sensor has been examined. However, the fabricated enzyme electrode responded successfully to glucose injections even in the presence of these interferents.

The fabricated enzyme based glucose biosensor has been, then, tested for the real sample analysis by using soft drink and blood samples. The results obtained have been compared with those obtained with HPLC/ Hospital Test methods and are given in Table 1.

Table 1 : Comparison of glucose determined using the fabricated biosensor and commercial HPLC/Hospital test method

Sample	Measured by Biosensor	Determined by HPLC/ Hospital Test
❖ <u>Soft drinks</u>		
<i>Orange</i>	23.41 ± 0.24 mg/dL	24.08 mg/dL
<i>Fanta</i>	27.59 ± 0.12 mg/dL	27.32 mg/dL
❖ <u>Human Blood</u>		
<i>Sample -1</i>	6.19 mM	6.52 mM
<i>Sample- 2</i>	4.12 mM	3.96 mM

The results indicate that the performance of the biosensor is at par with the commercially accepted methods.

The biosensor has been found to provide uniform performance over a continuous operation of 12 hours. Initial studies indicated a shelf-life of around three months under suitable conditions of storage after every use. Further work is currently in progress to study the influence of various other fabrication parameters, interferents, enzyme kinetics, environmental conditions etc. on in the performance, stability and shelf life.

Conclusions

The authors have reported the fabrication of an enzyme based low cost, portable and disposable type glucose biosensor. The sensors have been successfully tested for the determination of glucose concentration in soft drinks and human blood samples. The sensors have been found to exhibit excellent stability with a good shelf-life of about three months. The authors believe that the biosensor reported here may prove to be the low cost, portable and disposable alternates to the commercially available sensor methods. The further work is being aimed at accordingly.

References

1. A.F. Collings and Frank Caruso, Rep. Prog. Phys. 60 (1997) 1397
2. Brain Eggins in "Biosensors: An Introduction" Wiley Teubner (1996) U.K.
3. Baoli Wu, Guomei Zhang, Shaomin Shuang and Martin M.F. Choi, Talanta 64 (2004) 546
4. Dawei Pan, Jinhua Chen, Shouzhuo Yao, Lihua Nie, Jianjun Xia and Wenyan Tao, Sensors and Actuators B 104 (2005) 68
5. G. Fortier, E. Brassard and D. Belanger, Biotechnol. Tech., 2(1988)177
6. W.S. Kisaalita, Biosensors & Bioelectronics 7(1992) 613
7. G. Fortier, E. Brassard and D. Belanger, Biosensors & Bioelectronics 5(1990) 473

FABRICATION OF p-AgGaTe₂ / n-ZnSe PHOTODIODE

Shahera S. Patel* and B.H. Patel**

*University Science Instrumentation Centre (U.S.I.C.)

**Department of Electronics, Sardar Patel University
Vallabh Vidyanagar

Abstract

In this work we report the results of our study on the characterization of p-AgGaTe₂/n-ZnSe photodiode which is fabricated by flash-evaporation technique. Light and dark current-voltage, capacitance-voltage characteristics and spectral response of the device have been measured. Attempts have been made to study the device performance such as Responsivity, Detectivity etc. The implications are discussed.

Introduction

The utilization of several I-III-VI₂ chalcopyrite semiconductors in photodetector devices have been reported [1-6]. The major emphasis of these investigations has been directed towards the fabrication and characterization of heterojunction devices. Among these chalcopyrite type materials, CuInSe₂ possesses some exceptional characteristics for heterojunction applications. There are number of reports on the fabrication of semiconductor junctions with CuInSe₂ [5-9]. The transport properties of various types of semiconductor photodiode have been reported by several researchers[10-12].

Light induced processes in semiconductors are accompanied by photoelectrical, electrical and thermal phenomena. Illumination of semiconductors with photon energy above the band gap results in generation of excess electron-hole pairs and causes the internal electric fields to rise in the near-surface regions and also intolocal heating of the region.

In the present work we have presented the results of our study on the characterization of p-AgGaTe₂/n-ZnSe photodiode which is fabricated by flash-evaporation technique. Light and dark current-voltage, capacitance-voltage characteristics and spectral response of the device have been studied in detail. Attempts have been made to study the device performance such as Responsivity, Detectivity etc.

Experimental

The device consists of five layers as shown in Fig.1. The p-AgGaTe₂ thin film ($\approx 2000 \text{ \AA}$) was deposited by flash evaporation technique at a substrate temperature of about 573K

Fabrication of p-AgGaTe₂...

on silver coated glass substrate. The silver coating provides ohmic contact to the AgGaTe₂ thin film. Then ZnSe was evaporated from a quartz-wool baffled source at a substrate temperature of 473K. ZnSe films were polycrystalline and n-type having thickness of the order of 1200 Å. On top surface Indium Tin Oxide (ITO) was deposited which acts as anti-reflection coating, through which the light enters the device. Finally indium was evaporated at room temperature, to make ohmic contact to ITO film. Also, Indium solder was used as the ohmic contact to the ITO in this device. Suitable mask was employed from a square type device having an area of 1 square cm.

The current voltage characteristics were measured in dark and under illumination from a tungsten filament lamp (60W), kept at a distance of 5 cm from the fabricated photodiode. High impedance electrometer (Keithley 614) was used to measure the current. The capacitance-voltage measurements were carried out with a digital LCR bridge (HP DLCR 4284).

The spectral response was carried out at SICART, Vallabh-Vidyanagar using a UV-VIS-NIR Spectrophotometer (Make : PerkinElmer, Model : Lambda-19).

Results and Discussion

(1) Current -Voltage Characteristics :

Typical current-voltage characteristics for p-AgGaTe₂/n-ZnSe sample with and without tungsten lamp illumination is shown in Fig.2. The diode was illuminated through ITO layer. It was observed that in reverse bias condition when the diode was not illuminated, the reverse current was very small. The dark currents (measured at V=1.0Volt) were typically 1μA for forward direction and 0.3μA in the reverse direction for p-AgGaTe₂/n-ZnSe photodiode. When the device was illuminated with light, the forward and reverse current increases (measured at voltage 1V) upto a value 7μA and 3.9μA respectively.

Upon photoexcitation on a p-n junction diode, photons are absorbed mainly in the depletion region and also in the neutral regions, particularly on the top, where the light is incident.

The absorbed photons create electron-hole pairs. The photogenerated carriers in the depletion region are accelerated in opposite directions by the reverse bias and give rise to a photocurrent.

With increased reverse bias the depletion region gets wider. The photons incident on the depletion region produce electron-hole pairs (mobile charges), which can then be moved by the applied voltage across the junction. Since the depletion region is a high-resistance region, most of the voltage appears across that region and accelerates the generated

mobile electrons and holes. Some of the photons may be absorbed in the p and n regions outside the depletion region. The corresponding mobile charges, however, move by diffusion at a very low velocity, and most of them recombine along the way, contributing very little to the resulting photocurrent. Similar observations have been reported by Dzhafarov et al.[10] for photovoltaic GaAs p-n junctions.

(2) Capacitance-Voltage Characteristics :

Fig.3 shows a typical $1/C_2$ versus V curve obtained from C-V measurements at 1 KHz. The behaviour is quite linear, indicating the presence of an abrupt junction. The capacitance-voltage measurements for p-AgGaTe₂/n-ZnSe structure were carried out at room temperature. The diffusion potential V_d was determined as intersection point of a C^{-2} versus voltage plot with V axis. The diffusion potential was observed to be 0.58V.

(3) Spectral Response Characteristics :

A spectral response characteristics for p-AgGaTe₂/n-ZnSe photodiode is as shown in Fig.4. The low wavelength cutoff is due to the absorption by ZnSe and high wavelength cutoff is due to the absorption limit of AgGaTe₂ thin film. From the spectral response data, the detectivity was calculated to be $1.26 \times 10^7 \text{ cmHz}^{1/2} \text{ w}^{-1}$ at 500 nm for p-n photodiode.

The performance characteristics of p-AgGaTe₂/n-ZnSe of this photodiode in terms of responsivity at different wavelength are shown in Fig.5. The peak value of the Responsivity is found to be 0.7A/W at wavelength around 500 nm. Responsivity R (sometimes called the radiant sensitivity) defined as the ratio of photocurrent to the incident photon power. Again, the spectral response plot agrees with this value.

Gorlich[13] has reported that when the two semiconductors can be mixed to form solid solutions with spectral responses intermediate to those of the two end members. The value of this flexibility has been demonstrated by Weimer et al.[14] in the construction of visible-spectrum photoconductor arrays (which also included TFTS and thin-film diodes) for experimental television cameras.

Conclusions

The objective of this study was to assess the feasibility of p-AgGaTe₂/n-ZnSe junction which has rectifying property under illumination. The light and dark I-V characteristics have been presented. The barrier height has been calculated from the capacitance-voltage characteristics. Spectral response data correspond to expected peak values.

Fabrication of p-AgGaTe₂...

Acknowledgement

The financial assistance from University Grants Commission, New Delhi to Dr.B.H.Patel for her research project is greatly acknowledged.

References

1. Wanger S., Shay J.L., Migllorato P. and Kasper H.M. Appl. Phys. Letter **25**, 434 (1974).
2. Kazmerski L.L. and Sanborn G.A. J. Appl. Phys. **48**, 3178 (1977).
3. Brillson L.J. Surf. Sci. Reports **2**,123 (1982).
4. Shay J.L. and Wernick J.H. “ Ternary Chalcopyrite semiconductors- Growth, Electronic properties and Applications” P-175-214 (Pergamon , New York, 1975).
5. Kokubun Y. and Wada M. Jap.J.Appl.Phys. **16**, 579 (1977).
6. Kazmerski L.L., White F.R. and Morgan G.K. Appl. Phys. Letter **29**, 268 (1976).
7. Yu P.W., Park Y.S., Faile S.P. and Ehret J.E. Appl. Phys. Letter **26**, 717 (1975).
8. Mickelsen R.A. and Chen W.S. Appl. Phys. Letter **36**, 371 (1980).
9. Bettini M., Bachmann K.J., Buehler E., Shay J.L. & Wanger S. J. Appl. Phys. **48**, 1603 (1977).
10. Dzhafarov T.D., Sirin M. and Kciz S.A. J. Phys. D: Appl. Phys. **31** No.6, L 17 (1998).
11. Cengiz Besikci, Selcuk Ozer, Chris Van Hoof, Lars Zimmermann, Joachim John and Patrick Merken Semicond.Sci.Technol. **16**, 992 (2001).
12. Lile D.L. and Wieder H.H. Thin Solid Films **13**, 15 (1972).
13. Gorlich P., Adv. Electron, electron Phys. **14**, 37 (1961).
14. Weimer P.K., Sadasiv G., Meyer J.E., Meray-Horvath L. and Pike W.S., Proc. IEEE **55**, 1591 (1967).

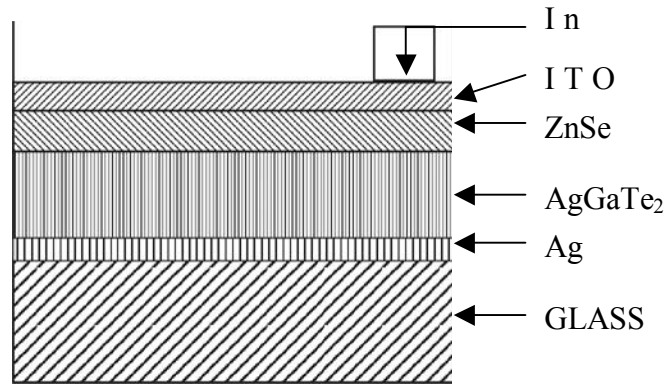


Fig.1 Schematic diagram of a p-AgGaTe₂/n-ZnSe Photodiode

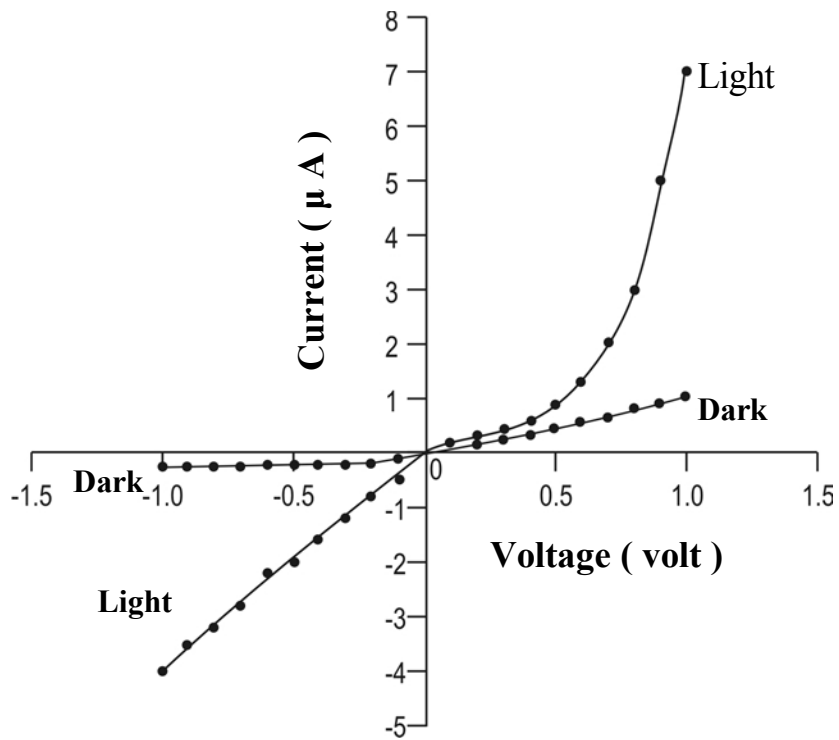


Fig.2 Current-Voltage characteristics of p-AgGaTe₂/n-ZnSe photodiode in Dark and after Illumination

Fabrication of p-AgGaTe₂...

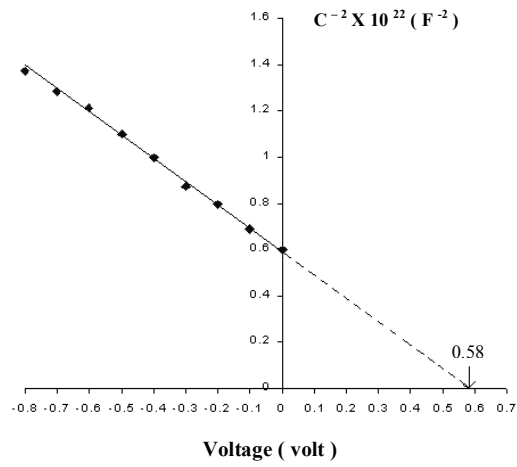


Fig. 3 Plot of C^{-2} versus Voltage of p-AgGaTe₂/ n-ZnSe Photo diode.

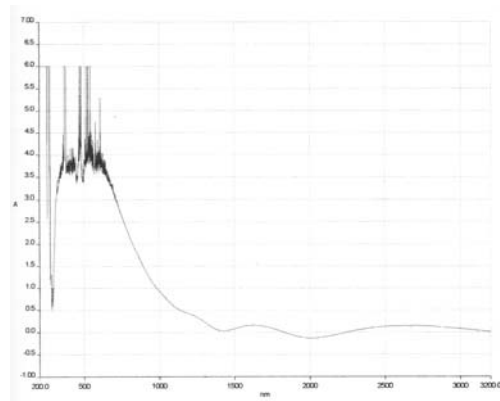


Fig.4 Spectral Response of p-AgGaTe₂/ n-ZnSe Photodiode.

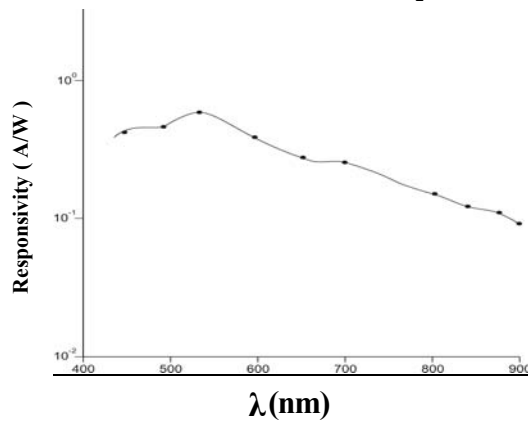


Fig.5 Performance Characteristics of p-AgGaTe₂/ n-ZnSe Photodiode.

THIAMIN AND RIBOFLAVIN STATUS OF RATS FED ON PHULKA SUPPLEMENTED WITH DIETARY FAT

Harshada J. Shah* and S.S. Sail**

*Department of Biochemistry, M.B. Patel Science College, Anand

**P.G. Department of Home Science, Vallabh Vidyanagar

Abstract

Phulka supplemented with 7 %, 15 % and 30 % fat were fed to weanling rats. Dietary and nutrient intakes were recorded. Observations indicate nearly similar dietary and nutrient intake for protein, thiamin and riboflavin. Intake of dietary fat varied with the groups. Study indicates decrease in thiamin and riboflavin storage in hepatic cell on feeding increased level of dietary fat. Decrease in storage of these two vitamins also influenced the hepatic storage of protein. Total lipid in the liver did not show variation but level of hepatic cholesterol increased with decrease in thiamin and riboflavin storage.

Introduction

Wheat has been a staple food for a large segment of the world population (Swaminathan M. 1968). About 80 - 90 % consumption of wheat is in the form of "Chapatti" (Austin et. al. 1979). Traditional preparation used as daily dietary consumption from wheat flour, are Bhakhri, phulka, paratha and poori. Addition of spices or spices along with vegetables to wheat flour gives varieties of recipes, when different methods of cooking are adapted.

Over 80% of the wheat produced in India is utilized for the preparation of various products like chapattis, phulka, tandori roti, nan, poori and other products which are mainly consumed as meal items (Saxena and Haridas 1995).

In the present study Phulka was prepared (Shah, 1999) and analyzed for chemical and biological parameters. Level of fat in the diet varies from person to person and therefore, experimental diet was supplemented with varying levels of fat. An attempt was made to study the effect of dietary fat on availability of thiamin and riboflavin.

Materials and Method:

Materials: Wheat and oil, were procured from the local market. Wheat was cleaned and ground to obtain whole wheat flour. Thiamin and riboflavin were procured from Sigma chemical company, St.Louis, Mo, U.S.A.; other chemicals used were of analytical grade.

DIET: PREPARATION OF PHULKA: Dough prepared from wheat flour was rolled on wooden roller. Rolled product roasted on both the sides for one min. and directly grilled

Thiamin and Riboflavin Status of Rats ...

on gas flame to puff the product. Prepared product was dried at 60°C and made into coarse powder.

MIXING OF GROUNDNUT OIL: Groundnut oil was mixed with the Phulka powder, to obtain diets containing 7%, 15% and 30% fat. The mixing of vitamins, minerals, starch, fiber and sucrose were avoided to observe the true effect of the nutrients present in Phulka.

CHEMICAL ANALYSIS: Diets prepared were analyzed for various nutrients content such as total protein (Oser and Hawks 1956), fat, thiamine and riboflavin (A.O.A.C. 1984).

ANIMAL EXPERIMENT: Male albino weanling rats, Charles Foster strain matched for age and weight at the start of the experiment. Animals were weighed using a triple beam balance [Oahu's U.S.A.]. Each group containing six albino rats (18 to 24 g) were selected and housed individually in clean galvanized pre labeled cages.

FEEDING TRIALS: Daily dietary intake of humans, do not contain supplementation of vitamins and minerals, therefore to study the true effect of diet addition of vitamins and minerals mixture was avoided. Rats fed on the following phulka diets for the period of 28 days;

- Group 1: 7% fat (12.9 gm% protein in the diet.)
- Group 2: 15% fat (12.86gm% protein in the diet.)
- Group 3: 30% fat (11.7 gm% protein in the diet.)

During the period of the experiment, on each day known weight of above diets were fed to rats. Left over diet was collected in pre weighed aluminum foil. Diet was dried at 60 °C to obtain constant weight. Left over was weighed to find out actual dietary intake. Records for dietary intake, gain in weight and PER were calculated according to Swaminathan M. (1985), FER was calculated using the formula- Gain in weight (g)/ Food intake (g).

Sacrifice of animals and removal of liver tissue: At the end of the experiment, animals were fasted over night and sacrificed under mild anesthesia.

Liver Processing:

Liver tissue were excised, blotted off blood and tissue fluids on a filter paper, cleared of extraneous tissue and weighed on a pre weighed aluminum foil. Known weight of liver tissue were divided for the estimation of total protein (Lowry et.al. 1951), lipid (AOAC 1984), cholesterol (Zlatkis, Zak and Boyle; 1953), riboflavin and thiamine (AOAC, 1984).

Results and Discussion:

Rats fed Phulka, containing 7%, 15% and 30% fat maintained nearly similar dietary and protein intake. Study indicates that the level of fat in the diet has no effect on the dietary intake. All diets showed nearly similar amounts of thiamine and riboflavin content, therefore intake of these nutrients remained similar (Table 1).

Data indicates that although dietary intake for all the groups remained the same, gain in weight of the rats decreased with increasing level of dietary fat. Gain in weight of the rats fed 7% fat was significantly higher ($p < 0.2$) compared to 15% fat fed rats ($p < 0.05$) and compared to 30% fat fed rats ($p > 0.0005$). This may be due to decreased availability of riboflavin for growth. Riboflavin deficient diet reported to decrease the growth (Olpin and Bates 1982). Rats fed Phulka containing 7% fat showed highest gain in weight, which decreased on increasing the fat content in the diet, (Fig-1).

Hepatic weight of rats did not change due to increased level of fat in the Phulka. Thiamin and riboflavin act as coenzymes in the metabolism of the proximate. Availability of these depends upon the intake of dietary proximate. Maximum amount of protein storage was observed for rats fed 7% fat in Phulka. (21.2g %) followed by 15% (17.1g %) and 30% (14.2g %) fat fed in Phulka. Values indicate significant differences ($p < 0.01$) and ($p < 0.0005$) compared to 7% fat diet and ($p < 0.005$) compared to 30% fat diet. Results indicate that level of dietary fat influences the storage of protein. High fat (20% higher than normal) diets require two times higher amounts of riboflavin (Roger et. al. 1950). Even though the total lipid level of the liver remained same, the level of liver cholesterol was increased significantly ($p > 0.025$) and ($p > 0.05$) on feeding 15% and 30% fat in the diet, respectively. Table - 2 represents the data for liver weight, protein, lipid and cholesterol. Hepatic level of thiamine and riboflavin were also found to be dependent, on the dietary fat intake. High fat diets influence the hepatic storage of thiamin and riboflavin. Feeding a high fat diet to weanling rats in a traditional product like phulka showed decreased hepatic thiamine and riboflavin storage. Phulka containing 7% fat showed 0.32 mg% liver thiamine levels followed by 15% (0.21 mg %) and 30% (0.18 mg %) fat diets. Table-3 indicates these values. Data indicates that higher amount of dietary fat (30%) decreased thiamine storage which was nearly the half the amount observed in the low fat (7%) diet. Values indicate significant decrease ($p < 0.1$) and ($p < 0.2$) on feeding 15% and 30% fat in the diet, respectively. Increasing the level of dietary fat decreased not only the thiamin storage but also the storage of riboflavin. Diets containing 7%, 15%, and 30% level of fat when fed for 28 day period showed 0.17mg%, 0.15mg% and 0.08 mg % riboflavin stores, respectively. Values indicates significant decrease ($p < 0.1$) and ($p < 0.2$) on feeding 15% and 30% fat in the diet respectively compared to 7% fat diet.

Conclusion:

Liver is a store-house for many nutrients. Analysis of hepatic parameters of rats indicated that the demand for vitamin and protein increases on a high fat diet. High fat diet demand more amounts of thiamine, riboflavin and protein for vital activities of the liver. Therefore, a higher amount of fat in a diet should be avoided or the dietary intake of thiamine, riboflavin and protein must be increased with high fat diet for the wellbeing of health.

Table - 1. Diet and nutrient intake of rats (four-week record)

Type of diet	Diet (g)	Protein (g)	Fat (g)	Thiamine (mg)	Riboflavin (mg)
Phulka 7% Fat	108.30±7.92	13.6±0.9	08.66±0.5	0.49±0.02	0.32±0.01
Phulka 15% Fat	104.16±3.97	13.4±1.0	16.66±0.5	0.47±0.02	0.31±0.01
Phulka 30% Fat	105.60±8.54	11.8±0.5	31.65±1.9	0.47±0.01	0.31±0.01

Values are mean of six animals ± SEM

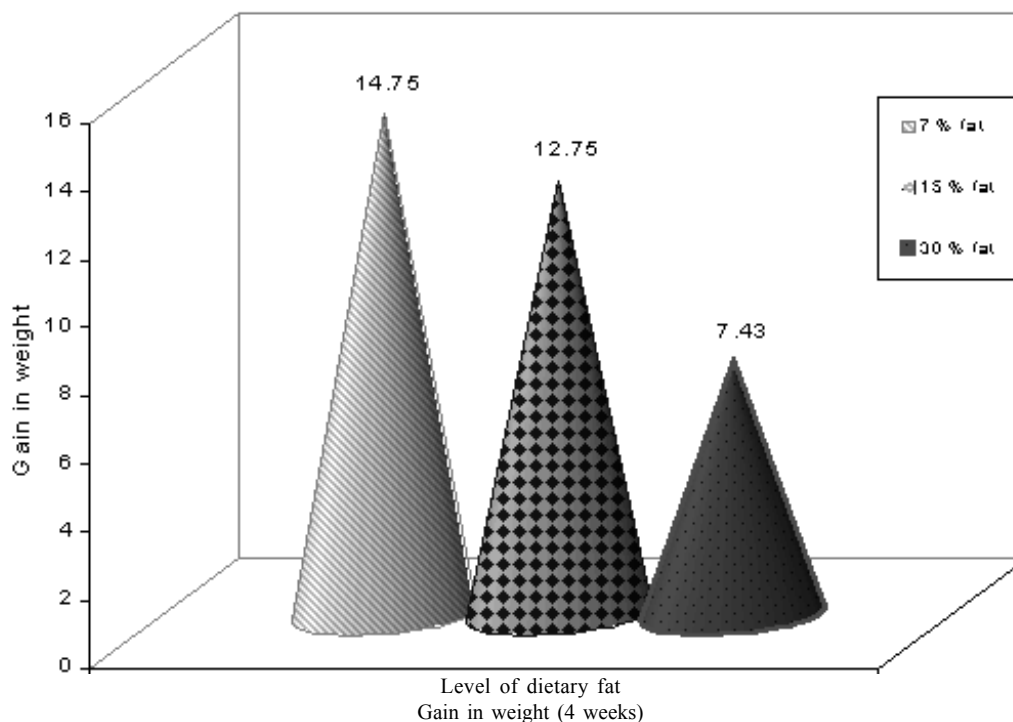


Fig. 1: Gain in weight of rats fed varying levels of fat in phulka

Table - 2. Liver weight, protein, lipid and cholesterol of rats

Type of diet	Liver weight (g)	Protein (g%)	Total Lipid (g%)	Cholesterol (mg%)
Phulka 7% Fat	2.13±0.17	21.22±0.63	3.36±0.43	94.63±14.70
Phulka 15% Fat	2.15±0.12	17.12±1.14	4.32±0.58	106.53±6.37
Phulka 30% Fat	2.01±0.12	14.20±0.62	4.48±0.57	137.82±8.65

Values are mean of six animals ± SEM

Table -3. Liver vitamin storage of rats

Type of diet	Thiamine (mg%)	Riboflavin (mg%)
Phulka 7% Fat	0.319±0.013	0.172±0.048
Phulka 15% Fat	0.211±0.044	0.153±0.027
Phulka 30% Fat	0.177±0.040	0.084±0.011

Values are mean of six animals ± SEM

References

1. A.A.V.C, American Association of Chemist (1951). Methods in Vitamin Assay. II ed. Inter science publisher inc. Newyork
2. A.O.A.C. (1984). Official Methods of Official Chemist. Washington D.C.
3. Austin, A. and Ram, A. (1979). Study on chapati making quality of wheat. I.C.A.R. New Delhi. Tech. Bull. 31:39 - 41
4. Lowry D.H. Rose Brough N.J., Forr A. K. and Randall P. J. (1951). Protein measurement with Folin - phenol reagent. J. Biol. chem. 193: 265-276
5. Reinhold, J.A (1953). Standard methods in clinical chemistry. Vol. - II. Academic Press. NY. 88
6. Roger, J. William, Robert, E. Eakin, Ernrt, Berstecher and Jr., William Shive. (1950). Factors influencing B vitamins requirements. Univ. of Texas, Reinhold Publishing Co. 330. West forty. Second st. New York. 18. U.S.A.

Thiamin and Riboflavin Status of Rats ...

7. Olpin, S.E. and Bates, C. J. (1982):Effect of dietary lipids on riboflavin status and fatty acid profile. *Br. Jr. nut.* 47,577
8. Oser, B. and Hawks, B.(1956).Hawks physiological chemistry. 13 edi.T.M.H. Publishing company Ltd. New Delhi
9. Saxena, D.C. and. Haridas, P. Rao. (1995). Survey of the quality characteristics of Tandoori dough and Tandoori roti. *Jr. Fd. Sci. Technol.* 32:1: 74-76
10. Shah, H.J.(1999). Nutritional Quality of food products prepared from selected cereals and pulses. Ph. D. thesis submitted to S.P.U.
11. Swaminathan, M.(1968). Diet and nutrition in India. *Indian Jr. of Dietetics.*5:225-228
12. Swaminathan, M.(1985). Essential of food and nutrition. Vol.- I. Fundamental aspects. II.ed158. Ganesh Pub. Co. Benglore.
13. Shrinivas, A.L.(1984). World wheat Situation.Indian miller. Vol. XV. 2 - 17
14. Zlatkis, A. Zak, B. and Boyled, A. J. (1953). A new method for direct determination of serum cholesterol. *Jr. Lab. Clin. Med.* 41: 486 - 488

EFFECT OF CHEMICAL ACTIVATION ON DEODORIZING PROPERTIES OF ACTIVATED CARBON FROM BANANA STEM

J.H. Bhagat and S. Manocha

Department of Materials Science
Sardar Patel University, Vallabh Vidyanagar -388 120

Abstract

The Banana stem abundantly available in *charotar* area is a waste fibrous biomass. Activated carbon was prepared from this waste dried banana stem by giving chemical treatment with acid, base and salt to ascertain the adsorption capacity of resulting activated carbon. The deodorizing properties of activated carbon were studied by using the Iodine adsorption method.

The results show that surface characteristic play a vital role in deodorization than the surface area of activated carbon.

Introduction

Activated carbons are widely used as industrial carbon in various sectors such as environment protection against both gaseous and liquid pollutant, pharmaceuticals, energy production, domestic appliance, consumer products and electronics industries [1-3]. These potential applications reveals the use of activated carbon of desired internal surface area, porosity and adsorption characteristics. These activated carbon can be prepared by selecting the appropriate precursor and by the control of the processing parameters. The carbonaceous precursor can be selected from naturally occurring biomass or synthetic precursor having high carbon content and low ash content [3, 4]. The biological origin raw materials like wood, coconut shell, agricultural wastes or coalified plant matter such as coal, lignite etc are the major precursors for making activated carbon.

Though, synthetic precursors such as polymeric fibers are being used to produce activated carbon with high surface area [3, 5-7], at the same time more and more agricultural wastes are also being investigated as precursors for making activated carbon. For adsorption from gaseous phase, mainly micro porous carbon are desired whereas, mesoporous carbon is used for liquid phase adsorption. Interest in utilization of bio-waste precursor is on regional basis and is primarily aimed at utilizing cheap bio- waste materials to produce low cost activated carbon. In Gujarat banana is one of the major crop. The complete plant along with the stem has fibrous structure .Therefore the studies on development of activated

Effect of Chemical Activation...

carbon from fibrous banana stem have been undertaken. Iodine adsorption is a measure of deodorization capacity. In the present paper, the deodorization capacity of activated carbon prepared by different chemical activation by acid, base and salt has been evaluated and are co-related with surface characteristics.

2.0 EXPERIMENTAL

2.1 Raw Material and Treatment

The banana stem obtained from Gujarat was used in the present studies. These were cut into small pieces (5-7 cm in length) and dried in sunlight. The dried pieces of banana stem were then used as a precursor for obtaining char and activated carbon. The dried banana stem was given treatment with acids e.g. H_3PO_4 and HNO_3 ; base such as KOH and salts e.g. $ZnCl_2$ followed by heat treatment at $1000^\circ C$. All the chemicals were of AR grade. The samples were immersed in the activating agent at room temperature for 24 hrs.

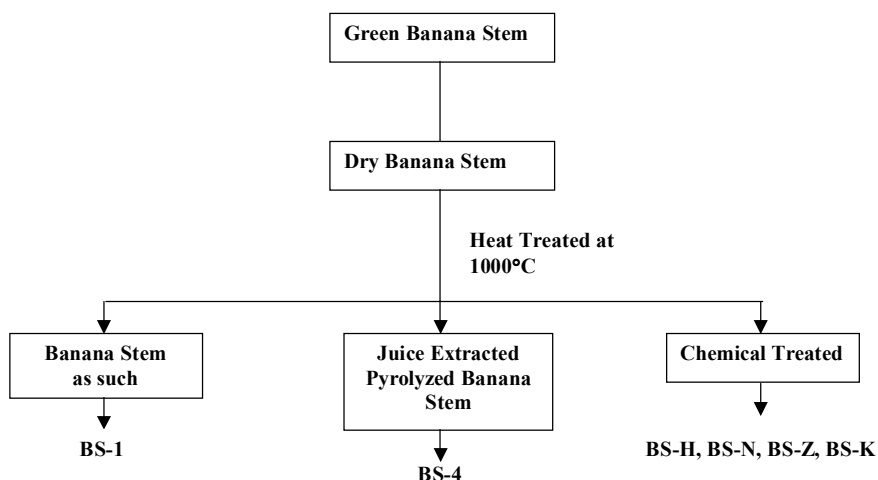


Figure.1. Schematic representation of experimental procedure

After the treatment, the samples were dried at $100^\circ C$. Pyrolysis of the sample was carried out in a Muffle furnace. In all series, samples were heated at the rate of $30^\circ C/hr$. Cooling was carried out at the rate of $60^\circ C/hr$. The activated carbon was also prepared from the banana stem by extracting the juice. The schematic diagram is shown in Figure- I.

2.2 Characterization of Samples

Specific gravity of all carbon samples were determined by Archimedes principal.

Thermogravimetric analysis of the samples was carried out using Mettler TA 4000 Thermal analysis system at heating rate of 10°C/min. Surface oxygen complexes [8,9] on chars as well as activated carbon were determined by selective neutralization technique.

The Surface area of the samples was measured on Micromeritics Gemini 2375 Surface area analyzer. The samples were cleaned prior to measurement by heating the sample at 250°C for 24 hours under continuous flow of Argon. Iodine adsorption studies were carried out as per standard technique. Accurately weighed 0.5 gm carbon sample was placed into 250 ml iodine flask. To this 10 ml of 5% HCl was added. The assembly was heated at 40°C for 5 min. and then cooled to room temperature. 100 ml of Iodine solution was added to these flasks. These were kept in dark for about 1-2 min and solutions were filtered to get clean solution. The clear solution was titrated with 0.01N sodium thiosulphate using starch as an indicator. The percentage Iodine adsorbed by the carbon sample was calculated using following equation:

$$\% \text{Iodine adsorbed} = \frac{\text{Iodine conc. before adsorption} - \text{Iodine conc. after adsorption}}{\text{Initial Iodine conc.}} \times 100$$

3.0 RESULTS AND DISCUSSION

3.1 Pyrolysis Behavior of Banana Stem

Pyrolysis behavior of banana stem as such as well as after chemical treatment was studied using thermo gravimetric analysis. The details are given elsewhere [9-11].

3.2 Ash Content

In comparison to commercially used woods for activated carbon, the banana stem carbons have been found to contain much higher ash. The ash content is in the range of 23-31%, being lower in chemically treated samples. The % ash content of the various carbon samples are given in Table-1. It further supports that chemical activating agents are reacting with the wood during pyrolysis. Silica content was found to be a round 75-80% of the total ash content.

3.3 Surface Oxygen Complexes

The surface oxygen complexes present on the carbon samples plays an important role in determining the total adsorption capacities of activated carbons. The results of the surface oxygen complexes present on the various carbon samples are given in Table 2. The surface oxygen complexes present on the carbon sample prepared by chemical activation (acid treated and salt treated) are found to be higher than that of alkali treated samples.

Effect of Chemical Activation...

3.4 Surface Area Measurement

The BET surface area of all carbon samples are given in Table 2. As seen from the table most of the chemicals do not have any significant effect on the ultimate value of surface area and porosity of the carbon. The inorganic materials act as catalyst for dehydration at lower temperatures when the pores are getting reorganized. Inorganic materials may fill or block some portion of macro pores. Nitric acid treatment show positive effect. The surface area of carbon is found to be enhanced almost double on treatment with nitric acid. This is because nitric acid does not show to leave behind any inorganic materials inside the carbon pores. However, nitric acid treatment shows significant improvement in micro pore area and micro pore volume. While the average pore diameter is found to remain same. The results are given in Table 2.

3.5 Iodine Adsorption Capacities

The deodorizing properties of carbon samples were adjudged by iodine adsorption test. The iodine adsorption (percentage) of all carbons are given in Table 2. The iodine adsorptions of BS-2 and BS-3 have similar value while BS-K has only 53% deodorization capacity. These appear mainly due to removal of some associated inorganic species and conversion of macro porosity to meso and micro porosity.

A comparison of deodorizing capacity with surface characteristics of activated carbon shows that in addition to surface area, surface oxygen complexes also play a vital role in the deodorization capacity of activated carbon.

Table 1 Physical Properties of Chars and Activated Carbon at 1000°C

Name of Sample	Yield (%)	Ash content (%)	Specific gravity (gm/cc)
BS -1	31.98	28.07	1.59
BS -4	22.50	22.87	1.52
BS -2	25.03	20.54	1.513
BS -3	30.75	20.03	1.531
BS-N	28.83	22.36	1.647
BS-Z	26.66	22.50	1.521
BS-K	23.70	23.40	1.503

Table 2 Surface Properties of Chars and Activated Carbon at 1000°C

Name of Sample	Surface oxygen complexes (meq/100 gm)	Iodine Adsorption (%)	BET Surface area (m ² /gm)	Micro pore area (m ² /gm)	Micro Pore vol. (cm ³ /gm)	Avg. Pore Diameter (Å)
BS -1	327.58	64.26	227.71	123.2735	0.056280	17.8785
BS -4	523.15	74.26	270.29	193.0889	0.019177	17.8346
BS -2	580.00	76.03	155.55	97.1254	0.044404	17.9207
BS -3	665.21	75.525	178.99	108.7093	0.069397	24.2913
BS-N	745.94	63.36	342.09	212.3466	0.097198	18.9517
BS-Z	637.40	61.06	184.244	123.7141	0.05658	18.9324
BS-K	573.04	53.33	140.84	71.0056	0.032272	17.9137

* The results reported in the paper form a part of Ph.D. Thesis of J.H. Bhagat submitted to Sardar Patel University, Vallabh Vidyanagar in Feb. 2001 under guidance of Dr.(Mrs.) S. Manocha, Professor, Dept. of Materials Science, Sardar Patel University, Vallabh Vidyanagar - 388120.

References

1. Dai, M. Collid Interface Sci. 1994, 164, 233
2. Byrne, C.E.; Nagle, D.C. Carbon 1997, 35(2), 259
3. Ryu, S.K. Chemical Industry & Technology (Korea) 1992,12,6
4. Gergora, K.; Esr, S. Carbon 1996, 34(7), 879
5. McEnaney, B.; Derbyshire, F.; Stencil, J. Carbon 1997, 30(7), 889
6. Thwaries, M.; Mc Enaney, B.; Botho, F.D. ACS Fuel Division 1992, 37(2), 497
7. Mochida, I.; Kisamori, S.; Fugitsu, H. Extended Abstracts Carbon 92, Essen Germany, 1992, 296
8. Mackway, D.W.; Robert, P.V. Carbon 1982, 20(2), 95
9. L.M. Manocha, J.H. Bhagat and S. Manocha, Carbon Vol. No. 22, June 2001
10. L.M. Manocha, J.H. Bhagat and S. Manocha, Advances in Carbon and Carbon Materials INDO CARBON 2001, Shipra Publication, Page No.48-57
11. L.M. Manocha, J.H. Bhagat and S. Manocha, 2nd Pacific Basin Conf. on Adsorption Science and Technology, May 2000, Brisbane (Australia)

PROPERTY MODIFICATION OF CONVENTIONAL CASTOR OIL BASED POLYURETHANE USING NOVEL FLAME RETARDANT POLYURETHANES

R.H. Patel and H.B. Patel

G.H. Patel Institute of Materials Science,
Sardar Patel University, Vallabh Vidyanagar-388120

Abstract

Polyurethanes were prepared from castor oil and phosphorous containing monomer and characterized by various chemical and instrumental analysis techniques. Thermal properties were determined using differential scanning calorimetry and thermogravimetric analysis techniques. Flame retardant properties of blended films were evaluated. Resistancy to UV light and certain chemical agents were determined. Incorporation of phosphorous containing polyurethane to castor oil based polyurethane improve the properties of the conventional castor oil based polyurethanes.

Introduction

Castor oil obtained from castor bean plant find a wide range of industrial applications due to its interesting chemical structure i.e. presence of different functional groups in the long aliphatic chain. Urethane polymers of castor oil are used in many commercial applications like coatings, foams, adhesives, elastomers, etc. [1,2]. But one of the major limitations of these polymers is their inherent flammability. To limit the flammability, it is necessary to incorporate fire retardants in the polymer [3, 4]. Polymers containing phosphorous group belong to these fire retardants, allow improved thermal and fire retardant properties [5, 6]. As these are halogen free products, attractive and welcome worldwide [7]. This work deals with the synthesis and characterization of novel phosphorous containing polyurethanes by reacting tris (m-hydroxy phenyl) phosphate with various diisocyanate. These polymers were blended with conventional castor oil based polyurethanes in different proportion to improve latter's flame retardant properties. Thermal, physical, flame retardant properties of the blended polymers in the film form have been evaluated.

EXPERIMENTAL

Materials

Resorcinol (RC), phosphorous oxychloride (POCl_3), Isophorone diisocyanate (IPDI), hexamethylene diisocyanate (HMDI), toluene diisocyanate (TDI) and diphenyl methane diisocyanate (MDI) were procured from fluka and were used without purification. Refined

R.H. Patel and H.B. Patel

grade castor oil was obtained from local market and was used after performing certain chemical tests. Solvents such as methyl ethyl ketone (MEK), ethanol (ETOH), dimethyl formamide (DMF), dimethyl sulphoxide (DMSO), dimethyl acetamide (DMAc) were used after distillation.

Synthesis of Castor oil based polyurethane

Castor oil based polyurethane (PU-A) was prepared [8] by reacting toluene diisocyanate (0.0946 mole) with castor oil (0.054 mole) at 45 °C for 1 hour with continuous stirring. The polyurethane was vacuum distilled to obtain pure polymer.

Synthesis of flame retardant polyurethane

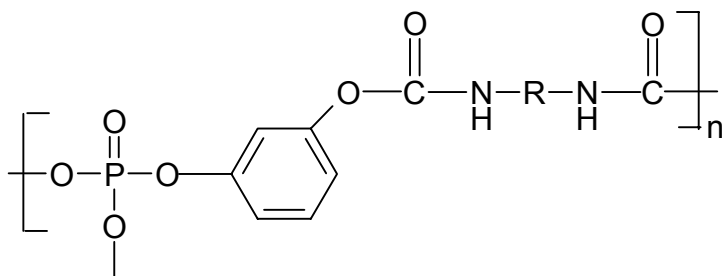
Monomer synthesis

The monomer tris (m- hydroxyl phenyl) phosphate (THPP) was synthesized [9] by reacting phosphorous oxy chloride (0.49 mole) with resorcinol (1.0 mole) at 110 °C for 2.5 hours. The resultant product was obtained by neutralizing and precipitating in cold water.

Synthesis of polyurethane

Polyurethane (PU-1) was prepared by reacting a prepolymer (diisocyanate monomer ratio 3:1) with excess monomer at 80 °C for 3 hours. The product was vacuum distilled to obtain pure polymer. Polyurethanes with isophorone diisocyanate (PU-2), diphenyl methane diisocyanate (PU-3) and hexamethylene diisocyanate (PU-4) were prepared in the similar manner.

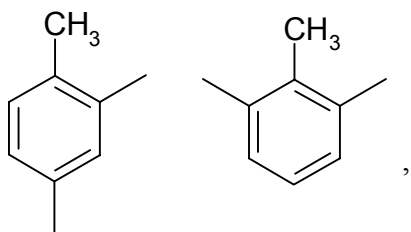
Property Modification of Conventional...



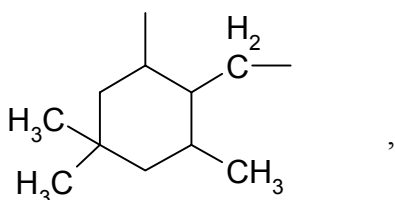
Structure of phosphorous containing polyurethane

Where R represents

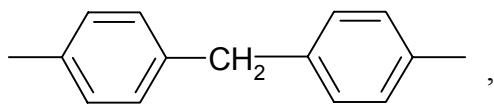
respectively in



PU-1



PU-2



PU-3

and



PU-4 resins

Properties and Characterization of the Polymers

The qualitative solubility of the synthesized polyurethanes in various solvents were examined at room temperature with concentration of approximately 1 % (W/V). The phosphorous

R.H. Patel and H.B. Patel

containing polyurethanes were soluble in DMF, DMSO, DMAc while castor oil based polyurethane was soluble in MEK. The intrinsic viscosity (Table 1) of these soluble polymers was measured using Ubbelohde suspended level viscometer in DMF at room temperature.

Number of hydroxyl group of the monomer and polymers was determined by hydroxyl group estimation [10, 11]. These values are reported in Table 1. Percentage yield of the monomer and polymers are in the range of 80-85%. Elemental analysis was carried out using Perkin-Elmer USA (Model 2400 series II). Observed values are in good agreement with the calculated value as shown in Table 1. Average molecular weights of the polyurethanes were determined by vapour pressure osmometer Model K - 7000. KNAUER instrument.

The infra-red spectra of the monomer and polymers were recorded in KBr pallet on Perkin Elmer USA (Model Spectrum GX, FT-IR) spectrophotometer.

The heat flow data of the polyurethanes were obtained by differential scanning calorimetry technique (DSC) using TA instrument USA (Model 5000/2920) at a heating rate 10 °C/min. using empty cell as reference. Thermogravimetric analysis (TGA) of the polymers were done on Perkin Elmer USA (TGA-7) thermal analyzer in air at a heating rate 10 °C/min.

Photostability and flame retardant properties were measured by casting blended polymer films from a glass mould. Required amount of castor oil based polyurethane, phosphorous containing polyurethane and ammonium phosphate were mixed thoroughly in suitable solvent and poured on the glass mould. Films were obtained (Table 3) by heating the content at 70 °C for 24 hours and then after cooling to room temperature. Stability of the films towards ultra-violet light was determined from ultra-violet spectrophotometer Perkin Elmer (Model Lambda 19). The limiting oxygen index (LOI) of the films were measured on a standard apparatus as per ASTM D 2863.

Results and Discussion

The IR spectra of the monomer shows a broad absorption band at 3388 cm^{-1} due to the presence of H-bonded hydroxyl species, the band at 1262 cm^{-1} corresponds to Ar-OH symmetric stretching frequency, C=C stretching of aromatic ring is observed at 1494 cm^{-1} , the band at 1252 cm^{-1} is due to the presence of P=O group and the band at 991 cm^{-1} is due to the P-O-C stretching frequency.

FIGURE 1 depicts the IR spectra of polyurethanes. The bands around 1600-1667 cm^{-1} are due to the -CONH asymmetric stretching vibration. The vibration for P=O group appears around 1226-1239 cm^{-1} . P-O-C stretching frequency is observed around 989

Property Modification of Conventional...

992 cm^{-1} . The broad bands around 3294-3337 cm^{-1} are attributed to N-H band.

The curing behavior of the polyurethane systems was studied in presence of 1 % $(\text{NH}_4)_2\text{HPO}_4$ using DSC techniques. Table 2 shows the curing characteristics such as the temperature at which curing is initiated (T_i), peaked (T_p) and completed (T_f). The exotherms obtained for various systems ranged in between 141 -220 $^\circ\text{C}$.

The thermal stability of the cured polyurethanes was studied by TGA analysis (FIGURE 2). Percentage weight loss data (Table 2) shows polyurethanes have good thermal stability. IPDT values give the idea of the overall decomposition temperature of the polyurethane systems. Polyurethane with TDI was stable up to 600 $^\circ\text{C}$. For this system char value was 68%. System with MDI (PU3) had char value 40%. This shows polyurethanes based on TDI and MDI have very good flame retardant properties. This fact was also supported by LOI values. LOI values are in the range of 30-36 % which also support good flame retardant properties.

Polyurethane of castor oil with ammonium phosphate shows initial decomposition temperature of 115 $^\circ\text{C}$. Char value is 24% for this system and LOI value is 18%. Further improvement of these value can be done by incorporation of phosphorous based polyurethanes. Addition of phosphorous polyurethanes with conventional castor oil based polyurethane in 70:30; 80:20 and 90:10 ratios improve the latter's flame retardant properties. LOI values for the blends were observed to be in the range of 20-30 %.

The polyurethane films were exposed to UV radiation for 3 hours. λ_{max} values are in the range of 360 to 375 nm. UV spectra of films were obtained at a time interval of every one hour. After exposure no remarkable change in the spectra has been observed. Thus it may be inferred that polymers are stable to UV light.

Shore hardness properties of the polyurethane films were measured. The shore D hardness value of the polymer films is in 30-45 range while the shore A hardness ranges in 35-55 as shown in Table 3. Hardness value decreases in blends which may be due to the flexible nature of castor oil based polyurethane.

The chemical and hydrolytic stability of the polyurethanes system were measured by dipping the films in methanol, 10% sodium hydroxide, 20% sodium hydroxide, 10% hydrochloric acid and in water. After seven days only minor change in the weights are observed while there was no change in the dimension of the films. A slight discoloration of the films was observed in sodium hydroxide solution but the color of the films remained unchanged in

R.H. Patel and H.B. Patel

other medium. The weight change data are given in Table 4. These data reveal that polymers have good chemical and hydrolytic stability.

Conclusion

The above study reveal that incorporation of flame retardant polyurethanes in castor oil based polyurethane improve the flame retardant properties of castor oil based polyurethanes.

Acknowledgement

The financial assistant from University Grants Commission, New Delhi is gratefully acknowledged.

References

1. Fabio M.D. ,Fransisco A. and Rocco L. , Mater. research. 7 (3) , 413 (2004)
2. Patel N. , Kansara S. , Somani K. and Raxit A. , Europ. Coat. J. 11, 34 (2003)
3. Spirckel M, Regnier N, Mortaigne B, Youssof B. and Bunel C., Polym. Degrand. Stab. **78**, 211-218(2002)
4. Kemmlein S., Hahn O. and Jann O., Atmos. Env.**37**,5485-5493 (2003)
5. Lin J.F. ,Ho C.F. , Huang S.K. , Polym Degrad. Stab.**67**, 137 (2000)
6. Modesti M., Loronzetti A., Simioni F. and Camino G., *Polym. Degrad. Stab.***77**, 195-202 (2002)
7. Modesti M. ,Loronzetti A. , Polym.Degrad.Stab.**78**,167 (2002)
8. Patel P., Shah T. and Suthar B., J. Appl. Polym. Sci. **40**, 1037-1047 (1990)
9. Patel S.R. and Patel R.G., High Performance Polymers. **3** , 237 (1991)
10. Vogel A.I. Elemental Practical Organic Chemistry, Part-3, Quantitative Organic Analysis , second edition Delhi, (CBS publishers & distributors) (1987)
11. Naughton F.C., J. Am. Oil Chem.. Soc. **51**, 65(1974)

Property Modification of Conventional...

Table 1 : Analytical data of polyurethanes

	System	Number of Hydroxyl group	Intrinsic Viscosity in DMF (η)	Average Molecular Weight \overline{M}_n	Elemental Analysis		
					dl/gm		
					C	H	N
Monomer	THPP	2.92		---	(57.40) 59.17	(4.01) 3.72	--- 0.26
PU-1	THPP+TDI	3.5	0.35	2010	(59.10) 58.40	(4.17) 4.12	(4.17) 4.15
PU-2	THPP+IPDI	3.4	0.24	2155	(58.46) 57.45	(5.01) 4.95	(3.89) 3.74
PU-3	THPP+MDI	4.2	0.30	2240	(62.67) 61.25	(4.28) 4.05	(3.75) 3.64
PU-4	THPP+HMDI	3.8	0.25	2005	(57.45) 56.34	(4.78) 4.65	(4.18) 4.10

Table 2 : Thermal properties of polyurethanes using $(\text{NH}_4)_2\text{HPO}_4$ as curing agent

	Curing Characteristics by DSC ($^{\circ}\text{C}$)			% Weight Loss from TGA ($^{\circ}\text{C}$)					IPDT ($^{\circ}\text{C}$)	Char Yield (%)
	Ti	Tp	Tf	10%	30%	32%	60%	70%		
PU-A	-	-	-	200	260	265	340	400	244	24
PU-1	190	195	205	290	535	600	-	-	475	68
PU-2	186	194	220	255	315	320	600	-	330	38
PU-3	190	196	210	255	290	295	-	-	378	40
PU-4	141	154	210	215	290	295	475	520	325	29

Table 3 : Flame retardant and hardness properties of polyurethane films

System	Proportion	LOI %	Hardness	
			Shore A	Shore D
PU-A	-	18	40	35
PU-1	-	36	80	70
PU-A:PU-1	70:30	30	55	45
	80:20	28	45	40
	90:10	24	40	35
PU-2	-	33	65	55
PU-A:PU-2	70:30	26	45	40
	80:20	23	40	35
	90:10	21	35	35
PU-3	-	34	70	60
PU-A:PU-3	70:30	26	50	40
	80:20	24	45	40
	90:10	20	35	30
PU-4	-	30	60	50
PU-A:PU-4	70:30	23	40	40
	80:20	21	35	35
	90:10	20	35	30

Property Modification of Conventional...

Table 4 : Chemical resistance properties of polyurethanes

System	Weight change data of polyurethane films (gm)				
	Methanol	Water	10% NaOH	20% NaOH	10% HCl Solution
PU-A:PU-1					
70:30	0.02	0.01	0.03	0.03	0.04
80:20	0.01		0.03	0.03	0.02
90:10	0.01	0.01	0.02	0.03	0.02
PU-A:PU-2					
70:30	0.03	0.02	0.04	0.04	0.05
80:20	0.02	0.01	0.03	0.03	0.04
90:10	0.01	0.01	0.02	0.03	0.04
PU-A:PU-3					
70:30	0.01	0.02	0.03	0.04	0.02
80:20	0.01	0.01	0.02	0.04	0.02
90:10	0.00	0.02	0.02	0.03	0.03
PU-A:PU-4					
70:30	0.02	0.02	0.03	0.03	0.06
80:20	0.00	0.02	0.03	0.04	0.04
90:10	0.00	0.01	0.01	0.03	0.04

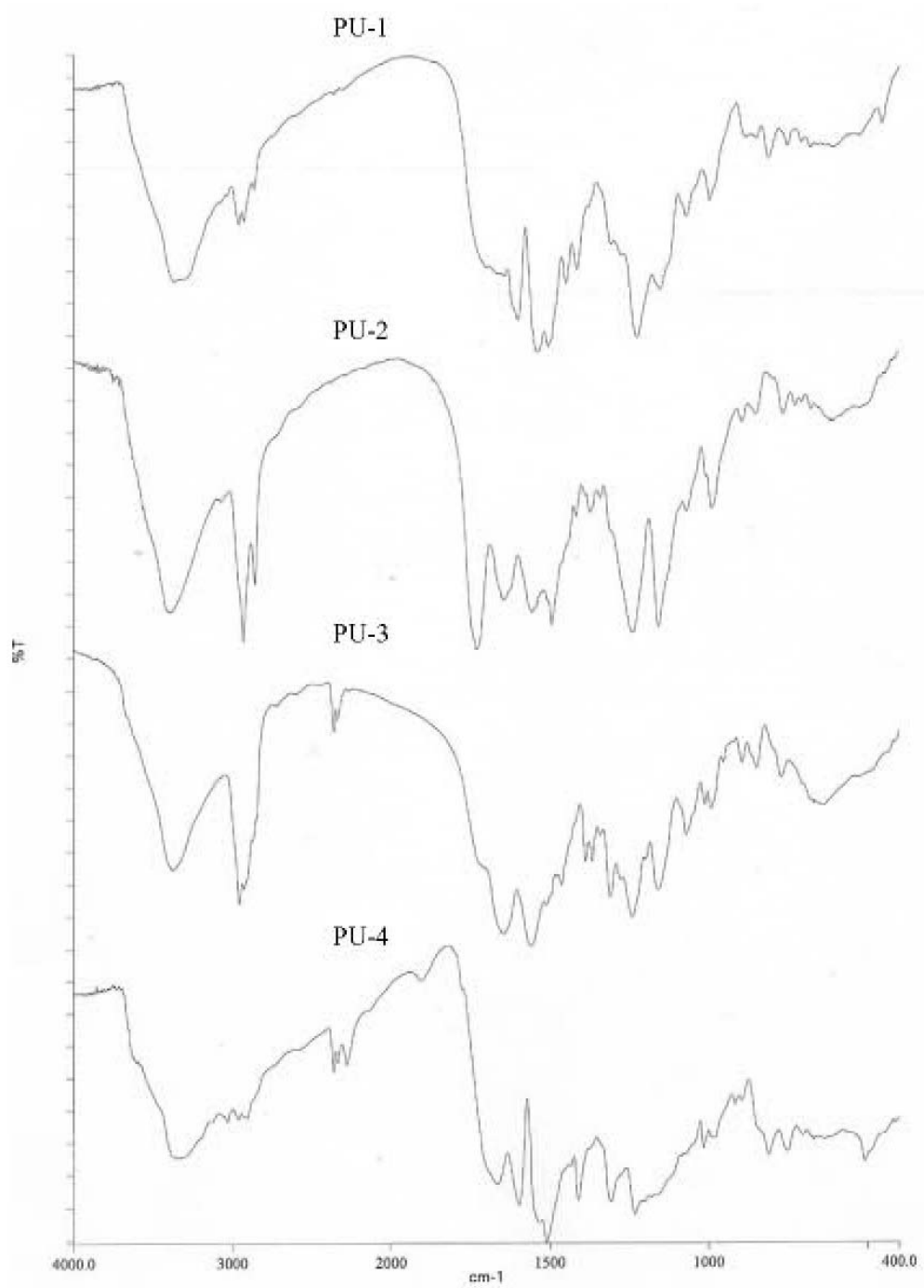


Fig. 1 : FT-IR spectra of polyurethane samples PU-1, PU-2, PU-3, PU-4

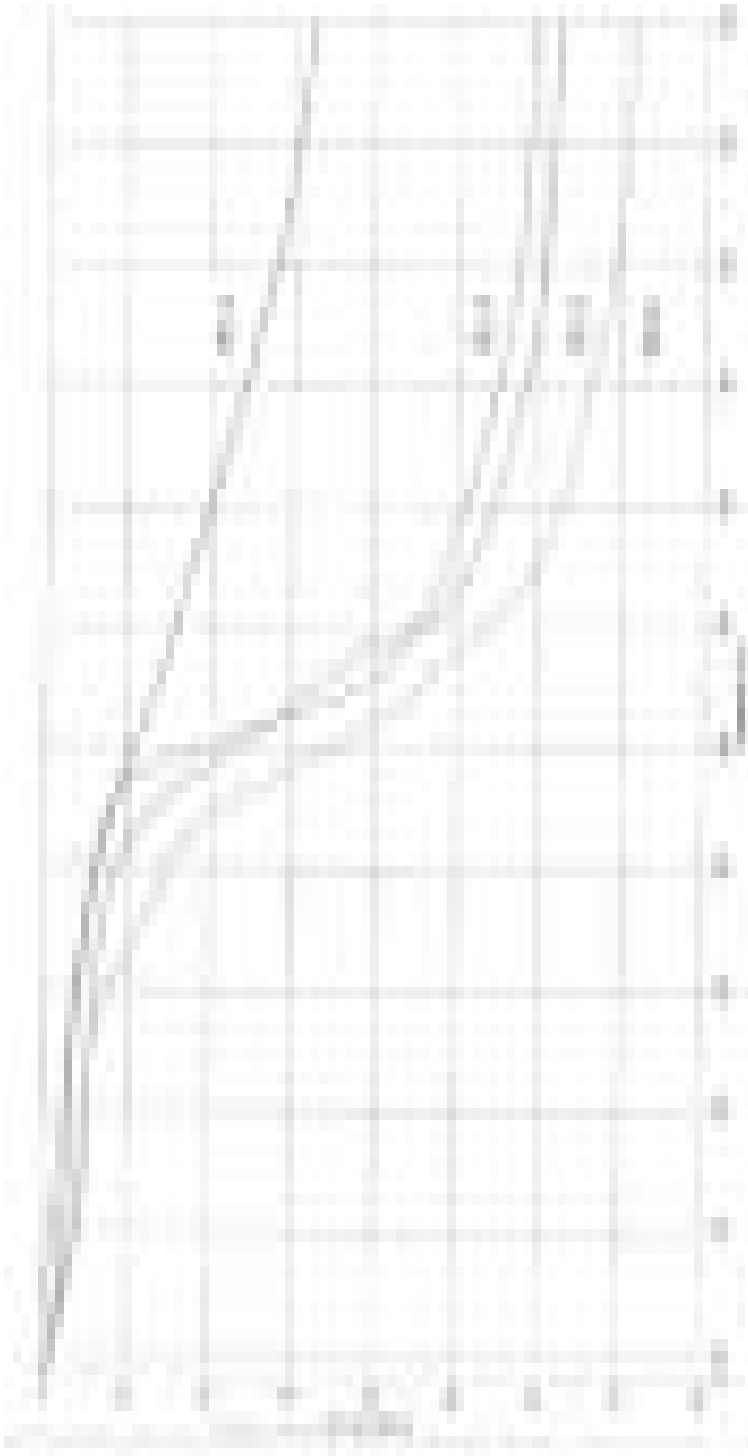


Fig. 2 : TGA curves of polyurethane samples PU-1, PU-2, PU-3, PU-4 in air at heating rate $10^{\circ}\text{C min}^{-1}$

AN ANISOTROPIC ANALOGUE OF SCHWARZSCHILD INTERIOR SOLUTION

S.K. Vaidya, V.J. Kaneria and V.H. Kyada

Department of Mathematics, Saurashtra University, Rajkot-360 005

Abstract

We present here an anisotropic version of Schwarzschild interior solution. The solution is matched with the Schwarzschild exterior solution at the boundary. The solution is interpreted as an exact relativistic model for a compact anisotropic star. The numerical estimates of various parameters are given and the physical features of the solution are briefly discussed.

Key words: General Relativity, Anisotropic fluid spheres.

PACS No. 04.20 jb

Introduction

The assumption of local isotropy is very usual in the astrophysical study of massive compact astronomical objects. However, the theoretical investigations of Ruderman (1972) and Canuto (1973) on more realistic stellar models indicate that stellar matter may be anisotropic at least in certain density ranges ($\rho < 10^{15} \text{ gcm}^{-3}$). According to them, the radial pressure may not be equal to the tangential pressure in such massive objects. No celestial body is composed of purely perfect fluid. Therefore it is very interesting to study the anisotropic fluid spheres in the frame work of general relativity. Existence of a solid core, presence of type-p superfluid or any other physical phenomena are responsible for anisotropic behavior. Our aim is not to study the ways of introducing anisotropy in the stellar matter but we are interested in the construction of exact relativistic models for anisotropic fluid spheres with physically reasonable behavior.

Bowers and Liang (1974) have discussed the possible importance of locally anisotropic equations of state for relativistic fluid spheres by generalizing the equations of hydrostatic equilibrium to include the effects of local anisotropy. Their study indicates that anisotropy-if present in the density range expected for relativistic stars (densities upto at least 10^{15} gcm^{-3}) may have non-negligible effect on such parameters as the maximum equilibrium mass and surface red shift. Consenza et al (1981), Bayin (1982), Krori et al (1984), Maharaj and Maartens (1989) and Gokharoo and Mehra (1993) have discussed different exact solutions of Einstein field equations. These solutions discussed various physical aspects of anisotropic fluid spheres. These solutions can be used as models of massive compact objects. Patel and Vaidya (1995) have obtained anisotropic analogue of Finch-Skea (1989)

An Anisotropic Analogue of...

It is easy to check that the Einstein field equation (2.2) along with (2.3) and (2.4) for the metric (2.1) reduce to the system of following equations (2.5) to (2.7).

$$8\pi\rho = \frac{1}{r^2} - e^{-\lambda} \left(\frac{1}{r^2} - \frac{\lambda'}{r} \right) \quad \dots \quad \dots \quad \dots \quad (2.5)$$

$$8\pi p_r = e^{-\lambda} \left(\frac{v'}{r} + \frac{1}{r^2} \right) - \frac{1}{r^2} \quad \dots \quad \dots \quad \dots \quad (2.6)$$

$$8\pi p_{\perp} = \frac{1}{4} e^{-\lambda} \left(2v'' + v'^2 - \lambda'v' + \frac{2}{r}(v' - \lambda') \right) \quad \dots \quad \dots \quad (2.7)$$

where the radial pressure P_r and tangential pressure P_{\perp} are given by

$$p_r = p + \frac{2S}{\sqrt{3}}, p_{\perp} = p - \frac{S}{\sqrt{3}}, S = \frac{1}{\sqrt{3}}(p_r - p_{\perp}) \quad \dots \quad \dots \quad (2.8)$$

Here overhead dash denotes differentiation w.r.t. r .

With the help of (2.6) and (2.7) one can easily check that

$$-16\pi\sqrt{3}Se^{\lambda} = v'' + \frac{1}{2}v'^2 - \frac{1}{r}(v' + \lambda') - \frac{1}{2}\lambda'v' + \frac{2}{r^2}(e^{\lambda} - 1) \quad \dots \quad \dots \quad (2.9)$$

$$\text{Substituting } e^{\frac{v}{2}} = F, r^2 = x \quad (2.10)$$

the equation (2.9) can be expressed in the form

$$4xe^{-\lambda} \frac{d^2F}{dx^2} + 2x \frac{d}{dx}(e^{-\lambda}) \frac{dF}{dx} + \left[\frac{1}{x}(1 - e^{-\lambda}) + \frac{d}{dx}(e^{-\lambda}) + 8\pi\sqrt{3}S \right] F = 0 \quad \dots \quad (2.11)$$

Let us assume that a solution of (2.11) for the isotropic fluid sphere is known. Let us denote this solution by $\lambda = \lambda_0(r)$ and $v = v_0(r)$. It is easy to verify that $\lambda = \lambda_0(r)$ and

$F = e^{\frac{v_0}{2}} + \alpha + \beta x$ satisfy the differential equation (2.11) provided the anisotropy function S is given by

$$-8\pi\sqrt{3}SF = \alpha \left[\frac{1}{x}(1 - e^{-\lambda_0}) + \frac{d}{dx}(e^{-\lambda_0}) \right] + \beta \left[\frac{1}{x}(1 - e^{-\lambda_0}) + 3 \frac{d}{dx}(e^{-\lambda_0}) \right] \dots \quad (2.12)$$

S.K. Vaidya, V.J. Kaneria and V.H. Kyada

where α and β are arbitrary constants. The choice of these constants depends upon the physical requirements of the solution. It is physically required that $S=0$ at the centre. i.e. $r=0$. If the function S is given by (2.12), then we get an anisotropic fluid sphere solution

from an isotropic fluid sphere solution by simply replacing $e^{\frac{v_0}{2}}$ by $e^{\frac{v_0}{2} + \alpha + \beta x}$. The physical parameters ρ , P_r and P_\perp can be obtained from (2.5), (2.6) and (2.12).

It can be easily proved that a perfect fluid (isotropic) solution with the metric (2.1) is conformally flat if and only if

$$\frac{1}{x}(1 - e^{-\lambda_0}) + \frac{d}{dx}(e^{-\lambda_0}) = 0 \quad \dots \quad \dots \quad \dots \quad (2.13)$$

In this case, the anisotropic function S is given by

$$-8\pi\sqrt{3}SF = 2\beta x - \frac{d}{dx}(e^{-\lambda_0}) \quad \dots \quad \dots \quad \dots \quad (2.14)$$

From (2.14), it is obvious that the anisotropic fluid generalizations of the isotropic conformally flat fluid sphere solutions can be obtained by the above method only if $\beta \neq 0$.

Any physically acceptable anisotropic fluid sphere solution must satisfy the following boundary conditions.

(i) At the surface of the sphere ($r=a$), our interior solution should match with the Schwarzschild exterior solution represented by the metric

$$ds^2 = \left(1 - \frac{2m}{r}\right) dt^2 - \left(1 - \frac{2m}{r}\right)^{-1} dr^2 - r^2(d\theta^2 + \sin^2\theta d\phi^2) \quad \dots \quad \dots \quad \dots \quad (2.15)$$

where m is the total of the sphere which is constant.

(ii) The radial pressure P_r at the centre should remain finite and it must vanish at the boundary $r = a$ of the sphere.

In the immediate section, we shall apply the above technique to Schwarzschild (1916) interior solution to get corresponding anisotropic analogue.

An Anisotropic Analogue of...

An Anisotropic Analogue of Schwarzschild Interior Solution

The metric for the Schwarzschild (1916) interior solution is given by

$$ds^2 = \left(A - B\sqrt{1 - \frac{r^2}{R^2}} \right)^2 dt^2 - \frac{dr^2}{1 - \frac{r^2}{R^2}} - r^2(d\theta^2 + \sin^2 \theta d\phi^2) \dots \dots \quad (3.1)$$

where R , A , B are arbitrary constants. For notations and standard form of this metric, we follow Adler et al (1975). According to technique and notations developed in preceding Section, the metric potentials $\nu_0(r)$ and $\lambda_0(r)$ for the metric (3.1) are given by

$$e^{\lambda_0} = \frac{1}{1 - \frac{r^2}{R^2}} ; e^{\frac{\nu_0}{2}} = \left(A - B\sqrt{1 - \frac{r^2}{R^2}} \right) \dots \dots \dots \quad (3.2)$$

and metric density is given by

$$8\pi\rho_0 = \frac{3}{R^2} \dots \dots \dots \quad (3.3)$$

It is well known that the space time of Schwarzschild interior solution is conformally flat. So we should take $\beta \neq 0$. For simplicity, we should put $\alpha = 0$. In this case the functions λ, ν and ρ satisfying the equation (2.9) are given by

$$e^\lambda = \frac{1}{1 - \frac{r^2}{R^2}} ; e^{\frac{\nu}{2}} = \left(A - B\sqrt{1 - \frac{r^2}{R^2}} \right) + \beta r^2 \dots \dots \dots \quad (3.4)$$

$$-8\pi\sqrt{3}S = \frac{2\beta x}{R^2 F} \dots \dots \dots \quad (3.5)$$

Here β is an arbitrary constant. It is clear that S vanishes at the centre $r = 0$. The radial pressure p_r and density ρ are given by

$$8\pi\rho = \frac{3}{R^2} \dots \dots \dots \quad (3.6)$$

$$8\pi p_r = \frac{3B\sqrt{1-\frac{r^2}{R^2}} - A + 4\beta R^2\left[1-\frac{r^2}{R^2}\right] - \beta r^2}{R^2\left[A - B\sqrt{1-\frac{r^2}{R^2}} + \beta r^2\right]} \dots \dots \dots \quad (3.7)$$

The above solution for anisotropic fluid sphere must satisfy the boundary conditions of section-2 at the boundary $r = a$. These boundary conditions specify the constants m , A and B as

$$m = \frac{a^3}{2R^2} \dots \dots \dots \quad (3.8)$$

$$A = \frac{3}{2}\sqrt{1-\frac{a^2}{R^2}} + 2\beta\left[a^2 - R^2\sqrt{1-\frac{a^2}{R^2}}\right] \dots \dots \dots \quad (3.9)$$

$$B = \frac{1}{2} + \frac{\beta}{\sqrt{1-\frac{a^2}{R^2}}}\left[a^2 - 2R^2\sqrt{1-\frac{a^2}{R^2}}\right] \dots \dots \dots \quad (3.10)$$

When $\beta = 0$, the anisotropy of pressure disappears and we recover the usual Schwarzschild interior solution.

Discussion

We shall now discuss some physical features of the above solution. This solution is with constant density which is given by equation (3.6). The central pressure P_{r_0} for the above solution is given by

$$8\pi P_{r_0} = \frac{3B - A + 4\beta r^2}{R^2(A - B)} \dots \dots \dots \quad (4.1)$$

OR

$$8\pi P_{r_0} = \frac{3\left[B - \frac{1}{3}A + \frac{4}{3}\beta R^2\right]}{R^2(A - B)} \dots \dots \dots \quad (4.2)$$

An Anisotropic Analogue of...

The physical requirements $p_{r_0} \geq 0$ and $\rho > p_{r_0}$ demand

$$f(A, B) \geq 0; 1 - f(A, B) \geq 0 \quad \dots \quad \dots \quad \dots \quad (4.3)$$

where $f(A, B)$ is defined by

$$f(A, B) = \frac{3 \left[B - \frac{1}{3} A + \frac{4}{3} \beta R^2 \right]}{A - B} \quad \dots \quad \dots \quad \dots \quad (4.4)$$

If $\frac{a}{R}$ and β is given then A and B can be computed from equations (3.9) and (3.10)

respectively. For $\beta = 0.1$ and $\beta = 1$ and for various values of a and R satisfying $0 < \frac{a}{R} < 1$,

the values of $f(A, B)$ and $1 - f(A, B)$ are abulated in the following two tables.

Table 1: For $\beta = 0.1$

a/R	$f(A, B)$	$1 - f(A, B)$
0.05	0.000614	0.999386
0.10	0.002302	0.997697
0.15	0.005005	0.994994
0.20	0.008805	0.991194
0.25	0.014077	0.985922
0.30	0.020732	0.979267
0.35	0.029092	0.970907
0.40	0.039503	0.960496
0.45	0.052423	0.947577
0.50	0.068529	0.931470
0.55	0.088810	0.911189
0.60	0.114791	0.885208
0.65	0.148948	0.851051
0.70	0.195614	0.804385
0.75	0.262905	0.737095
0.80	0.369063	0.630937
0.85	0.564062	0.435937
0.90	1.060360	-0.060360

Table 2: For $\beta = 0.1$

a/R	$f(A, B)$	$1 - f(A, B)$
0.05	0.000536	0.999464
0.10	0.002125	0.997875
0.15	0.004813	0.995187
0.20	0.008681	0.991319
0.25	0.013851	0.986149
0.30	0.020494	0.979506
0.35	0.028849	0.971151
0.40	0.039924	0.960076
0.45	0.052154	0.947846
0.50	0.068244	0.931756
0.55	0.088506	0.911494
0.60	0.114465	0.885535
0.65	0.148590	0.851410
0.70	0.195174	0.804826
0.75	0.262437	0.737563
0.80	0.368486	0.631514
0.85	0.563270	0.436730
0.90	1.058870	-0.058870

S.K. Vaidya, V.J. Kaneria and V.H. Kyada

From the above tables we can see that for $\beta = 0.1$ and $\beta = 1$, the function $f(A, B)$ is an increasing function of a/R . From the tables it is clear that for $a/R=0.9$, the central density becomes less than the central pressure. This is not desirable. Therefore for $\beta = 0.1$ and $\beta = 1$, the range of validity of our solution is $0 \leq a/R \leq 0.85$.

Conclusion

Thus, anisotropic version of Schwarzschild interior solution is obtained. Switching of the anisotropy from this solution we can recover the isotropic solution is the salient feature of our solution. Various numerical parameters are also estimated for the discussion of physical significance of the solution.

References

1. Bayin, S.S., Phys. Rev. D. **26**, 6 (1982)
2. Bowers, R.L. & Liang, E.P.T., Astro. Phys. J. **188**, 657 (1974)
3. Canuto, V., "Neutron Stars General Review" presented at Solvey conference on Astrophysics and Gravitation, Brussels (1973)
4. Consenza, M., Herrera, L., Esculpi, M. and Witten, L., J. Math. Phys., **22**, 118 (1981)
5. Finch, M.R. and Skea, J.E.F., Class. Quantum. Grav., **6**, 467 (1989)
6. Gokaroo, M.K. and Mehra, A.L., Gen. Rel. Grav., **26**, 1 (1993)
7. Krori, K.D., Borgohain, P. and Devi, R., Can. J. of Phys., **62**, 239 (1984)
8. Maharaj, S.D. and Maarten, R.L., Gen. Rel. Grav., **21**, 899 (1989)
9. Patel, L.K. and Vaidya, S.K., Math. Today, **43**, 23 (1995)
10. Patel, L.K. and Vaidya, S.K., APH. N.S., **3**, 177 (1996)
11. R. Adler, M. Bazin, M. Schiffer, Introduction to General Relativity McGraw-Hill-Kogakusha Ltd. (1975)
12. Ruderman, R., Ann. Rev. Astron. Astrophys., **10**, 427 (1972)
13. Vaidya, P.C. and Tikekar R., J. Astrophys. Astron. **3**, 325 (1982)

BIANCHI TYPE I BULK VISCOUS STRING DUST COSMOLOGICAL MODEL IN GENERAL RELATIVITY

Raj Bali and Anjali

Department of Mathematics,
University of Rajasthan, Jaipur-302 004

Abstract

Bianchi Type I Bulk viscous string dust cosmological model is investigated followed by technique used by Letelier [1979,1983]. To get a determinate model, we have assumed a condition $\sigma_1^1 \propto \theta$ which leads to $A = (BC)^n$ where σ_1^1 is the eigen value of shear tensor (σ_i^j) and θ the expansion in the model. The behaviour of the model in presence and absence of bulk viscosity is discussed. The physical and geometrical features of the model are also discussed.

Introduction

It is conjectured that material distribution behaves like a viscous fluid in early phase of the evolution of the universe (Ellis [1]). Misner [2] has studied the effect of viscosity on the evolution of cosmological models. Heller and Klimek [3] have investigated viscous fluid cosmological models without initial singularity. They have shown that the introduction of bulk viscosity effectively removes the initial singularity. Banerjee et al [4] have investigated Bianchi Type I cosmological models with bulk and shear viscosity. Bali and Jain [5,6] have investigated Bianchi Type I expanding and shearing viscous fluid cosmological models, in which coefficient of shear viscosity is proportional to the rate of expansion in the model and free gravitational field is Petrov Type ID and non-degenerate. Mohanty and Pradhan [7] investigated Robertson-Walker cosmological model with bulk viscosity and equation of state $p = (\gamma - 1)\rho$ where $0 \leq \gamma \leq 2$.

Cosmic strings play a significant role during an early stage of evolution of the universe (Kibble [8]) and give rise to density perturbation which leads to galaxy formations (Zel'dovich [9]). The general relativistic treatment of strings was initiated by Letelier [10,11] and Stachel [12]. Banerjee et al [13] have investigated an axially symmetric Bianchi Type I string dust cosmological model in presence and absence of magnetic field. Krori et al [14], Chakraborty and Nandy [15] have investigated Letelier strings cosmological models for Bianchi Type II, VIII and IX space-times. Chakraborty [16] has also investigated a class of cosmological solution of massive strings in Bianchi Type IX space-time using a supplementary condition $a = \alpha b^n$ where a, b are functions of t -alone and α, n are constants.

Tikekar and Patel [17] have investigated massive string cosmological model for Bianchi Type III space-time in the presence of magnetic field. Tikekar and Patel [18] have also investigated some exact solutions of string cosmology in Bianchi Type VI₀ space-time. Patel et al [19] investigated the integrability of cosmic strings in the context of Bianchi Types II, VIII & IX space-times. Roy and Banerji [20] have investigated some LRS Bianchi Type II string cosmological models in General Relativity. Bali and Singh [21] investigated Bianchi Type V bulk viscous fluid string dust cosmological model in General Relativity where coefficient of bulk viscosity (ζ) is inversely proportional to the expansion (θ) in the model. Bali and Dave [22] investigated Bianchi Type IX string cosmological model using the condition $\rho = \lambda$ and $a = e^{\alpha t}$ where ρ is the energy density, λ the string tension density, a is the metric potential and α is a constant. Bali and Dave [23] have also investigated Bianchi Type IX bulk viscous fluid string dust cosmological model assuming the condition $a = b^n$ and $\zeta\theta = \text{constant}$ where a and b are metric potentials, ζ the coefficient of bulk viscosity, θ the expansion in the model and n is a constant. Recently Bali and Upadhaya [24] have investigated an LRS Bianchi Type I bulk viscous fluid string dust cosmological model in which coefficient of shear viscosity is proportional to the rate of expansion in the model which leads to $A = \alpha B^n$, α and n are constants, A and B are metric potentials.

In this paper, we have investigated Bianchi Type I bulk viscous fluid string dust cosmological model assuming the condition $\sigma_1^1 \propto \theta$ which leads to $A = (BC)^n$ where A, B, C are metric potentials, n is constant, σ_1^1 is the eigen value of shear tensor (σ_i^j) and θ the expansion in the model. The physical and geometrical aspects of the model together with nature of the model in presence and absence of bulk viscosity are discussed.

We consider an Bianchi Type I metric in the form

$$ds^2 = - dt^2 + A^2 dx^2 + B^2 dy^2 + C^2 dz^2 \quad \dots (1.1)$$

where A, B and C are functions of t -alone.

The energy momentum T_i^j for bulk viscous string dust is given by Letelier [11], Landau and Lifshitz [25]

$$T_i^j = \varepsilon v_i v^j - \lambda x_i x^j - \zeta v_{;\ell}^{\ell} (g_i^j + v_i v^j) \quad \dots (1.2)$$

together with

$$v^i v_i = - x^i x_i = - 1 \quad \dots (1.3)$$

Bianchi Type I Bulk Viscous...

and

$$v^i x_i = 0 \quad \dots (1.4)$$

where $\varepsilon = \varepsilon_p + \lambda$, is the rest energy density for a cloud of strings, ε_p is the particle density, λ is the string tension density, v^i the flow velocity vector, x^i the direction of strings and ζ the coefficient of bulk viscosity.

The non-vanishing components of energy momentum tensor are given by

$$T_1^1 = -\lambda - \zeta v_{;\ell}^\ell \quad \dots (1.5)$$

$$T_2^2 = T_3^3 = -v_{;\ell}^\ell \quad \dots (1.6)$$

$$T_4^4 = -\varepsilon \quad \dots (1.7)$$

Using units $\frac{G}{C^4} = 1$, the Einstein field equation

$$R_i^j - \frac{1}{2} R g_i^j = -8 \pi T_i^j$$

for the metric (1.1) leads to

$$\frac{B_{44}}{B} + \frac{C_{44}}{C} + \frac{B_4 C_4}{BC} = 8 \pi (\lambda + \zeta v_{;\ell}^\ell) \quad \dots (1.8)$$

$$\frac{A_{44}}{A} + \frac{C_{44}}{C} + \frac{A_4 C_4}{AC} = 8 \pi \zeta v_{;\ell}^\ell \quad \dots (1.9)$$

$$\frac{A_{44}}{A} + \frac{B_{44}}{B} + \frac{A_4 B_4}{AB} = 8 \pi \zeta v_{;\ell}^\ell \quad \dots (1.10)$$

$$\frac{A_4 B_4}{AB} + \frac{A_4 C_4}{AC} + \frac{B_4 C_4}{BC} = 8 \pi \varepsilon \quad \dots (1.11)$$

Raj Bali and Anjali

where the suffix '4' after A, B, C denotes ordinary differentiation with respect to t. Equations (1.8)–(1.11) are four equations in five unknowns A, B, C, ϵ and λ . To get a determinate solution, we assume two extra conditions.

First we assume that the rest energy density of the system of strings (ϵ) is equal to the tension density of the system of strings (λ) i.e. string dust condition leads to

$$\epsilon = \lambda \quad \dots (1.12)$$

and a condition $\sigma_1^1 \alpha \theta$ which leads to

$$A = (BC)^n \quad \dots (1.13)$$

Where proportionality constant is taken as unity.

Equation (1.9) and (1.10) lead to

$$\frac{C_{44}}{C} - \frac{B_{44}}{B} = \frac{A_4}{A} \left(\frac{B_4}{B} - \frac{C_4}{C} \right) \quad \dots (1.14)$$

Using (1.13), equation (1.14) leads to

$$C^2 \left(\frac{B}{C} \right)_4 = \frac{L}{(BC)^n} \quad \dots (1.15)$$

where L is the constant of integration.

Putting $BC = \mu$, $\frac{B}{C} = \nu$ in equation (1.15), we have

$$\frac{\nu_4}{\nu} = \frac{L}{\mu^{n+1}} \quad \dots (1.16)$$

From equations (1.8) and (1.11) together with the condition (1.12), we have

$$\frac{B_{44}}{B} + \frac{C_{44}}{C} - \frac{A_4 B_4}{AB} - \frac{A_4 C_4}{AC} = 8\pi\zeta \left(\frac{A_4}{A} + \frac{B_4}{B} + \frac{C_4}{C} \right) \quad \dots (1.17)$$

where $v_{;\ell}^{\ell} = \frac{A_4}{A} + \frac{B_4}{B} + \frac{C_4}{C}$

Using condition (1.13) in (1.17), we have

$$\frac{B_{44}}{B} + \frac{C_{44}}{C} - \frac{n B_4^2}{B^2} - \frac{n C_4^2}{C^2} - 2n \frac{B_4 C_4}{BC} = 8\pi\zeta(n+1) \left(\frac{B_4}{B} + \frac{C_4}{C} \right) \quad \dots (1.18)$$

Bianchi Type I Bulk Viscous...

which leads to

$$\frac{\mu_{44}}{\mu} - \frac{(2n+1)}{2} \frac{\mu_4^2}{\mu^2} + \frac{v_4^2}{2v^2} = 8\pi\zeta(n+1) \frac{\mu_4}{\mu} \quad \dots (1.19)$$

where $BC = \mu$ and $\frac{B}{C} = v$.

From equations (1.16) and (1.19), we have

$$\frac{\mu_{44}}{\mu} - \frac{(2n+1)}{2} \frac{\mu_4^2}{\mu^2} + \frac{L^2}{2\mu^{2n+2}} = 8\pi\zeta(n+1) \frac{\mu_4}{\mu} \quad \dots (1.20)$$

which leads to

$$f f' - \left(\frac{2n+1}{2} \right) \frac{f^2}{\mu} - 8\pi\zeta(n+1) f + \frac{L^2}{2\mu^{2n+1}} = 0 \quad \dots (1.21)$$

where $\mu_4 = f(\mu)$, $f' = \frac{df}{d\mu}$.

In special case if $L = 0$, from equation (1.16), we have

$$\frac{v_4}{v} = 0$$

Thus $v = \alpha$ (constant) ... (1.22)

Equation (1.21) leads to

$$f' - \left(\frac{2n+1}{2} \right) \frac{f}{\mu} = 8\pi\zeta(n+1) \quad \dots (1.23)$$

which leads to

$$f = \frac{-16\pi(n+1)\zeta\mu}{(2n-1)} + N\mu^{\frac{2n+1}{2}} \quad \dots (1.24)$$

where N is constant of integration.

Raj Bali and Anjali

Which on integration leads to

$$\mu = \left[\frac{16 \pi (n+1) \zeta}{N (2n-1) (1 - M e^{8\pi(n+1)\zeta t})} \right]^{\frac{2}{2n-1}} \quad \dots (1.25)$$

where M is the constant of integration.

Using equations (1.22) and (1.25), the metric (1) leads to

$$\begin{aligned} ds^2 = & - dt^2 + \left[\frac{16 \pi (n+1) \zeta}{N (2n-1) (1 - M e^{8\pi(n+1)\zeta t})} \right]^{\frac{4n}{2n-1}} dx^2 \\ & + \alpha \left[\frac{16 \pi (n+1) \zeta}{N (2n-1) (1 - M e^{8\pi(n+1)\zeta t})} \right]^{\frac{2}{2n-1}} dy^2 \\ & + \frac{1}{\alpha} \left[\frac{16 \pi (n+1) \zeta}{N (2n-1) (1 - M e^{8\pi(n+1)\zeta t})} \right]^{\frac{2}{2n-1}} dz^2 \quad \dots (1.26) \end{aligned}$$

Using the transformation

$$1 - M e^{8\pi(n+1)\zeta t} = \sin \zeta T,$$

the metric (1.26) leads to

$$\begin{aligned} ds^2 = & - \frac{(1 + \sin \zeta \tau)^2 d\tau^2}{64\pi^2 (n+1)^2 \cos^2 \zeta \tau} + \left(\frac{16 \pi (n+1) \zeta}{N (2n-1) \sin \zeta \tau} \right)^{\frac{4n}{2n-1}} dX^2 \\ & + \left(\frac{16 \pi (n+1) \zeta}{N (2n-1) \sin \zeta \tau} \right)^{\frac{2}{2n-1}} dY^2 + \left(\frac{16 \pi (n+1) \zeta}{N (2n-1) \sin \zeta \tau} \right)^{\frac{2}{2n-1}} dZ^2 \quad \dots (1.27) \end{aligned}$$

In the absence of viscosity, the metric (1.27) reduces to

$$ds^2 = - \frac{d\tau^2}{64\pi^2 (n+1)^2} + \left(\frac{16 \pi (n+1)}{N (2n-1) \tau} \right)^{\frac{4n}{2n-1}} dX^2$$

Bianchi Type I Bulk Viscous...

$$+ \left(\frac{16 \pi (n+1)}{N (2n-1) \tau} \right)^{\frac{2}{2n-1}} dY^2 + \left(\frac{16 \pi (n+1)}{N (2n-1) \tau} \right)^{\frac{2}{2n-1}} dZ^2 \quad \dots (1.28)$$

Some Physical and Geometrical Features

The density ϵ for the model (1.27) is given by

$$8 \pi \epsilon = 8 \pi \lambda = \frac{64 (4n+1) \pi^2 (n+1)^2 \zeta^2 (1 - \sin \zeta \tau)^2}{(2n-1)^2 \sin^2 \zeta \tau} \quad \dots (2.1)$$

The expansion θ , shear (σ) and the spatial volume (R^3) for the model (1.27) are given by

$$\theta = \frac{16 \pi (n+1)^2 \zeta (1 - \sin \zeta \tau)}{(2n-1) \sin \zeta \tau} \quad \dots (2.2)$$

$$\sigma_1^1 = \frac{16 \pi (n+1) \zeta (1 - \sin \zeta \tau)}{3 \sin \zeta \tau} \quad \dots (2.3)$$

$$\sigma_2^2 = \sigma_3^3 = \frac{-8 \pi (n+1) \zeta (1 - \sin \zeta \tau)}{3 \sin \zeta \tau} \quad \dots (2.4)$$

$$\sigma_4^4 = 0 \quad \dots (2.5)$$

$$\sigma^2 = \frac{64}{3} \frac{\pi^2 (n+1) \zeta^2 (1 - \sin \zeta \tau)^2}{\sin^2 \zeta \tau} \quad \dots (2.6)$$

$$R^3 = \left(\frac{16 \pi (n+1) \zeta}{N (2n-1) \sin \zeta \tau} \right)^{\frac{2n+2}{2n-1}} \quad \dots (2.7)$$

3. Discussion

The model (1.27) starts with a big-bang at $\tau = 0$ and the expansion in the model decreases

as time increases. However, when $\tau = \frac{\pi}{2\zeta}$ and $n = -1$ then expansion in the model stops.

Raj Bali and Anjali

Also $\varepsilon \rightarrow \infty$ when $\tau \rightarrow 0$ and $\varepsilon \rightarrow 0$ when $\tau \rightarrow \frac{\pi}{2\zeta}$. The spatial volume is finite when $\tau = \frac{\pi}{2\zeta}$ and at $\tau = 0$, it is infinite when $n+1 > 0$. Hence the model (1.27) is anisotropic space-time.

However, the model isotropizes at $\tau = \frac{\pi}{2\zeta}$. The model (1.27) has Point Type singularity (MacCallum [25]) at $\tau = 0$.

In the absence of bulk viscosity i.e. when $\zeta = 0$, then the energy density (ε), string tension density (λ), the expansion (θ), the components of shear tensor σ_i^j and the spatial volume (R^3) are given by

$$8\pi\varepsilon = 8\pi\lambda = \frac{64(4n+1)\pi^2(n+1)^2}{(2n-1)^2\tau^2} \quad \dots (3.1)$$

$$\theta = \frac{16\pi(n+1)^2}{(2n-1)\tau} \quad \dots (3.2)$$

$$\sigma_1^1 = \frac{16\pi(n+1)}{3\tau} \quad \dots (3.3)$$

$$\sigma_2^2 = \sigma_3^3 = -\frac{8\pi(n+1)}{3\tau} \quad \dots (3.4)$$

$$\text{Thus } \sigma^2 = \frac{1}{2} \sigma_{ij} \sigma^{ij} = \frac{64}{3} \frac{\pi^2(n+1)^2}{\tau^2} \quad \dots (3.5)$$

$$\text{and } R^3 = \left[\frac{16\pi(n+1)}{3(2n-1)\tau} \right]^{\frac{2n+2}{2n-1}} \quad \dots (3.6)$$

The model (1.28) starts with a big-bang at $\tau = 0$ and the expansion in the model decreases as time increases. The energy density $\varepsilon \rightarrow \infty$ when $\tau \rightarrow 0$ and $\varepsilon \rightarrow 0$ when $\tau \rightarrow \infty$. The

spatial volume is finite at $\tau = 0$, it is infinite when $n+1 > 0$. Since $\lim_{\tau \rightarrow \infty} \frac{\sigma}{\theta} \neq 0$. The model

(1.28) in the absence of bulk viscosity, represents anisotropic space-time. However the model isotropizes for large values of τ . The model has Point Type singularity (MacCallum[26]) at $\tau=0$.

Bianchi Type I Bulk Viscous...

RB expresses his sincere thanks to the Department of Mathematics for visit under DRS-SAP and facilities in its NBHM Regional Library.

References

1. Ellis, G.F.R., General Relativity and Cosmology ed. R.K.Sachs, Academic Press, London (1971), p.124
2. Misner, C.W., Nature, **214**, 40. (1967), Misner, C.W., Astrophysical Journal, **151**, 431 (1968)
3. Heller, M. and Klimek, Z., Astrophys. & Space-Science, **33**, 37 (1975)
4. Banerjee, A.; Dutta Chaudhury, S.B. and Sanyal, A.K., J. Math. Phys. **26**, 3010 (1985)
5. Bali, R. and Jain, D.R., Astrophys. and Space-Science, **139**, 175 (1987)
6. Bali, R. and Jain, D.R., Astrophys. and Space-Science, **141**, 207 (1988)
7. Mohanty, G. and Pradhan, B.D, Astrophys. and Sp-Science, **181**, 1 (1991)
8. Kibble, T.W.B., J. Phys. **A9**, 1387 (1976)
9. Zel'dovich, Ya.B., Mon. Not. R. Astron. Soc. **192**, 663 (1980)
10. Letelier, P.S., Phys. Rev. **D 20**, 1294 (1979)
11. Letelier, P.S., Phy. Rev. **D28**, 2414 (1983)
12. Stachel, J., Phys. Rev. **D21**, 2171 (1980)
13. Banerjee, A.; Sanyal, A.K. and Chakraborty, S., Pramana – J. Phys. **34**, 1 (1990)
14. Krori, K.D.; Chaudhuri, T.; Mahanta, C.R. and Mazumdar, A., Gen. Relativity and Gravitation, **22**, 123 (1990)
15. Chakraborty, S. and Nandy, G.C., Astrophys. & Space-Science, **198**, 299. (1992)
16. Chakraborty, S., Astrophys. & Space-Science, **180**, 293 (1991)
17. Tikekar, R. and Patel, L.K., Gen. Rel. & Grav., **24**, 397 (1992)
18. Tikekar, R. and Patel, L.K., Pramana – J. Phys. (Ind.) **46**, 483 (1994)
19. Patel, L.K.; Maharaj, S.D. and Leach, P.G., Pramana – J. Phys. (Ind.), **46**, 331 (1996)
20. Roy, S.R. and Banerji, S.K., Class. Quantum Gravity, **11**, 1943 (1995)
21. Bali, Raj and Singh, D.K., Astrophys. & Space-Science, **288**, 517 (2003)
22. Bali, Raj and Dave, S., Pramana – J. Phys. (Ind.), **56**, 4 (2001)
23. Bali, Raj and Dave, S., Astrophys. & Space-Science, **288**, 503 (2003)
24. Bali, R. and Upadhaya, R.D., Astrophys. & Space-Science **288**, 287 (2003)
25. Landau, L.D. and Lifshitz, E.M., Fluid Mechanics, Pergamon Press, Oxford, Vol.6, p.505 (1963)
26. MacCallum, M.A.H., Comm. Math. Phys. **20**, 57 (1971)

MICROSTRUCTURAL ANALYSIS OF ZIRCONIUM TRISELENIDE SINGLE CRYSTALS

K.R. Patel, R.D. Vaidya, M.S. Dave, A.J. Patel and S.G. Patel

Department of Physics, Sardar Patel University,
Vallabh Vidyanagar

Abstract

The zirconium triselenide ($ZrSe_3$) single crystal has been grown by chemical vapour transport technique using iodine as a transporting agent. The optimum conditions for the growth of this crystal are given. The stoichiometry of the grown crystals was confirmed on the basis of energy dispersive analysis by X-ray (EDAX) and structural characterization was accomplished by X-ray diffraction (XRD) studies. The lattice parameters obtained from the XRD analysis were $a = 5.45 \text{ \AA}$, $b = 3.74 \text{ \AA}$ and $c = 9.44 \text{ \AA}$. These crystals were found to possess monoclinic, layered structure. The X-ray density was found to be 5.63 gm/cc and volume was calculated about 193.50 \AA^3 . The optical band gap of as grown crystals have been calculated with the help of optical absorption spectra in the range of $700 - 1400 \text{ nm}$.

Keywords: $ZrSe_3$ single crystal, EDAX, XRD, optical band gap

Introduction

The zirconium triselenide $ZrSe_3$ is a member of transition metal trichalcogenide, which possesses chain like structure belonging to the crystal space group $P2_1/m$ [1]. The linear chain of metal atoms is parallel to the crystallographic b-axis, which is the growth axis. Six chalcogen atoms surround each metal atom forming distorted trigonal prisms. The crystals were grown in the form of layers, which run parallel to the b-axis, and each chain in the layer are displaced from the neighboring chain by half of the unit cell along the b-axis. Resistivity, Hall coefficient and thermo electric power measurement of $ZrSe_3$ single crystals along the chain axis have been carried out in the temperature range $200 \text{ K} - 400 \text{ K}$ [2].

The ZrS_3 and $ZrSe_3$ exhibit a layer like semi conducting behavior [2-7]. At lowest temperature the $ZrSe_3$ measurements can be analyzed in terms of the familiar Debye T^3 law yielding characteristic Debye temperature at absolute zero $\theta_D = 110 \pm 2 \text{ K}$ in satisfactory arrangement with the value extracted from the available experimentally sound velocities. In contrast the ZrS_3 measurements do not behave according to the Debye law [8]. ZrS_xSe_{3-x} exhibit continuous regions of solid solubility. Diffuse reflectance measurement shows that ZrS_xSe_{3-x} exhibit semiconductor [9]. The (0 0 1) Van der Waals surfaces of $ZrSe_3$ and $ZrTe_3$ single crystals were studied by scanning tunneling microscopy at room temperature. It is shown that both the semiconducting $ZrSe_3$ and the semimetallic $ZrTe_3$

Microstructural Analysis of Zirconium Triselenide...

crystals show charge instability between various selenium/tellurium chains forming the surface [10]. The X-ray diffraction pattern of ZrS_3 shows the monoclinic cell with the lattice constants $a = 5.128 \text{ \AA}$, $b = 3.611 \text{ \AA}$, $c = 9.012 \text{ \AA}$, $\beta = 97.13^\circ$ [11]. The development of stresses by variation in high temperature of the two zones involved, resulting into slip lines and vapour inclusions, might possibly lead to generation of favorable screw dislocation sites for ZrS_3 single crystals [12].

In this paper, we report the growth of $ZrSe_3$ single crystals using chemical vapour transport technique with iodine as a transporting agent in order get single crystals with maximum dimensions. The structural characterization is carried out and results are discussed in detail.

Experiments

The single crystals of zirconium triselenide ($ZrSe_3$) have been grown by chemical vapour transport technique using iodine as a transporting agent. A 5 gm mixture of Zr (Purity: 97%) and Se (99.99%) was filled in the dried quartz ampoule. The quantity of 2 mg/cc iodine of the ampoule volume was sealed in the thin capillaries and placed in the ampoule as transporting agent. Then the ampoule was sealed at the pressure of 10^{-5} torr. The sealed ampoule was introduced into two-zone furnace at a constant reaction temperature to obtain the charge of $ZrSe_3$. The charge so prepared was rigorously shaken to ensure proper mixing of the constituents and kept in quartz ampoule. Then the ampoule was sealed at the pressure of 10^{-5} torr. The sealed ampoule was again placed in furnace under appropriate condition to obtain single crystals of $ZrSe_3$. The optimum conditions for growth of large size layered single crystals are as shown in Table 1. Fig. 1 shows the photograph of as grown crystals.

The compositions of the grown crystals were checked with the help of energy dispersive analysis by X-ray (EDAX). The energy dispersive spectra for determining the chemical composition of grown sample of $ZrSe_3$ single crystals is shown in fig. 2 and their results are shown in Table 2. X-ray diffraction (XRD) study was performed for the structural characterization. The X-ray diffractograms were obtained with Philips X-ray diffractometer (model:PW1820) employing CuK_α radiation. The microstructure study was accomplished with the help of computer aided optical zoom microscope (model: Axiotech 100 manufactured by Carl Zeiss, Germany).

The absorption spectra were obtained using UV-VIS-NIR DK 2A spectrophotometer in the range of 700 – 1400 nm. All measurements were taken at room temperature with the incident beam normal to the basal plane i.e. along the c-axis of the as grown flakes. The electrical band gap i.e. direct as well as indirect band gap of the grown crystals was found to be 1.48eV and 1.1eV respectively.

Results and Discussion

The single crystals of $ZrSe_3$ were grown by chemical vapour transport technique. The crystal structure of $ZrSe_3$ crystals is monoclinic with the space group $P2_1/m$. The X-ray diffractogram obtained for $ZrSe_3$ is shown in fig. 3. The pattern consists of well-defined sharp diffraction lines, indicating good crystallinity of the specimen. The lattice parameters (a, b and c), unit cell volume (V) and X-ray density (ρ) determined from the X-ray diffractograms are presented in Table 3, which are very well matched with the values obtained by Leif Bratts and others [13, 15, 16, 17].

The XRD data obtained for $ZrSe_3$ were used for the estimation of particle size using Scherrer's formula given by Srivastava [14],

$$\text{Thickness } t = \frac{K \lambda}{\beta \cos \theta}$$

where t is the crystallite (thickness) size as measured perpendicular to the reflecting plane, K the Scherrer constant whose value is taken to be unity assuming the particles to be spherical, λ the wave length of X-ray radiation, β the half intensity which is measured in radians and θ is the Bragg angle. (h k l) values corresponding to prominent reflection d-values, peak width, peak intensities and particle size for $ZrSe_3$ single crystals are shown in Table 4. The micrographs taken from the surfaces of the as grown single crystals of the $ZrSe_3$ is shown in fig. 4 which shows like layered screw dislocation.

Conclusion

- ❖ The chemical (iodine) vapour transport (CVT) technique is most suitable for the growth of large size; needle shaped layered single crystals of $ZrSe_3$.
- ❖ EDAX analysis of the grown samples has shown that stoichiometry is nearly preserved in the as grown crystals of the said compounds.
- ❖ X-ray diffraction analysis of the crystals have shown that the structure of $ZrSe_3$ is monoclinic layered.
- ❖ $ZrSe_3$ possesses layer type crystal structure, which can exhibit screw dislocation.

References

1. Furuseth S, Brattas L and Kjekshus A, Acta chem. Scand **A 29** (1975)623
2. Ikari T, Provencher R, Jandl S and Aubin M, Solid-State Communications **45** (1983) 113
3. Sourisseau C and Mathey Y, Chemical Physics **63** (1981) 143
4. Zwick A, Landa G, Renucci M, Carles R and Kjekshus A, Phy. Rev. **B26** (1982) 5694
5. Khumalo F, Olson C and Lynch D, Physica **105 B** (1981) 163
6. Deslandes J and Jandl S, Physics Rev **B-29** (1984) 2088
7. Wilson J A, Phys. Rev. **B-19** (1979) 6456
8. Provencher R. C. Ayuache, Jandl S and Gerin J. Solid State Communication **59** (1986) 553
9. Deville Cavellin C Martinez G. Gorochor O and Zwick A, J. Phys. C: Solid State Physics **15** (1982) 5371
10. Prodam A, Marinkovi V., Jug N, van Midden h, Bohm H, Bolwell F and Bemett J, Surface science **482-485** (2001) 1368
11. Huang L, Tang K, Yang Q, Shen G and Jia S, Materials research bulletin, **39 (7-8)** (2004) 1083
12. Patel S G, Agrawal M K and Arora S K, Crystal Research Technology, **31** (1996) 851
13. Brattas L and Kjekshus A, Acta Chem. Scand. **26** (1972) 3441
14. Srivastava S K and Avasthi B N, J. Less Common, **124** (1986) 85
15. Hahn H and Ness P, Anorg Allgem. Chem. **302** (1959) 37
16. Bear J and McTaggart F, J. Chem. **11** (1958) 458
17. Strozer E Built W and Meisel K, Anorg. Allgem Chem. **242** (1939) 249

Table: 1 Growth parameters of ZrSe₃ single crystals using chemical vapour transport technique.

Sample	Ampoule dimension		Temperature distribution		Physical characteristic of crystals			
	Length mm	ID mm	Reaction temperature (K)	Growth temperature (K)	Growth time (hr)	Plate area (mm ²)	Thickness (mm)	Colour & appearance
ZrSe ₃	250	22	1173	1023	370	10	0.09	Gray shining

Table: 2 The EDAX data of ZrSe₃ single crystals

Elements	Stoichiometric proportion	From EDAX
	Wt %	Wt %
Zr	27.80	25.26
Se	72.20	74.74

Table: 3 The crystallographic data of ZrSe₃ single crystals.

Parameter	Reported	Calculated
a (Å)	5.41 (15)	5.45
b (Å)	3.74 (16)	3.78
c (Å)	9.44 (17)	9.45
β	97.48 (17)	97.46
X-ray Density (gm/cc)	5.73 (13)	5.63
Volume V(Å) ³	189.9 (13)	193.50

Table: 4 The XRD data for ZrSe₃ single crystals

hkl	d spacing	Peak width 2θ	Peak intensity counts/sec	Particle size Å
001	9.4393	9.3614	2162.29	872.72
100	5.3959	16.4142	23.73	864.72
101	4.6981	18.8732	1597.31	867.61
110	3.1266	28.5241	1950.46	883.07
111	2.9309	30.4743	1767.13	665.29
004	2.3428	38.3888	1263.57	906.22
005	1.8742	48.5332	529.43	704.13
015	1.6927	54.1351	200.33	576.69
006	1.5609	59.1371	749.52	984.03
035	1.0425	95.2731	16.16	238.16

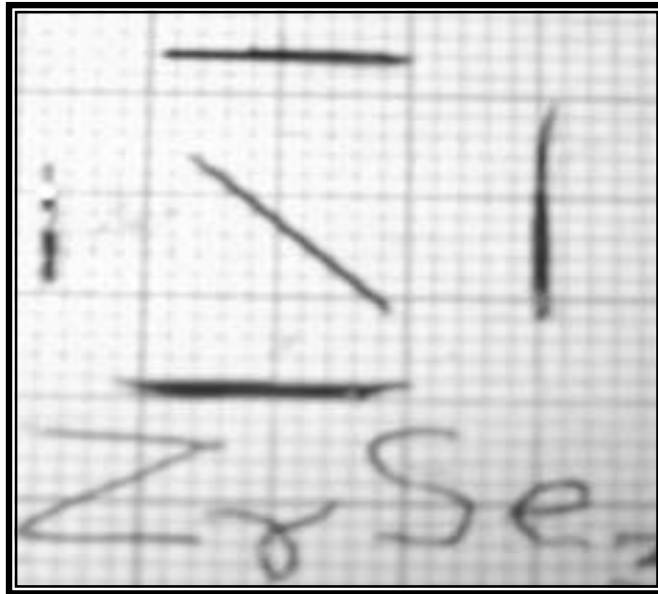


Fig. 1 The photograph of ZrSe₃ crystals.

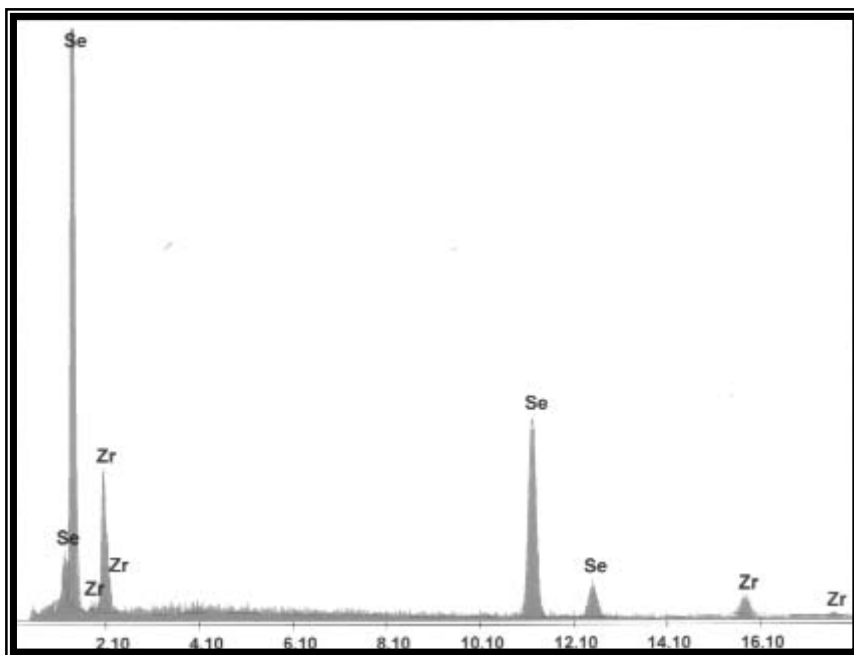


Fig. 2 The Energy Dispersive spectra of Zirconium triselenide single crystals

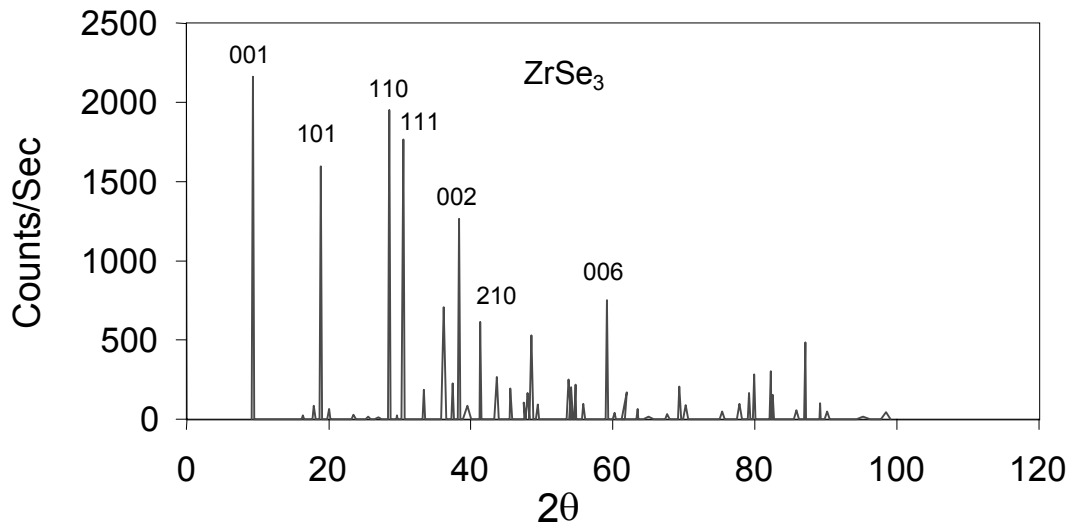


Fig. 3 The X-ray diffractograms obtained for $ZrSe_3$ single crystals

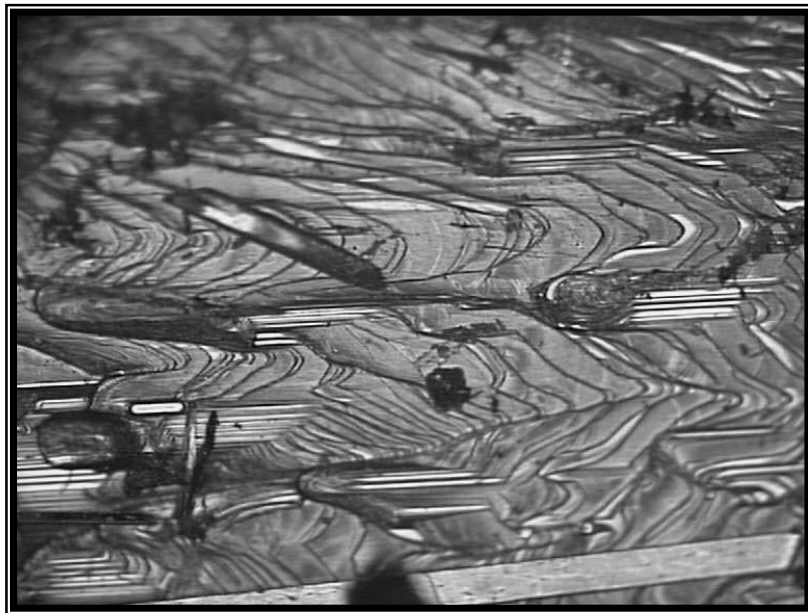


Fig. 4 The surface microstructure on the face of $ZrSe_3$ single crystal

GROWTH AND CHARACTERIZATION OF TaSe₂ SINGLE CRYSTALS GROWN BY CHEMICAL VAPOUR TRANSPORT TECHNIQUE

A.J. Patel, K.R. Patel, Rajiv Vaidya, A.R. Jani and S.G. Patel

Department of Physics, Sardar Patel University, Vallabh Vidyanagar

Abstract

The need for advanced materials has stimulated a large area of researches in which TaSe₂ (Tantalum diselenide) occupy a growing place due to its distinct atomic and electronic features. The present investigation focuses on the growth and characterization of TaSe₂ single crystals, which has important applications due to semiconducting nature. An attempt has been made to yield TaSe₂ single crystals by chemical vapour transport (CVT) using iodine as a transporting agent. Optimum conditions for growing these crystals are given. These crystals belong to transition metal dichalcogenides (TMDC) group, exhibiting very interesting physical properties. The energy dispersive analysis by X-rays (EDAX) gives the confirmation about stoichiometry of these crystals. The X-ray diffraction (XRD) studies were also carried out for the structural characterization. Hall-Effect and optical absorption measurements at room temperature have been made for the grown crystals. The resistance of layered crystal TaSe₂ is determined as a function of pressure up to 8 GPa using Bridgman anvils.

Introduction

Transition metal dichalcogenides possess various characteristics of metal, semiconductor and magnetic substances and have been studied widely [1-3]. A large amount of work on transition metals dichalcogenides has discussed some important properties of these materials [4]. Many authors [5-8] have studied 2H-TaSe₂ because of its very rich diversity of phenomena of CDWs, super lattice including transitions between commensurate phase, orthorhombic incommensurate stripe and hexagonal incommensurate phases and normal phase [7] with the onset temperature at 122 K and the "lock-in" phase transition temperature at 90 K [6]. The growth of single crystals of the transition metal dichalcogenides (TMDC) have been reported by many people by chemical vapour transport technique using iodine or bromine as transporting agent [9-12]. The size of the single crystals obtained by chemical vapour transport (CVT) depends upon a number of parameters [10], which include the dimension of the ampoule, the temperature T_1 & T_2 at the two ends of the ampoule and the concentration of transporting agent. Optimum values for these parameters can be obtained by trial and error and the conditions under which large single crystals can be obtained is studied.

A.J. Patel, K.R. Patel, Rajiv Vaidya, A.R. Jani and S.G. Patel

Single crystals of TaSe₂ have been grown by both methods, i.e. with direct vapour transport (DVT) and chemical vapour transport (CVT). Method of growing single crystals of TaSe₂ by direct vapour transport was reported with optimum conditions [13]. Tantalum diselenide, TaSe₂, is one of the most extensively studied members of the large lamellar transition metal dichalcogenides family. This is especially due to its transport properties. It is a layered materials consisting of covalently bonded Se-Ta-Se layers with van der Waal bonding between two layers. 2H-TaSe₂ single crystals were grown by iodine vapour transport and characterized by X-ray diffraction, magnetic susceptibility and resistivity measurements [14].

Among the transition-metal dichalcogenides, the polytype 4H-TaSe₂ show interesting atomic and electronic properties [14, 15]. Layer by layer etching of the surface of transition metal dichalcogenides has been used earlier using STM [16, 17] and atomic force microscope [18]. Due to weak van der Waals force between each layer, it is possible to etch away individual layers in a well-defined manner. Using this technique, it can be possible to choose each layer in the poly-type transition metal dichalcogenides by making successive layer-by-layer removal. A scanning tunneling microscope (STM) was used by to fabricate T-phase tantalum dichalcogenide (TaSe₂) nanocrystals with sizes ranging from 7 nm to more than 100 nm within the surface layer of 2H- TaSe₂ crystals at liquid helium temperature [19]. The superconducting transition temperatures for layer compounds in the system TaS_{2-x}Se_x have been measured by T. F. Smith et al. as a function of hydrostatic pressure up to 25 GPa [20].

Experimental and Results

There are two different methods for the growth of TaSe₂ single crystals such as DVT & CVT. Variety of transporting agents can be used for the growth. In the present paper we report the growth of TaSe₂ single crystals by CVT technique using iodine as transporting agent. Samples of TaSe₂ were prepared by reaction of the appropriate amount of tantalum powder (Make: Aldrich, USSR, purity: 99.95%) and selenium powder (Make: Koch-Light Laboratories Ltd., England, purity: 99.99%). Stoichiometric amount of the elements were introduced into a quartz ampoule of 22.5 cm internal diameter and 25 cm length. The ampoule was sealed at 10⁻⁵ torr. The mixture was distributed along the length of the horizontal ampoule, which was then introduced into a two zone furnace whose temperature was increased in steps of 50 °C from room temperature to a final temperature between 900 °C and 850 °C. This slow heating was necessary to avoid any possibility of explosion due to the strongly exothermic reaction between the elements. The ampoule was maintained at this final temperature for about 4 days and then allowed it to cool slowly. At this stage the compound was in the form of a free flowing fine black powder.

Growth and Characterization of TaSe₂ Single...

The powdered compound of 10 gm was introduced into a quartz ampoule of length of 25 cm, internal diameter 2.25 cm. Then 2 mg/cm³ of iodine (purity- 99.5%) was introduced into the ampoule by means of a capillary tube. The ampoule was evacuated to a pressure of about 10⁻⁵ torr and sealed. Ampoule was set horizontally in a two-zone furnace with the powder at one end of the ampoule, which is kept at the higher temperature. The ampoule was left in the temperature gradient of 2.5 °C/cm of the furnace for 7 days and then allowed to cool down slowly. The optimum conditions for the growth of TaSe₂ single crystals are given in Table 1. The EDAX gives the confirmation about stoichiometry of these crystals. Weight % of elements taken for growth and obtained from EDAX are shown in Table 2.

For X-ray diffraction, many small crystals were finely grinded with the help of an agate mortar and separated through 106-micron sieve to obtain grains of nearly equal size. X-ray powder patterns were recorded on X-ray Diffractometer (Make: Philips, Holland and Model: X' Pert) using CuK α radiation. The values of lattice parameters a, b and c, unit cell volume (V) and X-ray density (ρ) determined from the X-ray diffractograms are represented in Table 3.

Optical absorption spectra of the TaSe₂ single crystals have been taken in the range 200 nm to 3000 nm. The absorption coefficient is related to photon energy by expression

$$\alpha h\nu = (h\nu - E_g)^{1/n} \quad (1)$$

where the exponent n can take values 2, 1/2, 2/3, and 1/3 for the allowed direct, allowed indirect, forbidden direct and forbidden indirect transition respectively. In our case the best fit is obtained with n = 1/2 showing that TaSe₂ is indirect band gap material (Band Gap = 1.41 eV) where the wave vector difference between the electrons in valance band and conduction band is supplied by lattice phonons.

The Hall-Effect measurements have been carried out on the grown crystals to evaluate the type, mobility and carrier concentration. From the sign of Hall coefficient, the nature of charge carrier can be ascertained. The results obtained from the Hall-Effect measurement on these samples are given in Table 4.

Pressure is an important physical variable in material science. The development of high-pressure techniques has led to advances in fundamental scientific research and to industrial application. Electrical measurements are among the most known methods used for characterization of the sample at high pressure. In Bridgman opposed-anvil system [23], there is a decrease in volume of system and therefore the maximum pressure is limited by the flow of deformable gaskets in various geometries. This design uses Bridgman's principle

A.J. Patel, K.R. Patel, Rajiv Vaidya, A.R. Jani and S.G. Patel

of “massive support”. Bridgman anvils can be readily used up to about 10 GPa. The sample is in the form of a thin disc surrounded by pyrophyllite gasket [24] with talc as pressure transmitting medium. A four-probe method is used to evaluate the resistance of the TaSe₂ sample up to 8GPa pressure. The graph of resistance vs pressure for as grown crystals is shown in figure 2.

Conclusions

The chemical vapour transport technique has been used successfully to grow the single crystals of TaSe₂. The analysis of the absorption spectra clearly indicates the presence of indirect band gap in these single crystals. The crystal structure of 2H-TaSe₂ is found to be hexagonal with the space group . From the sign of the Hall coefficient it is confirmed that the grown crystals are p-type in nature. The resistance decreases as the pressure increases up to the pressure 8GPa. The sample shows conducting behaviour as pressure increases.

Acknowledgement

The author are indebted much to DAE-BRNS for providing financial assistance to Research Project Sanction No. 2004/37/21/BRNS/2382 dated 22-02-2005 for carrying out this work.

References

1. F. R. Gamble et al., Science, **174** (1971) 493
2. B. Morosin, Acta. Crystallorg. B, **30** (1974) 551
3. A. N. Vesi et l., Sov. Phys. Semicond., **13** (1979) 18
4. J. F. M. Rocha and A. Ribeiro, Ciencia e Cultura, Suppl. **43** (1991) 569
5. W. L. McMillan, Phys. Rev.j B, **12** (1975) 1187, 1197, B **14** (1976) 1496, B **16** (1977) 543, 4655
6. D. E. Moncton et al., Phys. Rev. Lett., **34** (1975) 734
7. D. E. Moncton et al., Phys. Rev. B, **16** (1977) 801
8. J. F. M. Rocha and A. Ribeiro filho, Proc. 17th IUPAP-Internat. Conf. Thermodyanamic and Statistical Mechanics, STATPHYS, RJ, Brazil, 1989
9. H. Guernoc, US Govt. Rept. **37** 101A (1961) AD265121
10. R. Nitsche et al., J.Phys.Chem. Solids **21** (1961) 199
11. H. L. Brixner, j. Electrochem. Soc **110** (1963) 289

Growth and Characterization of TaSe₂ Single...

12. H. Schafer, Chemical Transport Reactions (Academic Press, New York, 1964)
13. A. A. Al-Hilli et al., J. Crystal Growth **15** (1972) 93
14. J. A. Wilson et al., Adv. Phys., **24** (1975) 117
15. R. V. Coleman et al., Adv. Phys. **37** (1988) 559
16. B. Parkinson, J. Am. Chem. Soc. **112** (1990) 7498
17. A. P. Volodin and J. Aarts, Physica C **235** (1994) 1909
18. E. Delawski and B. A. Parkinson, J. Am. Chem. Soc. **114** (1992) 1661
19. J. Zhang et al., Science **274** (1996) 757
20. T. F. Smith, R. N. Shelton, R. E. Schwall, J. Phys. F: Metal Phys., **5** (1975) 1713
21. Bjerkekund and Kjekshus, Acta. Chem. Scand., **21**(1967) 513
22. Huisman et al., J. Less-Common Metals, **21** (1970) 187
23. P.W.Bridgmann, J.Appl. Phys. **12** (1941) 461
24. J.Lees, Advances in High Pressure Research, **1** (1966)

Table: 1 Growth parameters of TaSe₂ single crystals grown using chemical vapour transport

Sample	Reaction Temperature (°C)	Growth Temperature (°C)	Physical characteristics of the crystals			
			Growth time (hour)	Plate area (mm ²)	Thickness (mm)	Colour & Appearance
TaSe ₂	780	740	240	20x20	~0.1	Black shining

Table: 2 Weight % of elements taken for growth and obtained from EDAX analysis

Wt(%) of Elements	TaSe ₂	
	Ta	Se
Taken	53.50	46.50
from EDAX	51.68	48.32

A.J. Patel, K.R. Patel, Rajiv Vaidya, A.R. Jani and S.G. Patel

Table: 3 Crystallographic data of TaSe₂ single crystals grown using chemical vapour transport technique

a = b (Å)	3.438 ± 0.002
c (Å)	19.216 ± 0.026
Unit cell volume (Å)³	196.697
X-ray density (gm/cm³)	8.581

Table: 4 Resistivity, Hall coefficient, mobility and carrier concentration of TaSe₂ single crystal

Sample: TaSe₂			
ρ	R_H	μ_H	n
Ω cm	cm³/coul	cm²/Vsec	cm⁻³
0.8999	2041	2268.029	3.09x10 ¹³

Growth and Characterization of TaSe₂ Single...

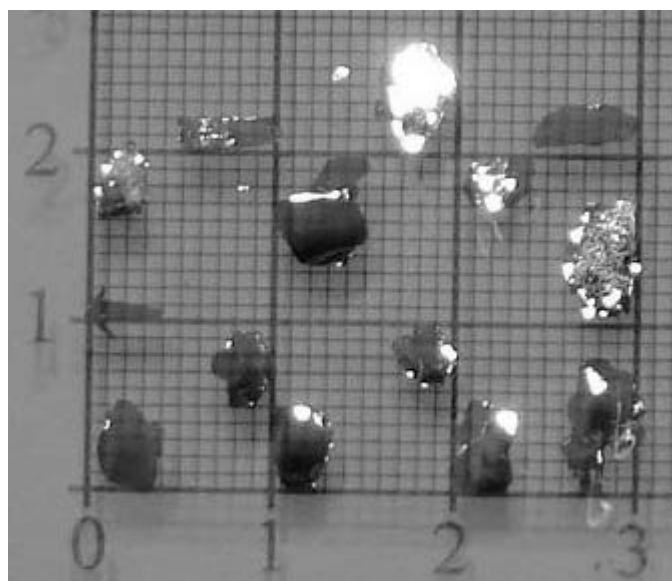


Fig 1 : Single crystals of TaSe₂ grown by chemical vapour transport technique

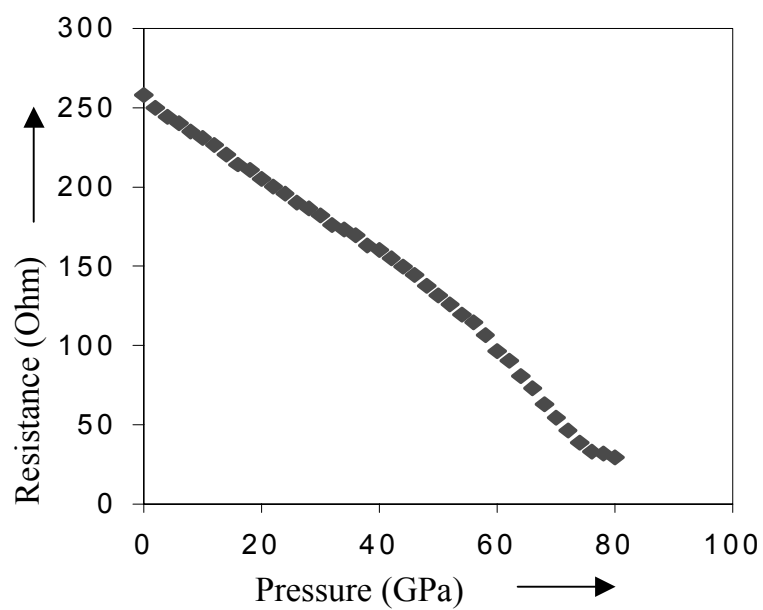


Fig 2 : Variation of resistance with pressure up to 8 GPa using Bridgman anvil set up

SYNTHESIS, THERMAL AND STRUCTURAL PROPERTIES OF ZINC SUBSTITUTED BARIUM HEXAFERRITE POWDERS PREPARED BY A GEL ROUTE

R.B. Jotania and C.C. Chauhan

Department of Physics, School of Sciences, Gujarat University
Ahmedabad

Abstract

This investigation deal with the study of thermal and structural prosperities of Zinc substituted Barium hexaferrite ($BaZn_2Fe_{16}O_{27}$) powders prepared by a Sol-Gel route. The $BaZn_2Fe_{16}O_{27}$ hexaferrite precursors were prepared using a Stearic acid gel technique and calcinated at $950^\circ C$ for 4 hours in a static air atmosphere. The gel and calcinated samples were characterized using various experimental techniques like DTA, TGA, FTIR and XRD and the results are compared.

Key words: Stearic acid gel method, Barium Zinc hexaferrite powders, Sol-Gel.

Introduction

Barium hexaferrite is a hard magnetic material having high saturation magnetization, high magnetic anisotropy field, high coercivity and excellent chemical stability. Barium hexaferrite powders have attracted much attention for applications in permanent magnets, high density perpendicular magnetic and magneto optic recording media [1-3]. Due to its low production cost and excellent magnetic properties the hexaferrites are widely used in fabrication of computer data storage devices, magnetic fluid and certain microwave devices [4-6].

Hexagonal ferrites are classified into six types according to their crystal structure. Out of six types, technical interests are gathered on M and W-types as these materials have found practical applications. The different unit cell structures for different types of hexagonal ferrites are illustrated in Table 1.

Type	Unit cell structures
M	SRS*R*
W	SSR*S*S*R
Y	STSTST
Z	RSTSR*S*T*S*
X	3 (RSR*SS)
U	RSR*S*T*S*

Table 1. Types and Unit cell structures of different types of hexaferrites

Synthesis, Thermal and Structural Properties...

(S, R and T refer to three types of block which exist in the unit cell, and * represents 180° rotation about the C-axis).

The smaller Fe³⁺ ions are arranged in five different kinds of interstitial sites. Three are Octahedral sites (12K, 4f₂ and 2a), one is a tetrahedral site (4f₁) and the last one site in which the ferric ion (Fe³⁺) is surrounded by five oxygen atoms forming a trigonal bi pyramid (2b). It is known that ferric ions provide the largest positive contribution at the 2b site, a relative weak positive contribution at the 4f₁, 4f₂ and 2a sites, and a negative contribution at the 12K site. [7]. Hexaferrites can be prepared by a large number of experimental techniques like conventional solid-state method. [8], Co-Precipitation [9], hydrothermal [10], glass crystallization [11], and Sol-gel processing [12, 13].

In this paper we report the synthesis and characterization of Zinc substituted Barium hexaferrite powders prepared by using a Stearic acid Gel techniques. The Stearic acid gel route has been recently applied to various barium hexaferrite [12, 13] and offers a quick and simple method to quite complex materials. It allows the resultant product very fine and free from agglomerates.

The structural behavior of hexaferrite powders depend on various factors like the method of preparation, chemical composition, sintering time and sintering temperature [14].

2. Experimental

2.1 Hexaferrite Synthesis

Research grade Ba(OH)₂, Zn(NO₃)₂, Fe(NO₃)₂·9H₂O and Stearic acid were used as a starting materials. Stoichiometric amount of Iron nitrate, Barium hydroxide, Zinc nitrate were dissolved one by one in appropriate of Stearic acid solution. The solution was heated at 100°C for two hours to obtain gel. The gel precursor was decomposed at 500°C for one hour and then calcinated at 950°C for four hours in air and slowly cooled in furnace to obtain BaZn₂Fe₁₆O₂₇ powder.

2.2 Sample Characterization

2.2.1. Thermal Analysis

Differential thermal analysis (DTA) and Thermo gravimetric analysis (TGA) were used to characterize the process of crystallization and to assess thermal stability of the final product. DTA and TGA curves of dried gel were recorded using SII Differential Thermal Analyzer Model No. 5100 in the region of 100°C to 800°C with a rate of 10°C/min.

2.2.2. Fourier Transformed Infrared Spectra

Fourier Transformed Infrared Spectra (FTIR) of Stearic acid gel and calcinated powders (500°C 1hr., 950°C 4hrs.) were recorded in KBr medium using a JASCO-FTIR-410 Spectrometer. The spectra were recorded in the full infrared range from 400-4000 cm^{-1} .

2.2.3. X-ray Diffraction

X-ray diffractograms of gel and calcinated samples were recorded on PW 1830 Diffractometer using $\text{CuK}\alpha$ radiation ($\lambda = 1.5405 \text{ \AA}$).

3. Result and Discussion:

DTA-TGA, FTIR and XRD measurements were undertaken in order to determine the temperature range in which those chemical and structural changes occur.

3.1 DTA-TG Analysis

DTA-TGA curves of dried gel, are shown in Fig.1. A weak endothermic peak appears at 223°C. The effect is attributed to the evaporation of the water molecules and decomposition of the residual salt and nitrate. The exothermic peak appear at 252°C, which is related to burning of organic substances. TGA curve also show fast weight loss between 252°C to 308°C. All the organic substances are combusted by 308°C and only small loss in weight is found beyond this temperature [15, 16].

3.2. FTIR Analysis

Fig. 2 shows the FTIR spectra of gel and calcinated samples, as a function of wave number (range from 400-4000 cm^{-1}). The absorption bands at 3400 cm^{-1} in gel Fig. (2a) is due to OH and H_2O vibration. This band disappears in calcinated sample; suggesting decrease in the quantity of water molecules. The band at 1383 cm^{-1} in gel corresponds to the presence of NO_3^- ions [17], which disappears at a higher temperature Fig. (2b). The absorption bands between 580 cm^{-1} to 440 cm^{-1} appear when heat treatment is performed on gel which is attributed to formation of Ba-Zn hexaferrite [16, 18].

3.3. X-ray Analysis

3.3.1. Phase Identification

The X-ray diffractogram of gel and calcinated samples (500°C 1hr., 950°C 4hrs.) are illustrated in Fig 3. The synthesized gel shows flat XRD pattern Fig. (3a) indicating no

Synthesis, Thermal and Structural Properties...

oxide crystallization occurs during solidification of the liquid solution where the sample heated at 500°C for 1 hr. Fig. (3b), XRD diffractogram shows some peaks indicating the starting of crystallization. However at 950°C, the W-type hexaferrite appears along with two more phases namely, M and α -Fe₂O₃.

Conclusion

- (a) A simple Stearic acid gel method is used to synthesized Zinc substituted Barium hexaferrite particles.
- (b) The preparation time and calcinated temperature in the present study is much lower than conventional ceramic technique (The preparation time of ceramic technique is about 24 hrs and calcilnation temperature is about 1100°C- 1300°C)
- (c) The Stearic acid gel method provides simple and yet technologically important processes of synthesis of haexaferrite, particularly at lower temperature.

Acknowledgement

Authors R.B.Jotania and C. C. Chauhan are thankful to University Grants Commission for the financial support under Minor Research Project F. No. 31-28/2005 (SR) and National Chemical Laboratory, Pune for providing experimental facilities.

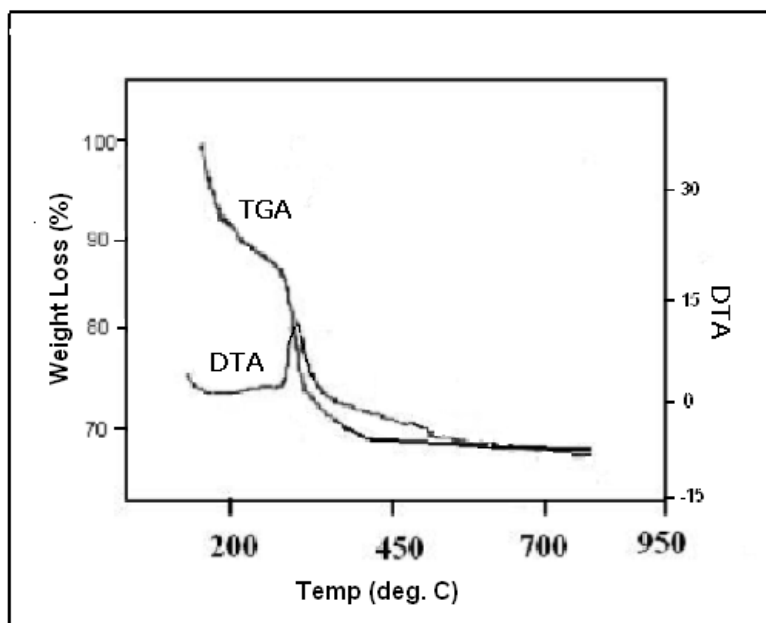


Fig. 1: DTA- TGA Curves of Dried Gel

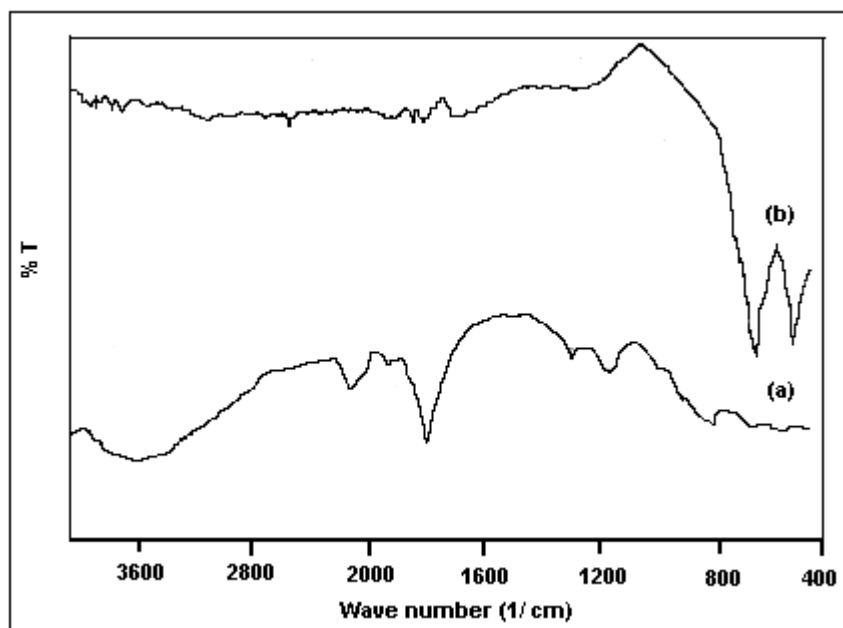


Fig. 2: FTIR spectra of (a) Gel (b) Calcinated sample (950°C for 4 hrs.)

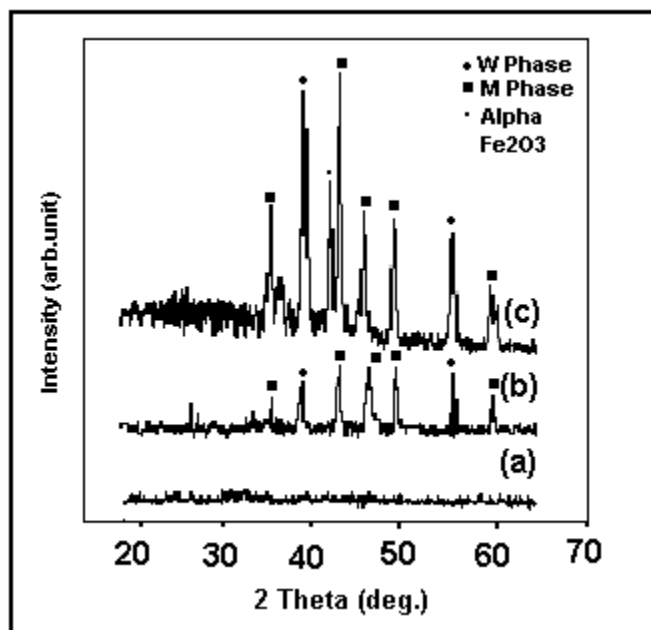


Fig. 3: The X-ray diffractogram (a) Gel, (b) sample heated at 500° C for 1 hour, (c) sample calcinated at 950° C for 4 hours

References

1. <http://www.aacg.bham.ac.uk/magnetic-materials/>.
2. Pillai V, Kumar P, Multani M. S., Shah D. O., Colloids Surf. A: Physicochem Eng. Aspects **69**, 80 (1993)
3. Dou Y.W, Ferrite Jiangsu Science and Technology, Nanjing, P. 417 (1996)
4. Gomi M, Cho J and Abe M, J Appl. Phys. Vol. **82**, 5126 (1997)
5. Harris J.E, Harrell J.W, Parker F.T and Kitahata S. J. Appl. Phys. **81**, 382 (1997)
6. Garcia D, Muro M, Batlie X, Laberta A, Gon Zalez J M and Montero M.I J. Appl. Phys. **81**, 3812 (1997)
7. Jacobo S.E, Cirale L, C Domingo-Pascual, Rodrigues Clements, Blesa M.S, J. Mater Sci. **97**, 1025 (1997)
8. Corp O, Barjega R, Segal E Brezeanu M, Thermochim Acta **318**, 57 (1998)
9. Chen D, Chen Y ,Colloid J. Interface Sci. **235**, 9 (2001)
10. Ataie A, Harries I, Ponton C, J. Mater Sci **30**, 1429 (1995)
11. Sato H, Umda T, Mater. Trans. **34**, 76 (1993)
12. Bernier J. Mater Sci. Eng. A. **10-9**, 233 (1989)
13. Matsumoto M, Morisako A, Hachiwa T, IEEE Trans. Magn. Jpn. **6**, 648 (1991)
14. Standly K.J, Oxide Magnetic Materials, Clarendon Press, Oxford 1962
15. Xinhua He, Qiugqiu Zhang Ling, Materials Letters **57**, 3031 (2003)
16. Temuujin J, Aoyama M, Senna M, Masuko T, C Ando, Kishi H, J. Solid State chem. **177**, 3903 (2004)
17. Salunkhe M.Y, Choudhry D.S, Kulkarani D.K. Vibration Spectroscopy **34**, 221 (2004)
18. Pullar R.C, Taylor M.D and Bhattacharya A.K, J Mater Science **32**, 873 (1997)

ELECTRON-MOLECULE INTERACTIONS IN COMPLEX POTENTIAL FORMULATION: e - H_2O EXAMPLE

Sumona Gangopadhyay and K.N. Joshipura

Department of Physics
Sardar Patel University
Vallabh Vidyanagar

Abstract

In this paper we have made a critical study of different model potentials of polarization and absorption interactions and their effects on various total cross sections (TCS) viz., total elastic cross sections (Q_{el}), total inelastic cross sections (Q_{inel}), total ionization cross sections (Q_{ion}), summed total excitation sections (ΣQ_{exc}), total (complete) cross sections (Q_T) and grand total cross sections (Q_{TOT}) of H_2O molecule on electron impact. The present calculations are based on the spherical complex optical potential formalism as outlined in [1, 2]. Non-spherical interactions are treated separately. The incident electron energy range is from threshold of ionization (~ 15 eV) to 2 KeV. Our results are compared with available theoretical and experimental data. Comparisons of model potentials are examined and cross section results are discussed.

Introduction

Collisions of electrons with water molecules play an important role in atmospheric and interstellar space processes, radiation biology and chemistry. [1, 2] Several experimental studies have been carried out since early 20th century. The first measurements of the total cross sections for H_2O molecule at lower energies were carried out by Bruche [3], Sueoka *et al* [4] and Szymtkowski [5]. Jain [6] employed a simple approach based on the spherical-complex-optical potential (SCOP) of the given electron-target system. At intermediate and high energies, measurements of total absolute cross sections for electron impact on H_2O were carried out by Zecca *et al* [7]. A recent review on all the processes of electron scattering with water molecule is due to Itikawa and Mason [8].

The cross sections of the e-molecule system depend critically on the interplay of the long range and the short range forces, and hence a comparative study is necessary. Therefore, in the present work we have examined different model potentials of absorption and polarization interactions and their effects on various TCSs for H_2O molecule at the incident energies (E_i) from ionization threshold (~ 15 eV) to 2000 eV. We have employed the Variable Phase Approach (VPA) of Calogero as discussed in [9] for calculation of total cross sections.

Electron-Molecule Interactions...

The target-projectile system is represented here in terms of a two channel scattering problem. Thus the total interaction potential between the incident electron and target water molecule is represented by a spherical complex optical potential (SCOP) as follows,

$$V_{opt}(r) = V_{st}(r) + V_{ex}(r) + V_{pol}(r) + iV_{abs}(r) \quad (1)$$

where different components of the SCOP are the static (V_{st}), exchange (V_{ex}), polarization (V_{pol}) and the absorption (V_{abs}) potentials. The basic electrostatic potential V_{st} is calculated from the parametric HF charge density given by,

$$\rho(r) = \frac{1}{4\pi r^2} \left[a_2 r^2 e^{-\frac{r}{b_2}} + a_3 r^3 e^{-\frac{r}{b_3}} \right] \quad (2)$$

where a_2 , a_3 , b_2 and b_3 are the fitting parameters whose values are 4478, 125, 0.0602 and 0.322 respectively. In H_2O the O-H bond length is $r_{OH} = 0.96 \text{ \AA}$. In our present work we have used Single Centre Approach to calculate the charge density for H_2O molecule. The hydrogen nuclei or protons are assumed to be distributed spherically and uniformly around the oxygen nucleus in the form of a shell with radius r_{OH} . Therefore a realistic static potential V_{st} as given by Katase *et al* [10] reads as under.

$$V_{st}(r) = -\frac{1}{r} \left[10G_{EB} - 2 + 2f_p \right] \quad (3)$$

Where

$$G_{EB} = \frac{1}{Z} \left[a_2 b_2^2 (r + 2b_2) e^{-\frac{r}{b_2}} + a_3 b_3^2 (r^2 + 4b_3 + 6b_3^2) e^{-\frac{r}{b_3}} \right] \quad (4)$$

with $Z=10$ as the number of electrons in H_2O . Further, we assume the H-nuclei to be uniformly distributed within a radius r_{OH} hence,

$$\begin{aligned} f_p &= \frac{r}{r_{OH}} \quad \text{for } r \leq r_{OH} \\ &= 1 \quad \text{for } r > r_{OH} \end{aligned} \quad (5)$$

The exchange potential is expressed presently as a function of charge density $\rho(r)$ and the incident wave-vector (k) by adopting the Hara Free Electron Gas Exchange [11] (HFEGE) model.

The specific purpose of this paper is to examine the relative importance and effect of the long range polarization potential (V_{pol}) and the short range absorption potential (V_{abs}) for

e-H₂O system. Apart from this we also consider the long range dipole potential of water molecule in two alternative models, which can yield the scattering amplitude in analytical forms. The details of theoretical aspects, including different model-potentials are discussed in the next section.

Theoretical Models and Calculations

Our calculations of different TCSs are based on a complex scattering potential vide equation (1). The total complex potential is employed in the Schroedinger equation and appropriate boundary conditions are applied along with numerical techniques to generate various scattering cross sections of the system. Details of our calculations and results for various atomic-molecular targets can be found in our recent publications [1, 2, 12, 13], and hence are not repeated in this paper.

While treating elastic as well as inelastic scattering of electrons by molecular targets, the effect of distortion of the target charge cloud by the projectile is very important. This effect is represented by the dynamic polarization model V_{pol} as given by,

$$V_{pol}(r) = -\frac{\alpha_d r^2}{2(r^2 + r_c^2)^3} \quad (6)$$

where α_d is the static dipole polarizability of the target and r_c is the energy dependent cut-off parameter expressed as

$$r_c = \frac{3k}{8I} \quad (7)$$

Here I is the first ionization potential of the target molecule. The above dynamic potential of equation (6) has a correct asymptotic form $-\alpha_d/2r^4$, but this model potential, equation (6) along with (7) does not hold good for lower energies say below 50 eV, where it begins to overestimate. Therefore a correlation-polarization potential V_{cp} was defined by Perdew & Zunger [14]. In this model the short range correlation is joined to the asymptotic form in the following manner,

$$\begin{aligned} V_{cp}(r) &= V_{SR}^{corr}, \quad \text{at } r \leq r_0 \\ &= -\frac{\alpha_d}{2r^4}, \quad \text{at } r > r_0 \end{aligned} \quad (8)$$

Here r_0 is the distance of intersection between the short range correlation part and long range form $-\alpha_d/2r^4$. The short range part of the potential in the above equation was given by [14].

Electron-Molecule Interactions...

The potential V_{cp} as defined above has been employed by several workers in the last two decades or so, but this model-potential suddenly assumes the asymptotic form at a finite distance r_0 . Also there is a kink in the potential function at $r=r_0$.

Yet another form viz., the polarization model of Zhang et al [15] goes by the following expression.

$$V_{Z,pol}(r) = -\frac{\alpha_d}{2(r^2 + r_{co}^2)^2} \quad (9)$$

It is essentially the same as in equation (6) but now in equation (9) the cut off parameter r_{co} is chosen in a way to ensure that the $V_{pol}(r)$ equals the short range correlation potential at the origin. Furthermore, the Zhang polarization model [15] contains some multipole and non-adiabatic corrections in the intermediate region and approaches the correct asymptotic form for large r .

In our polarization model we start with equation (6) but we choose the cut-off parameter r_c to be equal to r_0 as defined by the correlation-polarization potential vide equation (8). This is justified since r_0 defines a boundary between the short range and long range potentials. Our present polarization model is denoted by V_p . Since our cut off parameter r_0 is larger than the typical molecular bond-lengths, the present model potential weaker than the previous potentials. The present model (V_p) is more useful for highly polarizable targets.

Next we consider the imaginary part of the optical potential or the absorption potential which accounts for the total loss of scattered flux into all allowed channels of electronic excitation and ionization. A currently popular model form of V_{abs} is that of [16], who proposed quasi-free, Pauli-blocking, dynamic absorption potential given in au, as

$$V_{abs}(r, E_i) = -\frac{1}{2} \rho(r) v_{loc} \sigma_{ee} \\ = \rho(r) \left(\frac{T_{loc}}{2} \right)^{1/2} \cdot \left(\frac{8\pi}{10 k_F^3 E_i} \right) \cdot \theta(p^2 - k_F^2 - 2\Delta) \cdot (A_1 + A_2 + A_3) \quad (10)$$

In these expressions, v_{loc} is the local speed of the external electron, and σ_{ee} denotes the average total cross section of the binary collision of the external electron with a target electron. The local kinetic energy of the incident electron is obtained from

$$T_{loc} = E_i - V_R = E_i - (V_{st} + V_{ex} + V_{pol}) \quad (11)$$

There is practically no effect of V_{pol} on T_{loc} . For a given energy, the dominant term in equation (11) is V_{st} . Further $p^2 = 2E_i$, $k_F = [3\pi^2 \rho(r)]^{1/3}$ is the Fermi wave vector and Δ is an energy parameter. In equation (10), $\theta(x)$ is the Heaviside unit step function, such that $\theta(x) = 1$ for $x > 0$, and is zero otherwise. The dynamic functions A_1 , A_2 and A_3 defined in [16] depend differently on the molecular properties ρ , Δ and E_i . Full details of the V_{abs} potential in the present context of molecules are discussed in [13]. The energy parameter Δ determines a threshold below which $V_{abs} = 0$, and the ionization or excitation is prevented energetically. As a preliminary choice one can take $\Delta = I$. This will be called the original model of V_{abs} .

We have introduced a modification in the original model, by considering Δ as a slowly varying function of E_i around I . This is justified since Δ fixed at I prevents even discrete excitation at the incident energy $E_i = I$. We must allow for inelastic flux even at the ionization threshold. Thus, the modification that we introduce is to assign a reasonable minimum value $0.8I$ to Δ and to express the delta parameter as a function of E_i around I , as follows.

$$\Delta(E_i) = 0.8I + \beta(E_i - I) \quad (12)$$

Now let us say that E_p is the value of E_i at which our calculated Q_{inel} attains maximum. In equation (12) β is then obtained by requiring that $\Delta = I + 1$ (eV) at $E_i = E_p$, beyond which Δ is held constant. The expression for $\Delta(E_i)$, equation (12), is meaningful since Δ fixed at I would not allow even excitation at incident energy $E_i \leq I$. On the other hand, if parameter Δ is much less than the ionization threshold, then V_{abs} becomes unduly high near the peak position. In short the present form of delta equation (12) balances all these aspects and allows us to obtain satisfactory values of Q_{ion} for a given target.

The next task is to set up the Schrödinger equation with the modified V_{abs} , and find the complex phase shifts $\delta_l = Re \delta_l + i Im \delta_l$ for various partial waves l by following the Variable Phase Approach [9]. The said approach is highlighted in Gangopadhyay et al [17]. The coupled differential equations [17] for the phase functions involved in this approach are solved by the standard fourth order RK method to calculate total (complete) cross sections given by,

$$Q_T(E_i) = Q_{el}(E_i) + Q_{inel}(E_i) \quad (13)$$

Here Q_{el} is the total elastic cross section and Q_{inel} is the total inelastic cross section. Now the Q_{inel} cannot be measured directly, but it contains Q_{ion} .

Electron-Molecule Interactions...

In recent years, we [1, 13] have developed and successfully employed a semi-empirical approach called ‘Complex Scattering Potential-ionization contribution’ (CSP-ic) method for determining the total ionization cross section Q_{ion} from Q_{inel} . In the present work, we have followed this method for obtaining the total ionization cross sections for H₂O molecules. In the CSP-ic method we introduce the following ratio function.

$$R(E_i) = \frac{Q_{ion}(E_i)}{Q_{inel}(E_i)} \quad (14)$$

Such that, $0 \leq R(E_i) \lesssim 1$. This ratio is expressed as a continuous function of energy and the required Q_{ion} are obtained as discussed in our recent papers [13].

Now we turn to anisotropic or non-spherical potential of electron-molecule scattering. Our potentials of the previous discussion are spherical and hence the cross section Q_T does not include the effects of rotational-vibrational excitations due to non-spherical potentials. H₂O is a polar molecule and these effects cannot be neglected. We have included these effects by defining the grand total cross section Q_{TOT} as under,

$$Q_{TOT}(E_i) = Q_T(E_i) + Q_{NS}(E_i) \quad (15)$$

where Q_{NS} stands for the TCS of the non-spherical interactions. Presently, we have adopted a modification in the form of cut-off dipole potential (V_D) defined below.

$$\begin{aligned} V_D &= -\frac{\bar{D} \cdot \hat{r}}{r_d^2} & 0 \leq r \leq r_d \\ &= -\frac{\bar{D} \cdot \hat{r}}{r^2} & r > r_d \end{aligned} \quad (16)$$

where \bar{D} is the molecular dipole moment, and r_d is chosen to be the bond length r_{OH} (0.96 Å) for H₂O molecule. The above form is more justified than the simple asymptotic dipole potential $-\bar{D} \cdot \hat{r} / r^2$. When r_d approaches zero, we recover the original dipole potential as discussed by Itikawa [18]. The differential cross section for rotational excitation ($J \rightarrow J'$) can be calculated analytically in the present dipole potential, and are given by

$$\frac{d\sigma}{d\Omega}(\theta, E_i) = \frac{32k'}{3k} \pi D^2 \frac{J'}{2J+1} \left[\frac{1}{K^6 r_d^4} (1 - \cos(Kr_d))^2 \right] \quad (17)$$

Where, k and k' are the initial and final momenta of the scattering electron. Further K is the magnitude of wave vector transfer. The rotational cross section $Q_{NS}(E_i)$ with $J=0$ and $J'=1$ is then obtained by numerical integration over scattering angle θ . The Q_{NS} thus calculated are added to the Q_T for obtaining the grand total cross sections Q_{TOT} .

Results Discussion and Conclusions

In this paper we have investigated some aspects of the electron molecule interactions in the complex potential formalism, with an example of e-H₂O scattering. The two long range potentials considered here are the polarization potential and the dipole potential. The behaviour of the polarization potentials is examined relatively in figure 1. The four polarization models considered here are V_p , V_{pol} , $V_{Z,pol}$ and V_{cp} , and all of them tend to the correct asymptotic limit. All these model-potentials are shown comparatively for water molecule in figure 1.

Clearly the asymptotic form $-\alpha_d/2r^4$ breaks down at short range distances, therefore appropriate models are required to represent the polarization effect. The correlation polarization model V_{cp} is satisfactory except for a kink at $r=r_0$.

The Zhang polarization model $V_{Z,pol}$ is smooth and continuous (figure 1) but this particular form depends on the choice of r_{co} in equation (9). The dynamic form with energy dependent r_c (equations 6 & 7), as well as the present polarization model with $r_c = r_0 = 3.79 a_0$, both go over to zero at the origin, and therefore they are both weaker than the previous two models. The present model V_p is the weakest (figure 1) amongst these models since the present cut-off is fairly large. This would be necessary for highly polarizable targets having large values of α_d .

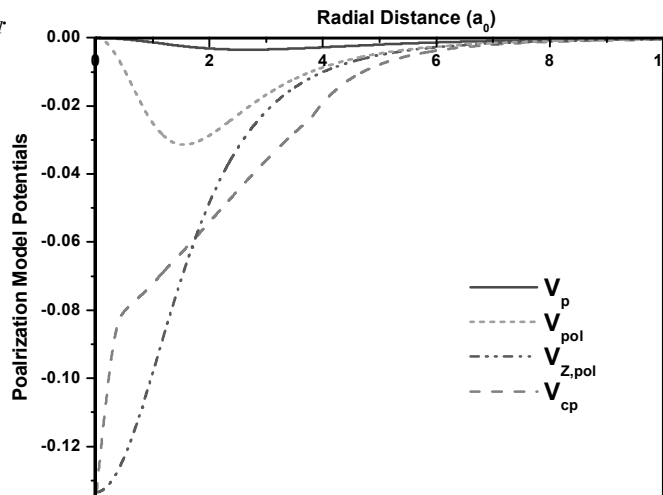


Figure 1 Various Polarization models potentials for e - H₂O scattering, as functions of r in Bohr radius a_0

Electron-Molecule Interactions...

We turn now to the absorption potential shown graphically in figure 2. In this figure the spherical charge density and the variation of the absorption potential with the change in Δ at 100 eV have been plotted separately.

The attractive absorption potential (lower part of figure 2) shows a peak in the valance electron region. This is understood from the outer peak position of the radial charge distribution $4\pi r^2 \rho(r)$. The V_{abs} is slightly weaker in our present model, in view of equation (12). The fact that the V_{abs} is a short range potential also becomes clear from this figure.

Let us note that the potential V_{abs} is not affected by the choice of any polarization potential discussed above.

Now let us discuss the effects of these model potentials on the various total cross sections of e-H₂O scattering. First we consider the grand cross sections Q_{TOT} and the elastic cross sections Q_{el} in this system, along with some comparisons as shown in figure 3.

There is some difference in Q_{TOT} (upper curves of figure 3) due to these models, and it arises mainly at the low and intermediate energies. The present results with correlation-polarization model V_{cp} are essentially those of Jain [6] and are on the higher side. Low energy Q_{TOT} are slightly different in the (present) V_p and the $V_{Z,pol}$ models. The

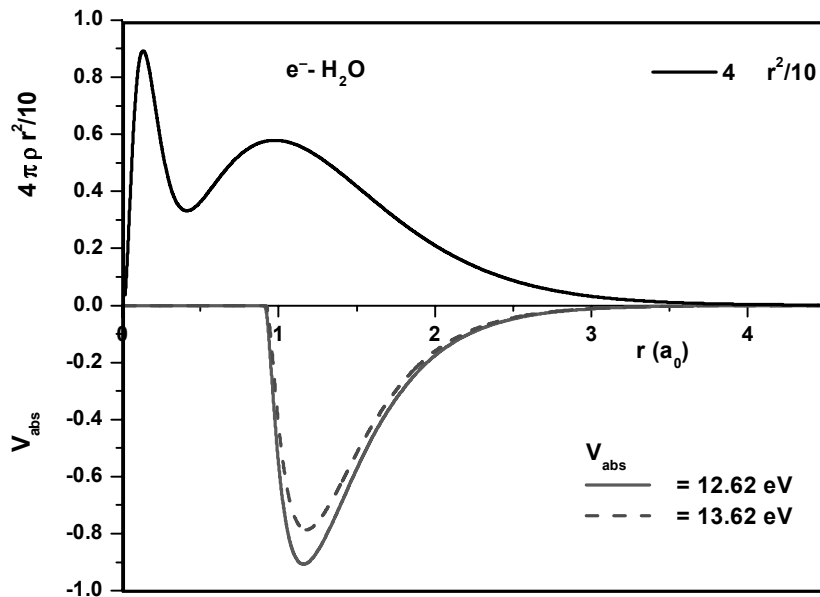


Figure 2 Radial charge density and absorption potential for H₂O at 100 eV

polarization models show greater effects on differential rather the total cross section. Other data [19-21] are also shown in figure 3 for comparison.

Let us focus next on rotational excitation cross section Q_{rot} calculated in the Born approximation with the present dipole potential V_D . These are depicted as middle curves (figure 3), and the present Q_{rot} are consistently smaller than the original model. The present V_D form, equation (16) is more appropriate for highly polar molecules with large value of D . Finally in figure 3, only one calculation of Q_{el} is shown for the sake of clarity.

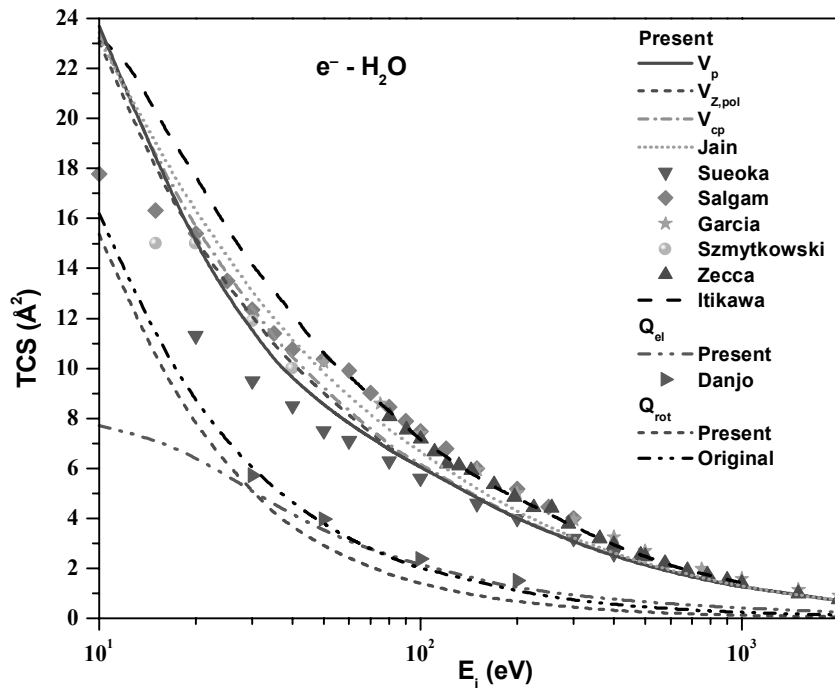


Figure 3 Total elastic (Q_{el}) and grand total cross sections (Q_{TOT}) for H_2O molecule under different model potentials

Consider now figure 4 in which the ionization and the electronic excitation cross sections are plotted for e- H_2O system. For Q_{ion} we have also shown the BEB theory results of Kim et al [22] and the measured data of Straub et al [23].

In conclusion, the present paper highlights comparatively the four different forms of the polarization potential and two forms of the absorption potential in the electron scattering by water molecules. The polarization model V_p proposed presently would be more meaningful for highly polarizable targets. The difference among all this polarization potentials is expected to be more significant in the angular distribution, i.e. differential cross sections

Electron-Molecule Interactions...

at intermediate energies. Similarly the cut-off dipole model V_D proposed here would be appropriate for highly polar molecules. Finally it is more appropriate to consider V_{abs} including variable Δ in order to derive reasonable theoretical values of ionization cross sections Q_{ion} . This model also yields information on electronic excitation cross sections ΣQ_{exc} (figure 4), about which the current knowledge is sparse.

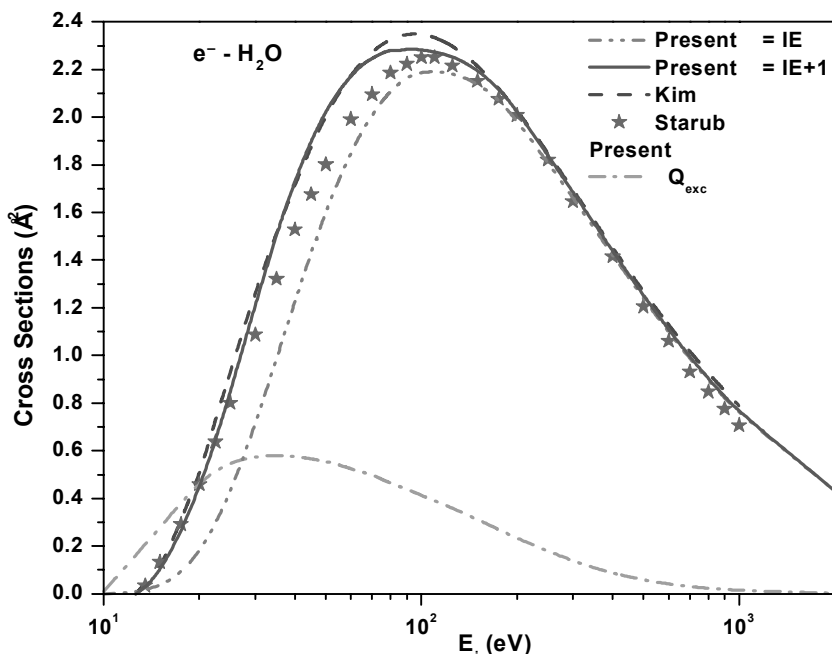


Figure 4 Total ionization (Q_{ion}) and excitation (ΣQ_{exc}) cross sections for H_2O molecule

Acknowledgement

This work was done as a part of a Research Project of K N Joshipura, being funded by ISRO (Bangalore, India).

References

1. Minaxi Vinodkumar, K N Joshipura, C G Limbachiya & B K Antony, Eur. J. Phys. **D 37** (2006) 67
2. Minaxi Vinodkumar, Joshipura K N, Limbachiya C G & Mason N, Phys. Rev. **A 74** (2006) 022721
3. Bruche E, Ann. Phys., Lpz. **1** (1929) 93
4. Sueoka O, Mori S & Katoyama L, J. Phys **B 19** (1986) L373

Sumona Gangopadhyay and K.N. Joshipura

5. Szmytkowski C, Phys. Lett. **136** (1987) 363
6. Jain A, J. Phys. **B 21** (1988) 905
7. Zecca A, Karwasz G, Oss S, Grisentu R & Brusa R S, J. Phys. **B 20** (1987) L133
8. Itikawa Y & Mason N, J. Phys. Chem. Ref. Data **34** (2005) 1
9. Calogero F., Variable Phase Approach to Potential Scattering (Academic, New York, 1974)
10. Katase A, Ishibashi K, Matsumoto Y, Sakae T, Maezono S, Murakami E, Watanbe K & Maki H, J. Phys **B 19** (1986) 2715
11. Hara S J, Phys. Soc. Jpn. **22** (1967) 710
12. Joshipura K N, Vaishnav B G & Limbachiya C G, Pramana- J. Phys. (India) **66** (2006) 403
13. Joshipura K N, Gangopadhyay Sumona & Vaishnav B G, J. Phys **B 40** (2007) 199
14. Perdew J P & Zunger A, Phys. Rev. **A 23** (1981) 5048
15. Zhang X, Sun J & Liu Y, J. Phys. **B 25** (1992) 1893
16. Staszewska G, Schwenke D M, & Truhlar D G, J. Chem. Phys. **81** (1984) 3078
17. Gangopadhyay Sumona, Vinodkumar P C & Joshipura K N, Prajna Journal of Pure & Applied Sciences **14** (2006) 108
18. Itikawa Y, Physics Reports (Review Section of Physics Letters) **46**, (1978) 117
19. Garcia G, private communication (2006)
20. Salgam Z & Atkins N, J. Phys **B 23** (1990) 1529; **24** (1991) 3491
21. Danjo A & Nishimura H, J. Phys. Soc. Japan **54** (1985) 1224
22. Kim Y. K., from NIST Web-Site, <http://physics.nist.gov/PhysRefData/Ionization/EI/table.html>
23. Straub H C, Lindsay B G, Smith K A, and Stebbings R F, J. Chem. Phys. **108**, (1998) 109

TEMPERATURE SENSITIVITY OF CHARACTERISTIC PARAMETERS OF MoSe₂ SOLAR CELLS

Deepa Makhija, T.S. Maniar, R.J. Pathak*, K.D. Patel, V.M. Pathak and R. Srivastava

Department of Physics, Sardar Patel University, Vallabh Vidyanagar

*R.R. Mehta College of Science, Palanpur

Abstract

MoSe₂ belongs to a class of group II-VI chalcogenides having C7 type crystal structure, which possesses a layered structure. These MX₂ (M=W or Mo, X= S, Se or Te) compounds form a structurally and chemically well defined family. The basic structure of loosely coupled X-M-X sheets makes these materials extremely interesting. This compound has attracted considerable attention due to its use in the construction of regenerative electrochemical solar cells. In present investigations, MoSe₂ crystals grown by direct vapour transport method have been used. The photoconversion characteristics of n-MoSe₂/I₂/I/Pt PEC solar cells have been investigated under polychromatic illumination from an incandescent lamp at various intensities, which show that the photoconversion efficiency is low. The series resistance is one of the major parameters that control the photoconversion behaviour of these solar cells. Efforts have been made to estimate its value. In addition, the effect of temperature on the series resistance and various other parameters of PEC solar cells have also been investigated. It has been observed that the series resistance decreases and it improves the behaviour of PEC solar cells.

Introduction

MX₂- type layered chalcogenides having corrosion resistant d-d phototransitions (e.g. MoSe₂, WSe₂) are of special significance in the fabrication of viable photoelectrochemical solar cells [1-4]. However, the achieved photoconversion efficiencies so far reported on as grown crystals are far behind the expected optimum values [5]. The photoconversion characteristics of semiconducting material used as photoelectrode are determined primarily by parameters like doping density, the diffusion length of minority carriers, the series resistance of such cells etc [6, 7]. Among these, the series resistance is a parameter [8,9] whose effect on the photoconversion efficiency of solar cells is very prominent. This parameter should have low value for better characteristic of such cells. In view of this, the authors report here the estimation of the series resistance of n-MoSe₂/I₂/I/Pt PEC solar cells and the effect of temperature on this parameter and various other parameters of such PEC solar cells.

Experimental

As grown MoSe₂ crystals have been used to fabricate a photoelectrode for PEC solar

Deepa Makhija, T.S. Maniar, R.J. Pathak, K.D. Patel, V.M. Pathak and R. Srivastava

cells. These electrodes have been used as photoanodes in I₂/I⁻ electrolyte with platinum as counterelectrode (as shown in figure 1). Using a specially designed potentiometer system,

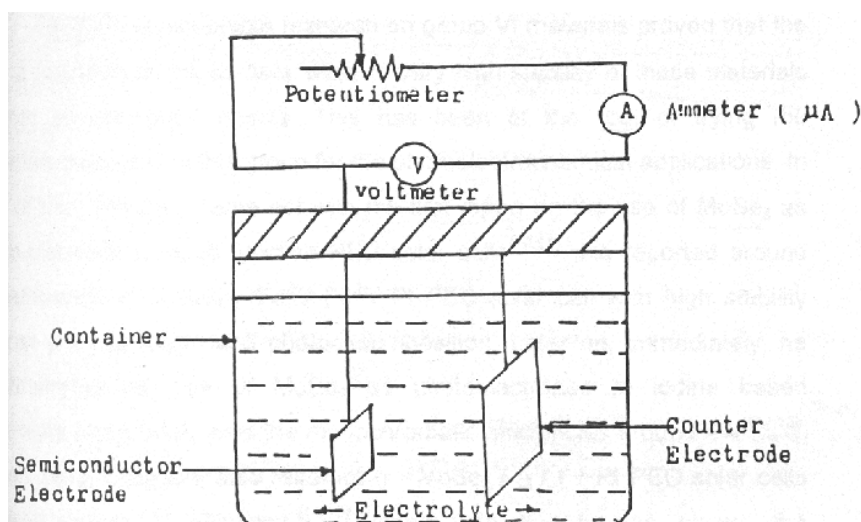


Fig. 1: Schematic diagram of a Photoelectrochemical solar cell

the photocurrent and photovoltage have been measured at different light intensities of incident polychromatic radiation.

Results and Discussions

The photoconversion characteristics of n-MoSe₂/I₂/I⁻/Pt PEC solar cells have been investigated at different intensities of illuminations, which show low photoconversion efficiencies. Results on one such typical cell is shown in figure 2. From this figure, it is quite evident that the efficiency decreases as the intensity of illumination increases and after

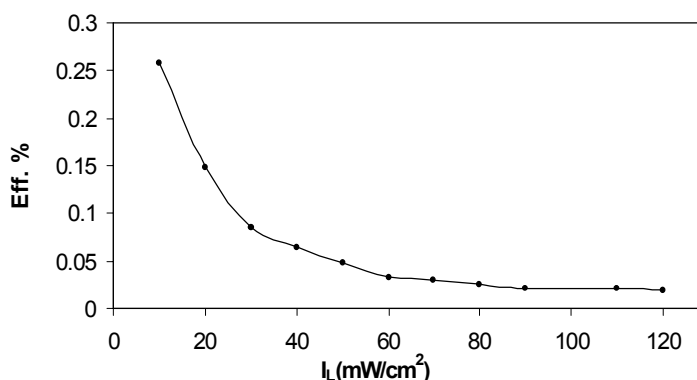


Fig. 2 : Variation of efficiency with intensity of illumination (Electrode - 1)

Temperature Sensitivity of...

certain stage, it tends to be stabilized. This may be attributed to various parameters like poor quality of exposed surface, the series resistance, the defect density in semiconductor etc. The increase in illumination intensity increases the photogeneration of carriers in semiconductor. But the semiconductor-electrolyte interface does not respond to this increase due to the poor interfacial electrochemical kinetics. These electrochemical kinetic limitations are reflected in the low values of efficiency for higher illumination intensities. In addition, a significant portion of generated photovoltage drops across the high series resistance of the electrode and this is not transported across the load.

Since, for TMDC based solar cells, the series resistance is a significant parameter controlling the overall behaviour of PEC solar cells, effort has been made to estimate it. There are various methods like the slope method, area method and deviation method known for its estimation [9 -12]. In present investigation the slope method has been employed to estimate this parameter. This method was first proposed by M. Wolf and H.Rauschenbach [13]. The photovoltage – photocurrent characteristics of MoSe₂ based PEC solar cells at 300K are given in figure 3.

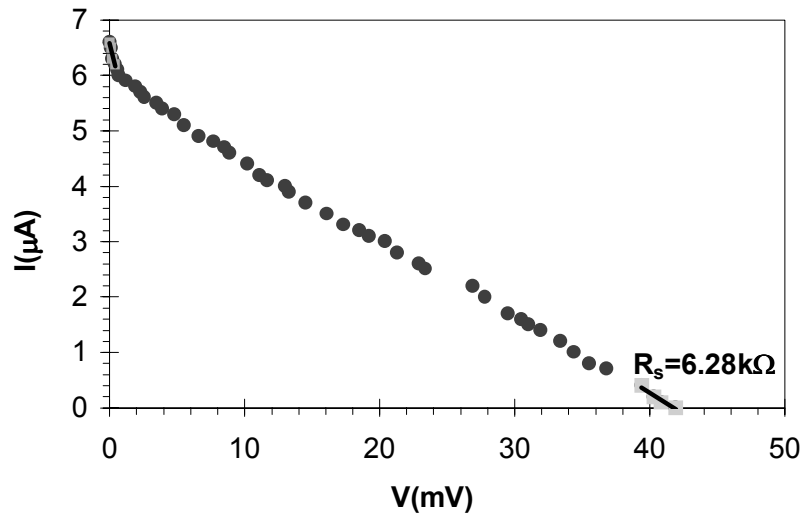


Fig. 3 : Photovoltage - photocurrent characteristics of MoSe₂ based PEC solar cell at I_L=10mW/cm²

These characteristics have been used here to evaluate the series resistance. Accordingly, the series resistance can be given as

$$R_s = - \left(\frac{dV}{dI} \right)_{I=0} \quad (1)$$

Therefore, the slope of the curve shown in figure 3 near the open circuit voltage directly gives the value of the series resistance. In present case this value has been found to be $6.28 \text{ K}\Omega$, which is considerably high. The main reason for high series resistance in this material is the layered type structure. In PEC solar cell fabricated from these materials, photogenerated carriers have to be transported along the c-axis where the layers are bound to each other with weak van der wall forces and thus face high resistance [14-15].

It is important to note that the series resistance and other parameters like efficiency, fill factor etc. are expected to depend upon the temperature. Therefore, the variations of these parameters with temperature have been investigated and the results are shown in figure 4(a), 4(b) and 4(c).

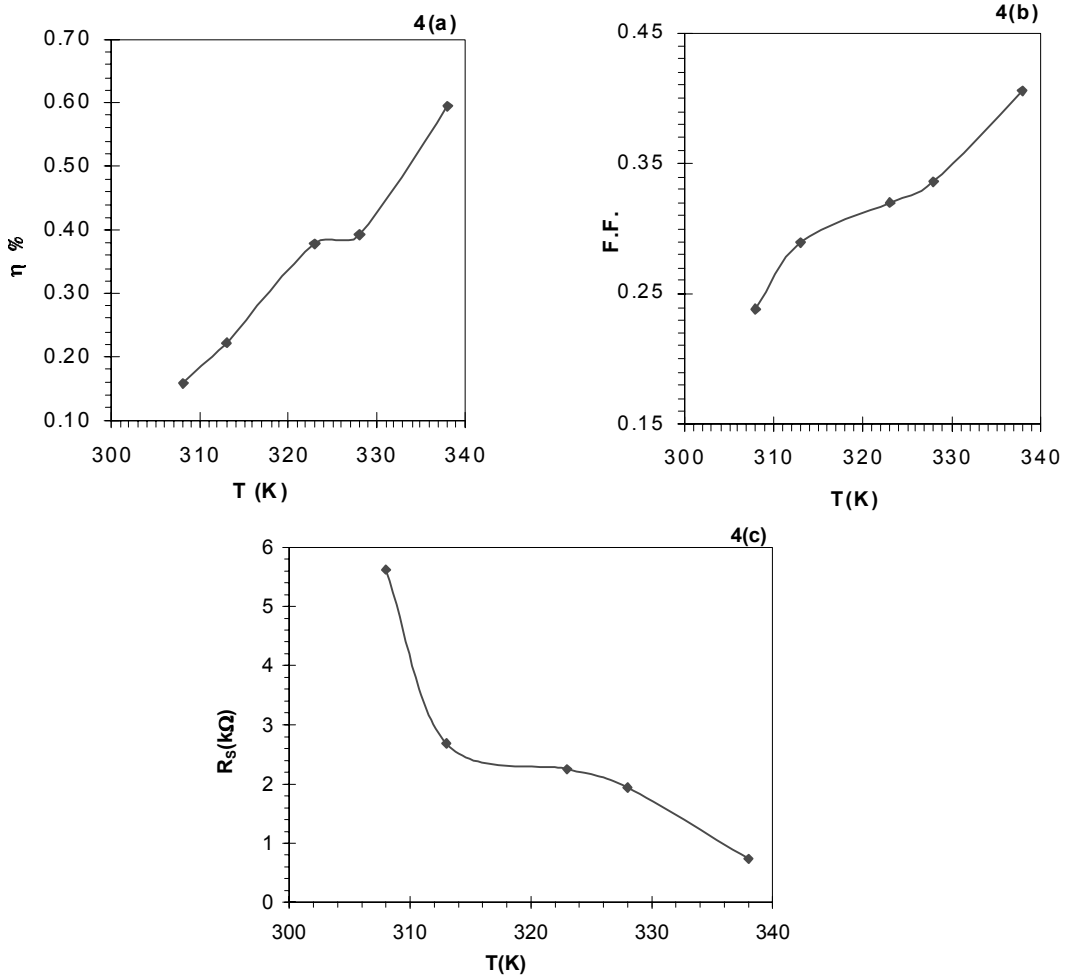


Fig. 4 : Variation of (a) efficiency (b) fill factor and (c) series resistance with temperature (Electrode – 2)

Temperature Sensitivity of...

It is quite apparent from figures 4(a), 4(b) and 4(c) that the fill factor and efficiency increase with temperature while the series resistance of MoSe₂ PEC solar cells decreases with temperature. This is in good conformity with the semiconducting behaviour of photoelectrode. Moreover, due to the reduction in series resistance, the transport of photogenerated carriers becomes more efficient, which is the main reason for improvement in the parameters of such cells.

References

1. Tributsch H. Ber Bunsenges. Phys. Chem., **81**, 362 (1977)
2. Tributsch H and Bennett J C, J. Electroanal. Chem. **81**, 97 (1977)
3. Gobrecht J. Gerischer H and Tributsch H. Ber. Bunsenges. Phys. Chem. **82**, 1331(1978)
4. Gujarathi D.N., Solanki G.K., Deshpande M.P., Agrawal M.K., Solar Energy Materials and Solar cells, **90**, 2630 (2006)
5. Gerischer H., Semiconductor Liquid Junction Solar Cells ed. A Heller (Pennington, NJ: The Electrochemical Soc. Inc.) (1977)
6. Butler M.A. and Ginley D.S., J. Mat. Sci., **15**, 7 (1980)
7. Sureshchandra in “Photoelectrochemical solar cells” Gordon and Breach Science Publication, New York
8. Pathak V.M. and Srivastava R., Solar Energy, **50**,123 (1993)
9. Pathak V.M., Patel K.D., Pathak R.J. and Srivastava R., Solar Energy Materials and Solar cells, **0**, 1 (2001)
10. Gerardo L. Araujo, Enrique Sanchez, IEEE Transactions on Electron Devices, **ED-29**, **No.10**, 1511(1982)
11. Chan D.S. H., Philips J.R. and Phang J.C.H., Solid-State Electronics, **29**,**No.3**, 329 (1986)
12. Dieter K. Schorder “Semiconductor Material and Device Characterization” Wiley Interscience Publication, (1990)
13. Wolf M. and Rauschenbach H. Adv. Energy Conv., **3**, 455(1963)
14. Wilson J.A., Yoffe A.D., The transition metal dichalcogenides: Discussions and interpretations of the observed optical, electrical and structural properties, Adv. Phys. **18**, 193 (1969)
15. Srivastava R. and Pathak V.M., Energy bands and PEC behaviour of n- MoSe₂ solar cells, B. Electrochem., **5**, 537 (1989)

GROWTH AND X-RAY DIFFRACTION STUDIES OF ZnSe CRYSTALS

J.R. Gandhi, G.K. Solanki, K.D. Patel and S.G. Patel

Department of Physics, Sardar Patel University
Vallabh Vidyanagar

Abstract

ZnSe is a wide band gap compound and has attracted many researchers due to its interesting luminescence properties. In this paper authors present their investigations on growth of ZnSe crystals by Physical Vapor Transport Technique. The structural characterization was accomplished by X-Ray diffraction (XRD) studies and it was found to be cubic. Lattice parameters, volume and X-ray density have been measured for the grown crystals. The particle size for a number of reflections has been calculated by using Scherrer's formula.

KEY WORDS : ZnSe crystal, Physical vapor transport, XRD, EDAX

Introduction

The wide band gap II-VI compounds are the promising materials for their use in many optoelectronic applications. ZnSe having a direct band gap of 2.7 eV at room temperature (H. Wenisch et al. [1]) is one of this group and has many potential applications in optical devices and components. Crystalline ZnSe is very important material to be used as substrate for operating in blue range. Optical devices based on ZnSe having a ZnSe substrate (homojunctions), have many advantages over the optical devices having GaAs substrate (heterojunctions) as explained by Huanyong [2], Ching-Hua[3], Urbietta[4], and Wang[5].

In early 1990's, GaAs was used in optical devices (particularly in laser industries) as substrate to make ZnSe based optical devices. But the lattice mismatch and difference in the thermal expansion coefficient between GaAs and ZnSe had shortened the lifetime of such devices (Hiroyuki Kato et al. [6]).

Thus to increase the lifetime of the devices based on ZnSe and to enhance their performance by reducing the defects in them, it was necessary to improve the basic characteristics of ZnSe. But due to the lack of high purity commercially available ZnSe bulk crystals, limited work has been done in this field. Hence, there was a need of large and high purity substrates for homoepitaxial growth.

Most of the bulk crystal growth techniques used for the growth of ZnSe crystals yield heavily twinned and impure materials whose luminescence spectra are dominated by impurity

Growth and X-Ray Diffraction...

bound excitons and /or donor-acceptor pair (DAP) bands (Tourine [7], Bhargava [8]). In recent years, significant progress has been achieved in terms of material purity and structural quality (Taguchi [9], Cantwell [10], Mochizuki [11], Rudolph [12]).

EXPERIMENTAL

ZnSe crystals have been grown by a Physical Vapor Transport Technique (PVT). A 10 gram of mixture of Zn (4.53 gram, Purity : 99.99%, Make: Fluka Chemi) and Se (5.47gram, Purity : 99.99%, Make : Aldrich, USA) were taken in stoichiometric proportion in a quartz ampoule for charge preparation. This ampoule was evacuated at the pressure of 10^{-5} Torr and then sealed. This sealed ampoule was placed in a dual zone furnace of constant reaction temperature to obtain a charge of the material. For the synthesis of the charge, temperature was slowly increased up to 1023 K with 10 K/hr. The ampoule was kept at this temperature for 4 days. Then the furnace was slowly cooled at the rate of 20 K/hr and brought to room temperature. The resulting orange yellowish charge was obtained in the ampoule. This charge was crushed and transferred to other quartz ampoule. This ampoule was also evacuated at a pressure of 10^{-5} Torr and placed in a two zone horizontal furnace for 10 days with a temperature gradient of 50 K between the source zone (1173 K) and growth zone (1123 K). After that furnace was cooled down to room temperature at a rate of 10 K/hr. Thus the material has been found to be converted into single crystals at the cooler end of the ampoule. The grown crystals of yellow color were collected after breaking the ampoule.

To achieve the temperature gradient of 50 K between the source zone and the growth zone, several runs were taken. The process was initially started with the temperature gradient of 100 K between both the zones. This gradient was then reduced to 10 K after investigating the results. Thus finally after six runs, the gradient was set to 50 K that resulted in formation of small crystals. The selection of upper temperature and the gradient of temperature between the growth and source zone were made on the basis of an extensive literature survey. All six runs with their corresponding zone temperatures are tabulated in Table -1.

Table - 1: Temperature distribution of various runs taken for crystal growth

Initial Material : ZnSe (10 gram)

Run No.	Ampoule Dimensions			Temperature Distribution			Growth Time (Hour)	Result
	OD (mm)	ID (mm)	Length (mm)	Source Zone (K)	Growth Zone (K)	Difference (K)		
1	25	22	250	1173	1073	100	168	Ingots
2	25	22	250	1173	1083	90	168	Ingots
3	25	22	250	1173	1093	80	168	Ingots
4	25	22	250	1173	1103	70	168	Ingots
5	25	22	250	1173	1113	60	168	Ingots
6	25	22	250	1173	1123	50	168	Crystals of Size app.3 mm ²

For X-ray diffraction (XRD) work, several small crystals were finely ground with the help of an agate mortar and filtered through 106-micron sieve to obtain grains of nearly equal size. The X-ray diffractograms were taken with Philips X-ray diffractometer (model: PW1820) employing CuK_α radiation. The energy dispersive analysis by X-rays (EDAX) has been carried out for determination of the stoichiometric proportion of Zn and Se.

Results And Discussion

The crystals of ZnSe were grown by Physical Vapor Transport (PVT) Technique. The crystal structure is cubic. The X-ray powder diffractogram obtained for ZnSe is shown in figure-1.

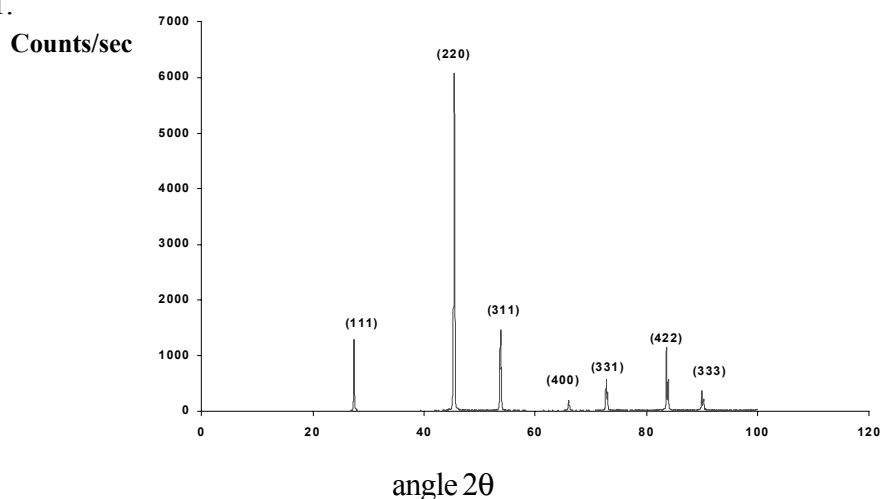


Figure-1 : X-ray powder diffractogram of ZnSe crystal

Growth and X-Ray Diffraction...

The sharp peaks indicate the good crystalline structure of the grown compound. The values of lattice parameters a, b and c (here a=b=c), unit cell volume (V) and X-ray density (ρ) determined from x-ray diffractogram are presented in table – 2 which are very well matched with the values of JCPDF data.

Table -2: Crystallographic data of ZnSe crystal grown using PVT

Parameter	JCPDF data	Present Work
a =b=c (Å)	5.66	5.65
Unit cell Volume V (Å) ³	182.17	180.69
X-ray density ρ (gm . cm ⁻³)	5.26	5.305

The X-ray data for ZnSe was used for estimation of particle size using Scherrer's formula given by-

$$t = \frac{K\lambda}{\beta \cos \theta}$$

where t is the particle size as measured perpendicular to the reflecting plane, K is the Scherrer constant whose value is taken to be unity assuming the particles to be spherical, λ is the wavelength of X-ray radiation, β the half intensity width measured in radians and θ is the Bragg angle. The (h k l) values corresponding to prominent reflection, d-values, half width, peak intensities and particle size for ZnSe crystals are shown in Table - 3.

Table - 3 : X-ray diffraction data for ZnSe grown by PVT Technique

(h k l)	d-spacing (Å)	Peak Width (°2 θ)	Peak Intensity (Counts/second)	Particle size (Å)
(1 1 1)	3.2526	0.21	1307.40	389.52
(2 2 0)	1.9955	0.21	5526.33	410.21
(3 1 1)	1.7035	0.28	1361.00	318.18
(4 0 0)	1.4146	0.28	185.04	338.34
(3 3 1)	1.2982	0.35	478.03	282.01
(4 2 2)	1.1561	0.21	1075.28	507.31
(3 3 3)	1.0903	0.21	227.81	534.51

Conslusion

Crystals of ZnSe were grown by Physical Vapor Transport (PVT) Technique. The temperature difference between the source zone and the growth zone has been varied from 10 K to 50 K and it has been found that at 50 K difference in these temperatures resulted in small, yellowish shining crystals of ZnSe.

The EDAX study gives a confirmation that crystals are stoichiometrically perfect. The X-ray diffraction analysis confirms a cubic structure of the as grown crystals and all structural parameters that have been determined are in good agreement with the standard JCPDF.

References

1. H.Wenisch, K Schull, D Homanel, G Landeehr, D Siche and H Hartmann, *Semiconductor Science Technology* **11**, 107-115 (1996)
2. Huanyong Li and Wangi Jie, *Journal of Crystal Growth* **257**, 110-115 (2003)
3. Ching- Hua Su, M.Dudley, R. Matyi, S.Feth, and S.L.Lehoczky *Journal of Crystal Growth* **208** 237-247 (2000)
4. A.Urbieta, P.Fernandez, J. Piqueras and V.Munoz *Materials Science & Engineering* **B78** 105-108 (2000)
5. J.F.Wang, A. Omino and M.Isshiki *Materials Science & Engineering* **B-83** 185 191 (2001)
6. Hiroyuki Kato, Harahiko Udono and Isco Kikuma *Journal of Crystal Growth* **229** 76-86 (2001)
7. E.Tournie, C.Morhain, G.Neu, C.Ongaretto, J.P.Faurie, R.Triboulet and J.O.Ndap, *Journal of Applied Physics*, **80 (5)** (1996)
8. R.N.Bhargava, *Journal of Crystal Growth* **59**, 15 (1982)
9. T.Taguchi, T.Kusao and Hiraki , *Journal of Crystal Growth* **72** 46 (1985)
10. G Cantwell, W.C.Harsch, H.L.Cotal, B.G.Markey S.W.S. Mc Keever and J.E.Thomas *Journal of applied Physics*, **71** 2931(1992)
11. K.Mochizuki, K.Masumoto, T.Yasuda, Y.Segawa and K. Kimoto, *Journal of Crystal Growth*, **135** 318 (1994)
12. P.Rudolph K. Umetsu, H.J.Koh and T.Fukada, *Journal of Crystal Growth* **143** 359 (1994)